UNIVERSIDAD NACIONAL AUTÓNOMA DE MEXICO

DOCTORADO EN CIENCIAS (FÍSICA)
INSTITUTO DE CIENCIAS FÍSICAS

EFFECT OF UNNECESSARY PROTEIN SYNTHESIS ON THE GROWTH OF E. COLI

TESIS
QUE PARA OPTAR POR EL GRADO DE:
DOCTOR EN CIENCIAS (FÍSICA)

PRESENTA:
MAYRA PATRICIA GARCÍA ALCALÁ

DR. MAXIMINO ALDANA GONZÁLEZ
INSTITUTO DE CIENCIAS FÍSICAS, UNAM

DR. PHILIPPE CLUZEL
HARVAD UNIVERSITY

DR. HERNÁN LARRALDE RIDAURA
INSTITUTO DE CIENCIAS FÍSICAS, UNAM

DR. ALEJANDRO FRANK HOEFLICH
INSTITUTO DE CIENCIAS NUCLEARES, UNAM

CUERNAVACA, MOR., JULIO 2021

Agradecimientos

Este trabajo debe su existencia y resultados a la intervención de personas que generosamente han facilitado el proceso de investigación con su conocimiento, trabajo y apoyo.

Gracias al Dr. Maximino Aldana por su guía, y porque desde inicios de mi doctorado me animó a seguir en investigación y ofreció la oportunidad de trabajar haciendo experimentos. Tuve la fortuna también de contar con el apoyo de la comunidad de estudiantes, amigos e investigadores del ICF: gracias.

Al Dr. Philippe Cluzel le agradezco que me haya abierto las puertas para trabajar en su laboratorio, y su paciencia en mi comienzo en la práctica experimental. Gracias a los miembros del laboratorio del Dr. Cluzel, en especial a Mark Kim. Gracias a los compañeros y amigos que conocí en Cambridge, además de su colaboración científica, me ayudaron a vivir en un país extranjero, a adaptarme en un área de investigación nueva para mí, y a sobrellevar los retos que esto representaba.

Gracias a toda mi querida familia por el apoyo y confianza a lo largo de toda mi vida académica.

Finalmente, expreso mi reconocimiento al apoyo institucional que permitió cada fase de este trabajo: las becas otorgadas por el CONACyT y el Centro de Ciencias de la Complejidad de la UNAM, con las amables gestiones del Dr. Alejandro Frank.

•»❋«•

Contents

1. Introduction

E. coli is presumably the simplest and most studied model organism, and yet, for this and all microorganisms, it is not fully understood how they regulate their cell size and division time [8,57].

A bacterial population can present different phenotypes depending on the environmental conditions in which they are growing. Changes in the nutrients, temperature, PH, etc., lead to changes in cell size, division time, and gene expression [2, 16, 17].

Although there is cell-to-cell variability within a population, even on an isogenic population in a constant environment, the average values of cell size and growth rate are stable. The average values can even be reproduced if a population of the same strain grows in the same condition.

Since 1950, there has been significant research based on the measurement and characterization of bacteria's physiological parameters, as the growth rate, doubling time, protein content, etc., under different growth conditions. The goal being the finding of quantitative relations between cell's physiological parameters in order to infer the restrictions on the growth's underlying molecular mechanism.

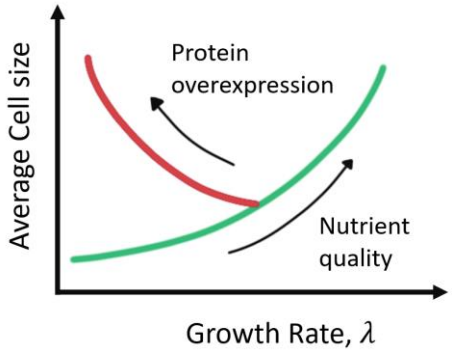

Figure 1.1. Relation between the average cell size and the growth rate of a bacterial population under different growth limitations. When the growth rate is modulated by nutrient quality (green), average cell size follows an exponential function which is known as a "nutritional growth law" [2, 11]. In contrast, when cells are forced to overexpress unnecessary proteins (red), the average of the cell size increases, but the growth rate decreases [11]. Both curves represent the trend across the average values of different populations. The image is a representation of the results in [11].

With this approach, Schaechter et al. identified in *Salmonella* a relation that is known as a nutrient growth law: the macromolecular composition of cells (mass of RNA, DNA, protein, and cell mass)

is essentially a function of the doubling rate alone, irrespective of the content of the growth medium (Fig.1.1).

In the same spirit, T. Hwa and coworkers studied the concentration of diverse proteins in *E. coli* across different growth conditions modulating the growth rate by changing the growth medium [12, 56]. They observed that the concentration of some proteins across such conditions increases, decreases, or is constant, depending on the protein's function in the cell (Fig.1.2a). For instance, ribosomal proteins (the proteins involved in the protein synthesis) increase linearly with the nutrient-modulated growth rate. These observations demonstrate the critical dependence on gene expression and growth rate and are also considered growth laws. . Hwa and coworkers proposed a model in which a cell's resources are allocated among different types or sectors of proteins [12].

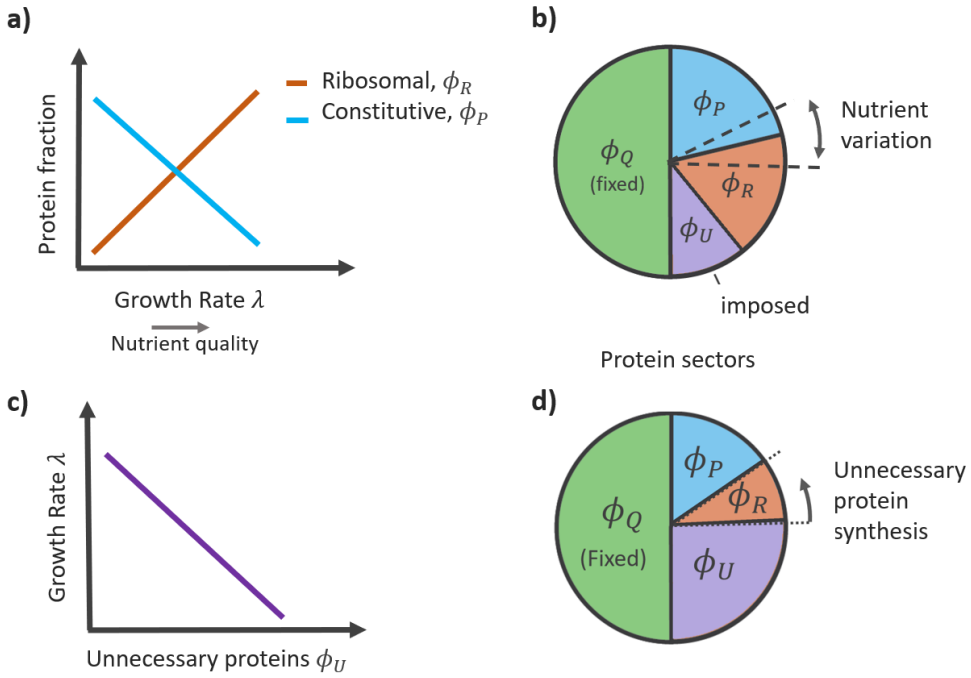

Figure 1.2. T. Hwa and coworkers observed that the fraction of ribosomal proteins increases linearly with the growth rate when the growth medium's nutrient quality modulates the latter (a, brown line) [12, 666]. The constitutively expressed proteins show the opposite dependence on the growth rate (a, blue line), implying a linear constraint between ribosomal and constitutive proteins. Then, the minimal proteome division can be considered as (b): a fixed sector of housekeeping proteins ϕ_Q (green), if imposed, a sector of unnecessary proteins ϕ_U (purple), and the constitutive ϕ_P (blue) and ribosomal sectors ϕ_R (brown), which change their size depending on the nutrient condition. When cells are forced to synthesize unnecessary proteins U, while maintained in the same nutrient conditions, the growth rate decreases (c).

Since the fraction of unnecessary protein increases, it effectively decreases the fraction allocable to the P and R sectors (d).

The minimal model contemplates three sectors, the ribosomal proteins ϕ_R, housekeeping ϕ_Q, and constitutive proteins ϕ_P, plus, if imposed the expression of unnecessary proteins, an extra sector ϕ_U. These sectors increase, remains unchanged and decrease respectively as a function of the nutrient modulated growth rate, as in their experimental results (Fig.1.2a and b). Since the cell has finite proteomic resources, any increase in investment in a sector must coincide with a corresponding decrease in investment in another. With the model, they also could predict the cost in the growth rate of a population due to the cell overproduction of an "extra" unnecessary protein. When forced to synthesize unnecessary proteins, the population growth rate decreases approximately linearly, while changing the fraction of the protein sectors (Fig.1.2c and d).

Basan et al. also analyzed the growth of *E. coli* under unnecessary protein synthesis. Their main observation is that when there is an expression of unnecessary proteins, the mean cell size of a population increases while the growth rate decreases [11] (Fig.1.1 red). Such relation goes in the 'opposite direction' than the nutrient growth law (Fig.1.1 red).

The studies mentioned above were done by performing experiments with bacteria growing in "bulk". However, the mean population behavior of bacteria does not give enough information to understand the process by which individual cells control their growth.

In recent years there has been a rapid development in microfluidic designs and techniques that allow the measurement of individual bacterial cells growing in a controlled environment. For instance, the Mother Machine is a microfluidic device used to monitor single cells trapped in small channels where they can grow and divide while fed with a constant flow of growth media [48].

Several studies have used this technique to analyze the cell size and division time fluctuations in a bacterial population driven by intrinsic noise in the molecular composition.

The correlations between cell size at birth, size at the division, and division time in a steady-state help characterize the cell-size control mechanism [8]. One classic model for cell-size control is the *sizer model*, which proposes that a bacterium needs to reach a critical size (or a critical size per DNA) for it to divide [1] (Fig.1.3). The *timer model* proposes a fixed time interval between cell

cycle events [1, 18]. And a recent model, named *adder,* considers that for the cell to maintain its cell size, it needs to increment its mass by a fixed value [7]. Some studies have demonstrated that the $E.coli$ growth agrees with the adder model [6, 9]. Nevertheless, the underlying molecular mechanism of the fixed size is not yet understood [23]; therefore it is still a source of investigation how single cells respond to different perturbations and if the physiological changes they acquire fit with any of the size control models.

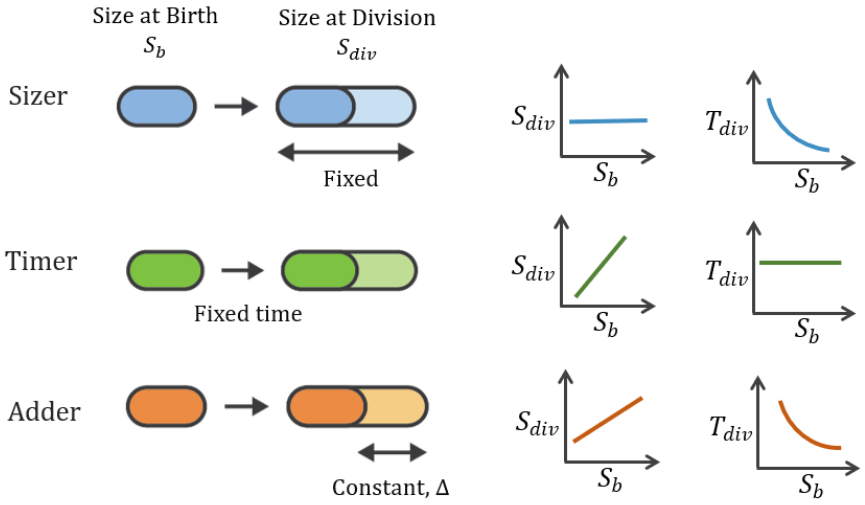

Figure 1.3. Bacterial size control models. In the 'sizer' model (top), cells divide once they reached a fixed size S_{div}, independent of the size at birth S_b. In the 'timer' model (middle), the size depends solely on the age of the cells and divide after a fixed duration since birth, such that the division time T_{div} is constant. In the 'adder' model (bottom), there is a constant mass (or content) Δ that cells need to reach to trigger its division. On the right side are the relations between the variations in size at division S_{div} and of the division time T_{div} as a function of size at birth S_b for a population of bacteria that follows each model. Those relations help determine which model a certain bacteria or strain follows. Figure modified from [8].

Specifically, Taheri-Aragui et al., using the mother machine, monitored *E. coli* cells and found that the adder model relations are verified when bacteria grow in media with different nutrient quality. They also found deviations in the nutrient growth law at the single-cell level [6, 23], which can be explained by the adder mechanism as well.

Similarly, analyzing how individual cells grow when they overproduce unnecessary proteins at different levels can give information on the molecular mechanisms. Are relationships between the

physiological parameters that characterize the Adder model conserved when growth is perturbed by overexpression? Are there deviations from the population-level behavior? Is there a cost in growth associated with the fluctuations in production?

To address these questions, in the present work, I explore the effect on bacterial growth due to overexpression of unnecessary protein in different conditions, at population and single-cell levels.

I constructed a set of *E. coli* strains, the ProVenus set, which have different synthesis levels of the fluorescent protein Venus, a protein that is unnecessary for bacteria, see Fig.1.4. I used the mother machine device and fluorescent microscopy to monitor the growth and protein content over time of cells of all such strains. I also grow the cells under a flow of various growth media. Then, I can characterize the growth for cells changing the protein production and nutrient quality.

In the next chapter, I describe the steps I followed for constructing the microfluidic device, the protocol I used to transform the ProVenus strains, and report the experimental setup for monitoring the cells using fluorescent microscopy.

With the data obtained from the ProVenus set, first, I explore the population-level relations of bacterial growth, such as the nutriment growth law and the ones from the resource allocation model.

In chapter 4, I consider the single-cell nature of the data and analyze how cell growth changes as a function of the expression of the unnecessary protein Venus in individual cells across the strains. I characterize the correlation between the different measured parameters (size, division time, fluorescence) and how such correlations change for a different level of unnecessary synthesis to test some cell size models and division control mechanisms.

My goal is that the relations of protein production and the cell size, growth rate, and other cell parameters shed light on the mechanisms that cells follow to grow and divide. Also, how these relations give rise to the known population-level behavior.

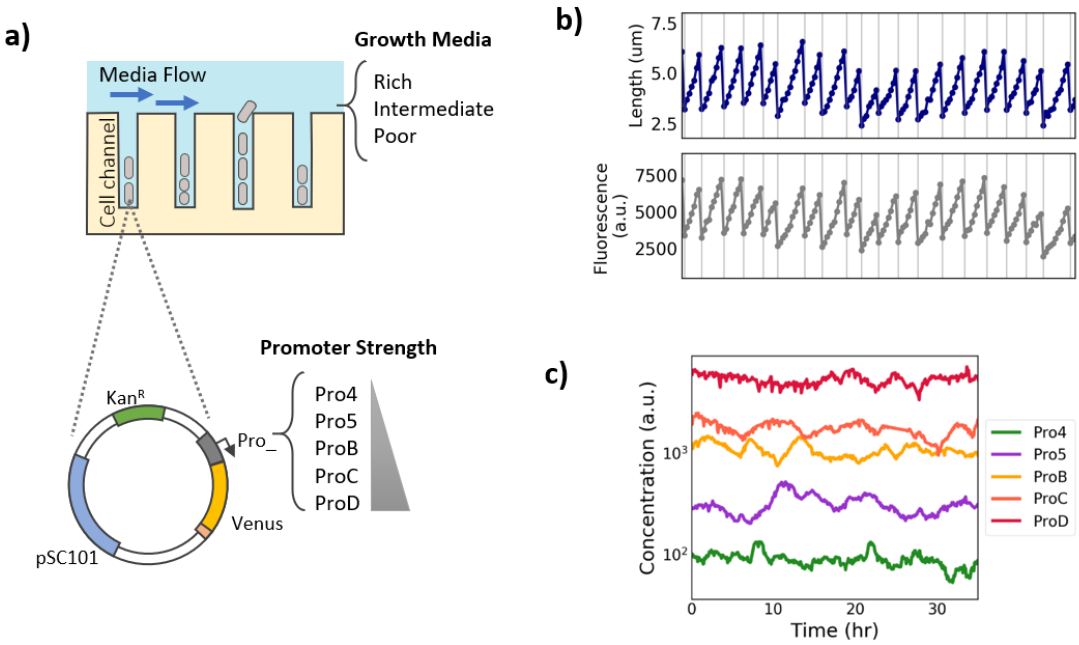

Figure 1.4. a) Schematics of the microfluidic experimental setup and ProVenus strains. In the Mother Machine device, cells get constrained into the cell channel where they can grow and divide while fed by a constant flow of fresh growth media. The 'mother' cell in the base can be monitored for many generations using time-lapse imaging. The ProVenus strains, which I monitored, produce fluorescent proteins in multiple levels. Each strain has a plasmid that expresses the fluorescent protein Venus controlled by a constitutive promoter from a group (Pro4, Pro5, …, ProD) with various promoter strengths. All the strains were grown under the flow of three different growth media, referred to as poor, intermediate, and rich. b) Typical time trace of a ProBVenus cell growing in the mother machine in rich medium. The cell length (top) and fluorescence (bottom) increase continuously until cell division occurs (vertical gray lines). **c)** Concentration (fluorescence/area) over time of a cell from each strain of the ProVenus. The rainbow color code corresponds to the level of strength of the Venus promoter.

The ProVenus strains express the unnecessary protein constitutively, so they have a constant synthesis of Venus. For this reason, with such strains, it cannot be analyzed the effect on growth when cells have a sudden decrease or increase of protein production.

There are some proteins that cells natively synthesize in oscillatory or pulse-like dynamics.

Such cases are an interesting system for analyzing the impact in growth due to the sudden protein synthesis in the same strain, thus allowing as well to study the effect over time.

Some proteins that *E. coli* produces in pulses are proteins related to the assembly and functioning of the flagella, the organelle that allows bacteria to move [47].

The flagellar transcriptional system is organized into a transcriptional hierarchy of three promoter classes that are temporally regulated for the flagella assembly, see Fig.1.5a. The class-1 promoter *flhDp* regulates the formation of a macromolecular complex $FlhD_4C_2$, also called the master regulator. $FlhD_4C_2$ governs the activation of the class-2 promoters that control the expression of the genes for the flagellar hook and basal body. One of the class-2 promoters controls the production of the protein FliA that mediates the expression of the class-3 genes for the filament synthesis and motor elements that power the flagellum rotation.

In [47], we reported that the class-2 promoters present sharp bursts of activity followed by long periods with no activity that can extend across several cell divisions. Hence, the class-2 flagellar proteins are synthesized with intermittences while bacteria grow. For this reason, I decided to study the effect on cell growth due to flagellar protein production. To do this analysis, I used a mother machine device to monitor an *E. coli* strain named here DCF, which expresses the fluorescent protein Venus when class-1 is activated and a cyan fluorescent protein CFP when a class-2 promoter is activated (Fig.1.5b). In Chapter 5, I analyze the response of individual cells subject to the perturbations on protein production: How cells change in size, division time, and other parameters before, during, and after a burst in protein expression.

In summary, in the following chapters, I present an analysis of the variations of the physiological parameters within a population and across populations when cells are subject to different levels of unnecessary protein synthesis and grow in diverse nutrient quality. I compare the results with the expectation of various growth models, both population-level and for the cell size and division control mechanisms of individual cells.

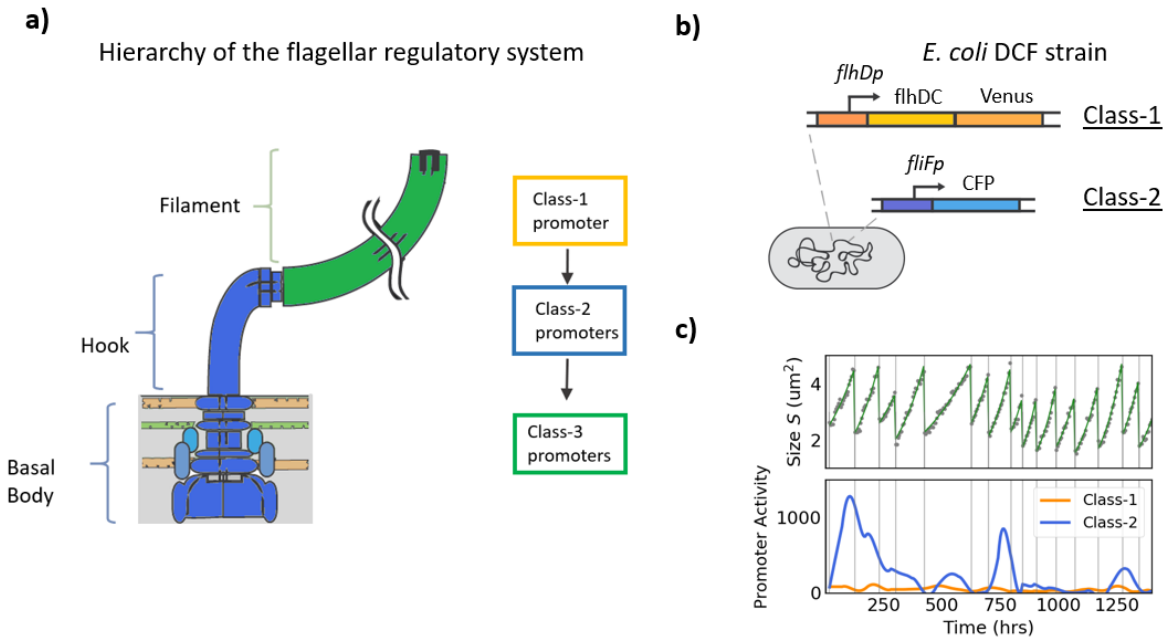

Figure 1.5. a) Hierarchy of the flagellar regulatory system. The assembly of the flagellum in *E. coli* is coordinated by the orderly activation of three promoter classes. The class-1 promoter, flhDp, produces the master regulator FlhDC that directs the transcription of the class-2 promoters. Class-2 promoters control the genes that codify the proteins that form the hook and basal body substructure (structures in blue). One of the class-2 proteins is a sigma factor that directs the expression of class-3 promoters, which controls the genes for the structure of the filament and chemosensory pathway. **b)** The strain DCF has two mutations in the chromosome to report the activity of class-1 and class-2 promoters [47]. The gene for Venus fluorescent protein expression was inserted downstream the class-1 native promoter and operon. The promoter for the class-2 promoter *fliFp*, controls the activity of the cyan fluorescent protein CFP. **c)** Top: Area of a DCF cell over multiple generations. The gray vertical lines correspond to a time point where the cell divide. Bottom: Activity (derivative of the fluorescence) for the class-1 (yellow) and class-2 (blue) promoters. The activity of Class-2 displays pulse-like dynamics, in which burst of activity followed by periods of no activity that can last several generations.

2. Method Development

2.1 Introduction

Our experimental setup's goal is to measure bacteria's physiological characteristics when they overproduce unnecessary proteins.

To convey this, I constructed a set of *E. coli* strains that overproduce the unnecessary protein Venus in various quantities called ProVenus. To these strains, I want to measure the cell size, division time, growth rate, and fluorescence, which is a proxy of the number of unnecessary proteins Venus in the cells.

The experiments that I performed are single cells growing inside a microfluidic device called the 'Mother Machine' [14]. In this device, cells can grow under stable conditions with a constant flow of growth medium that feeds them for long periods. Inside de device, cells get trapped in small channels while they can still grow and divide. Using microscopy techniques, I took time-lapse images of the cells growing. From the images, it can be extracted different physiological parameters like cell size, division time, and the fluorescence of the cells over time.

In the following sections, I describe the different steps that I followed to make these experiments: from the constructions of the strains, fabrication of the microfluidic device, the setup of the microscopy experiments, and the process to extract the dataset from the images.

2.2 Construction of *E. coli* strains with different levels of unnecessary protein synthesis

To analyze the relationship between unnecessary protein synthesis and bacterial growth, I use two types of *E. coli* strains:

- ProVenus strains. This set of strains synthetize the fluorescent protein Venus at various levels, each with a steady synthesis rate over time.
- DCF strain. Reports the activity of the genes that code for a class of flagellar proteins that are synthetized with a pulse-like dynamics [47].

The description and protocol for the construction of the ProVenus set is bellow, while the DCF strain construction is in [47].

a) Strains with constitutive expression of Venus

For cells to synthesize the Venus proteins, they need to be programmed to do so: the gene's genetic sequences that code for Venus and the promoter to initiate its transcription need to be added into their genome. The cell's own machinery for replication, transcription, and translation will then synthesize the Venus protein. There are two possibilities for adding these sequences into the genome: one is to include it in the cell's chromosome, and the other is to add that sequence in a plasmid[1]. I decided to produce Venus from a plasmid since a cell can maintain multiple plasmid copies (as dictated by their copy number, which is the average number of plasmid copies per cell); thus, there would be a higher protein synthesis.

I use a set of constitutive promoters[2] from the Pro-series, Pro1, Pro4, … ProB, ProD, which are artificial promoters with various strengths, to control Venus transcription [22]. In this way, cells with different promoters will have as well different levels of Venus expression.

The plasmid also has an antibiotic resistance gene (resistance to Kanamacyn) and the sequence of the origin of replication pSC101, Fig. 2.1. The antibiotic resistance gene is a selectable marker, and the origin of replication is the sequence necessary for the bacteria to replicate the plasmid with ~5 copies per cell.

The steps I followed to construct the plasmids are:

1. I amplified (using PCR) the sequences of the origin of replication plus the gene that confers antibiotic resistance from a backbone of a plasmid that already contained them.

[1] A plasmid is a structure in bacterial cells consisting of DNA that can exist and replicate independently of the chromosome. Plasmids provide genetic instructions for certain cell activities (e.g. resistance to antibiotic drugs). They can be transferred from cell to cell in a bacterial colony. Plasmids are widely used as vectors to produce recombinant DNA for gene cloning.

[2] Constitutive Genes are genes that are expressed following interaction between a promoter and RNA polymerase without additional regulation [61].

2. I ordered the sequence for the linear fragment of the promoter Pro5 plus a ribosomal binding site (RBS) plus the Venus gene, 'Pro5_Venus', from a custom oligonucleotide supplier company.
3. Using Isothermal Assembly, I assembled the two linear sequences, the backbone and the 'Pro5_Venus' , to circled into the plasmid pPro5Venus, i.e. to join the linear fragments in order to form the circular molecule that is a plasmid.
4. I transformed the plasmid into an *E. co*li strain (Dh5α), selected the colonies resistant to kanamycin, and have yellow fluorescence under the microscope.
5. For the rest of the plasmids, I amplified the complete linear sequence of pPro5Venus with primers that helped to swap the Pro5 10-box with the respective sequence for each promoter Pro1, Pro2, …, ProD. Each plasmid was circularized using the NEB KLD Enzyme Mix (New England Biolabs).

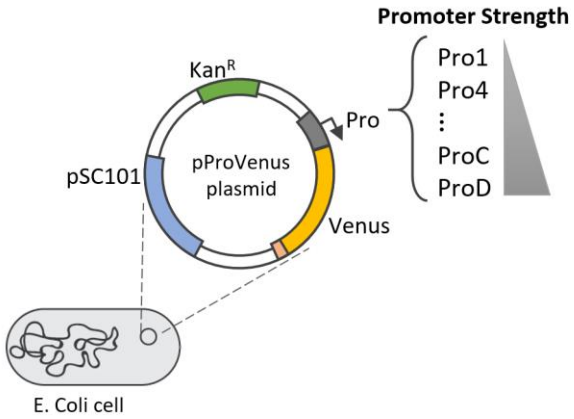

Figure 2.1. Schematic of a ProVenus strain. An *E. coli* strain (MG1655) was transformed with a plasmid, pProVenus, which constitutively expresses the yellow fluorescent protein Venus. A promoter Pro from a set of synthetic promoters with variable strength, Pro∈{Pro1, Pro4, …, ProD} from [22] controls Venus expression. The plasmid also contains a selectable marker, a kanamycin antibiotic resistance gene (Kan^R), and the origin of replication pSC101.

Once I constructed the plasmids, I transformed each of them into an *E. coli* strain via electroporation. The strain in which the plasmid was transformed is a MG1655 strain, with a point

mutation in the *motA* gene (E98K) that disables flagellar rotation and prevents cells from swimming out of the channels in the "mother machine".

After growing the transformed cells on LB medium for recovery, I plated them in agar plates with kanamycin, from where I selected resistant colonies. I verified the presence and sequence of the plasmid on the strains by colony PCF and sequencing. I also used Fluorescence microscopy to choose fluorescent colonies, ensuring the cells synthesize the Venus proteins.

Then, I measured the fluorescence level of the ProVenus set using flow cytometry. Such technique consists of directing a UV beam into a liquid flow that contains bacteria in low density, where the beam gets scattered. Fluorescence detectors sense the spectrum of wavelengths of the scattered light. If the bacteria contain a fluorescent protein, the emitted light has a particular wavelength that is detected and then processed to measure the fluorescence intensity. In Fig.2.2, I show the fluorescence distributions of a population from each of the ProVenus strains. The order of the strains by fluorescence is expected from the promoter strength reported by Davis et al. [22].

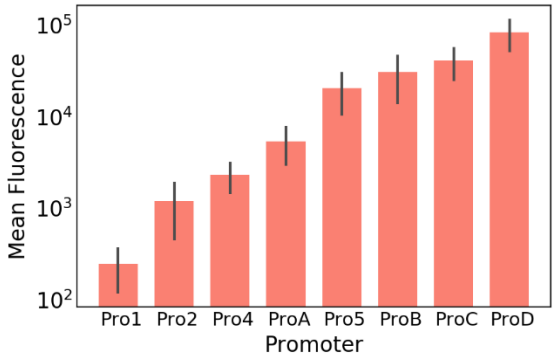

Figure 2.2. Fluorescence of ProVenus Strains. Strains with a different promoters (Pro1, …, ProD) controlling Venus expression were grown in liquid growth medium until exponential phase and measured their fluorescence using a flow cytometry instrument. The bars' height shows the mean yellow fluorescence over a population of cells of each strain and the error bars the standard deviation.

b) Strain flagellar genes reporters

As mention in Chapter 1, *E. coli*'s flagellar promoter genes are divided into three coordinately regulated classes. This regulatory hierarchy acts to ensure the orderly synthesis of the proteins that conform the different parts of the flagella.

Class-1 promoter, *flhDp*, controls the production of the master regulator of the network, FlhDC, which directs the transcription of class-2 genes, genes that produce the proteins necessary for the assembly of the hook and basal body of the flagella. One of the class-2 gene products FliA, is a sigma factor [13] that controls the activation of class-3 promoters, whose products are the proteins that compose the flagellin and the motor system.

In the present work, in chapter 5, I analyze the cell growth and the flagellar promoter activity of the DCF strain (called E98KFC in [47]). This strain has the following mutations in its gnome:

- Class-1 reporter. The Venus gene was added downstream the class-1 operon *flhDC* (the set of genes controlled by class-1 promoter), as a reporter of the activity of this class.
- Class-2 reporter. A copy of the class-2 promoter and the gene that codes for the cyan fluorescent protein SCFP3A was inserted in the galK region of the chromosome (this region is a standard region in molecular engineering to make transformations in bacteria). The native *fliF* gene was left intact.
- The strain has a point mutation (E98K) in the MotA gene, which disables flagellar rotation and prevents cells from swimming out of the channels in the "mother machine".
- A detailed protocol for the chromosomal engineering steps followed in the construction on this strain can be found in [47].

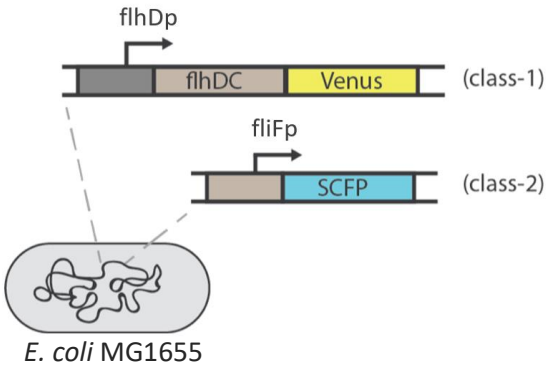

Figure 2.3 Diagram of a DCF strain. The *E. coli* strain has two mutations in the chromosome to report the activity of class-1 and class-2 promoters [47]. The gene for the Venus fluorescent protein expression was inserted downstream the class-1 native promoter and operon. In a different region of the chromosome, a copy of the class-2 promoter *fliFp* controls the activity of the cyan fluorescent protein CFP.

2.3 Microfluidic device construction

The Mother Machine is a microfluidic device where individual bacteria can grow and be monitored under controlled conditions for a long time [14].

The device consists of small channels closed on one end and connected perpendicularly on the the end to a wide channel in which liquid growth media can flow, see Fig.2.4. Once the device is loaded with bacteria, individual cells get trapped at the closed end of the cell channels, where there is enough space to grow while the liquid media also feeds them. As the cells grow and divide, the newly born cells get pushed out of the cell channels and washed away with the growth media flow, while the 'mother' cell remains at the bottom. The mother cell can easily be monitored over time since, in principle, it remains at the same position while growing and dividing under controlled conditions.

In this section, I describe the steps to fabricate a mother machine device: the modifications to the classical design, the fabrication of the mold, and the device casting.

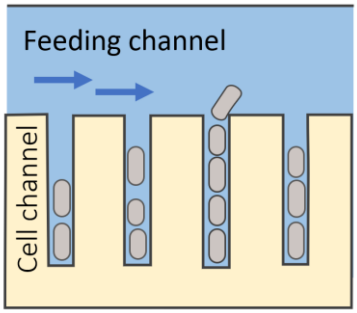

Figure. 2.4. The Mother Machine device confines bacteria into channels, where they can grow while being monitored with a microscope over long periods of time. Bacteria grow and divide inside the channels, allowing the daughter cells to move and eventually leave the cell channels. There is a continuous flow of fresh medium in the Feeding channels, so the cells remain in balanced growth throughout the experiment.

Modifications of the standard Mother Machine

Using the computer drawing package AutoCAD, I designed the microfluidic device to maximize the number of cell channels and positions captured in the 5 min intervals when the pictures of the time-lapse are taken.

As pictured in Fig.2.5, the design consists of two layers: the small features, the cell channels, and the other for big features, the feeding channels, and the wide-area for the growth medium's inlet and outlet. The first layer supports the cell channels (A in Fig. 2.5) that are 1.2 µm wide and 25 µm long. I included an extra area along the open side of the channels (B in Fig.2.5). This structure enhances the efficiency of cell load in the channels and helps the halo-effect that can appear in the intersection of the two layers does not disturb the clearness of the tracked cells in the image.

The second layer implements the features for the feeding channels (C in Fig. 2.5). These are 8.1 mm long and 150 µm wide. At the start and end of the feeding channels, there is a circular area (E and D in Fig.2.5) that serves as inlets and outlets, respectively, to connect the tubing to flow media.

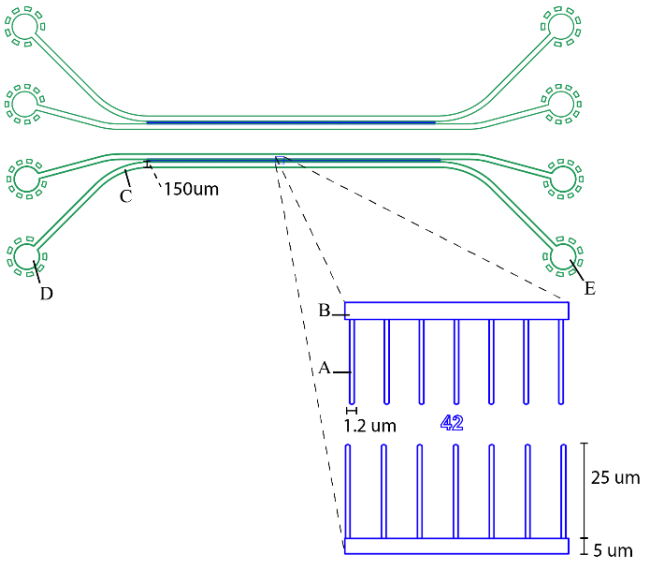

Figure 2.5. Mother Machine mold design. It consists of two layers for different UV light expositions. The first layer (blue) contains the cell channels (A) and an extra area (B) to avoid a halo effect in the microscope. The second layer (green) has four independent feeding channels (C), and the wide circular area that corresponds to the inlets and outlets for the liquid growth media.

Fabrication of the device mold using Photolithography

Using the design described above, I created a mold from which we can cast many identical devices. For constructing this mold, I used Photolithography, a technique used to pattern a 2-D design on a thin silicon substrate (a wafer).

The first step consists of coating the silicon wafer with a negative photoresist named SU-8. This photoresist is a light-sensitive viscous substrate that hardens when exposed to light and is soluble to a liquid photoresist developer. Typically, a mask is used in the SU-8 covered wafer to block light selectively with the microfluidic device pattern. Thus, only the exposed features (i.e., the channels) will be hardened while the not exposed area will be dissolved when 'washed' with the photoresist developer [14].

I modified such protocol so the device's features are exposed directly to the wafer without the need for a mask. I used a direct laser writer, which receives as an input the file with the device's design (Fig. 2.6), and with a laser, it exposes it directly to the resist-covered wafer.

To ‘print’ the mother machine design illustrated in Fig.2.6, I followed two rounds of coating, exposition, developing, and hardening, one for each layer (feeding channels and flow channels). These ‘two rounds’ are necessary because for each layer it is used a photoresist with different viscosity, leading to different heights (more viscous photoresist results in a thicker coat and therefore a larger height, in comparison with a less viscous photoresist). The protocol I followed aims to have a height of 1.2μm for the microchannels and 11μm for the feeding channels. I corroborated the sizes of the features by measuring with a stylus contact profilometer.

In Appendix 1 there is a detailed protocol with the parameters I used in the different steps in the mold fabrication.

Device casting and loading

The material I used for the microfluidic device is a solid but soft material named PDMS (Polydimethylsiloxane), which is non-toxic for bacteria, easy to work with, and transparent [59]. The following are the general steps to make the device:

1. The mold is placed in an empty Petri dish with the device’s features facing up. A mixture of liquid PDMS and a curing agent are poured.
2. The dish is placed into a vacuum chamber for a few minutes to discard possible bubbles of air due to the mixing and pouring.
3. Then it is incubated at 65°C for some hours, so the polymer becomes a solid.
4. Once solid, the device is cut and separated from the mold, and some holes are made transversally. These holes are the inlets/outlets where the growth media enters/exits.
5. The device then is Plasma bonded [3] to a slice of glass to cover the grooves and seal the actual channels where cells can be confined, and growth media can flow.

[3] Plasma bond, consists of exposing the surfaces to an oxygen plasma. This process cleanses the surfaces and modifications of the OH groups in the glass and sianol groups in the PDMS, allowing, once attached to the exposed surfaces, to create a strong covalent bond between them [60].

2.4 Fluorescence microscopy

The first step to set up a mother machine experiment is to load the bacteria into a device. I convey this by pipetting in a high-density culture of the bacteria. For the media to flow inside the feeding channels, the device's inlets need to be connected to syringes filled with media, which are controlled by pumps that maintain a constant flux of 4-5µl/min throughout the experiment. The outlets also need to be connected to a waste container.

Once the device is loaded and connected to the media, I place it on the stage of an inverted microscope and select different device regions with cells trapped in the channels. Pictures of these regions are taken automatically every 5 minutes. I set the microscope to acquire two different pictures for each position, one using phase-contrast imaging and the other with fluorescence microscopy.

The automated acquisition of the images is controlled by a Matlab script interfacing µManager [47]. This program controls the stage of the microscope (so the microscope can focus on the selected different regions), the LED light source (to excite the fluorophores), the camera, and a shutter (to acquire and control the settings of the pictures).

In Fig.2.6, I show an example of the images taken during an experiment. The phase-contrast image (black and white) and fluorescence image (yellow) are overlapped. Bacteria inside the microchannels have different levels of fluorescence since they correspond to a different ProVenus strain.

Before starting the time-lapse, I wait ~6 hours since the device is mounted in the microscope so that cells can adapt to the growth conditions (the temperature, the growth media, etc.). Typically an experiment lasts ~24 hours to have a statistically significant number of division events.

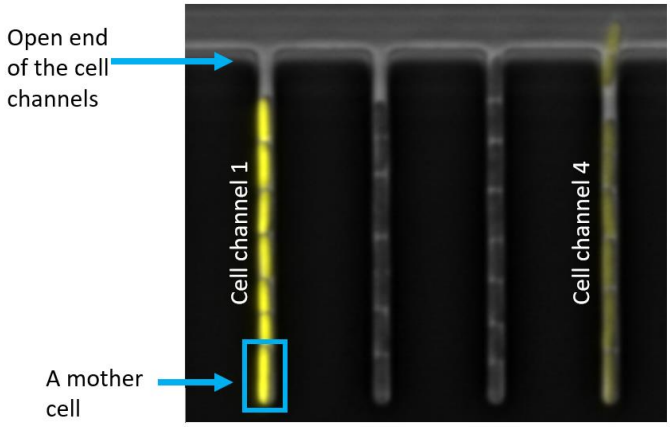

Figure 2.7. Picture of bacteria inside microchannels. The phase-contrast (in gray) and fluorescence (in yellow) images are overlapped. The different brightness from the yellow fluorescence is because there are three different strains from the ProVenus set in the channels. The 'cell channel 1' has cells from a strain with high production of Venus; the two channels in the middle do not produce it, and in 'cell channel 4', there is an intermediate level of Venus production.

2.5 Image processing

For the extraction of the data as cell size, division time, etc., from the cells in the images, I used the software Bacmman [58]. This software allows customizing a pipeline with multiple image-processing transformations to segment the cells and track their position and progeny across the different images of the time-lapse.

In Fig.2.7, I show a screenshot of the program's output, a phase-contrast image of a single cell channel over a short period of time. Segmentation and tracking are calculated from the phase-contrast images. The segmented cells are outlined in pink. The lines that connect the channels from different time points correspond to tracks of the same bacteria; each time there is a division, the color of the tracks changes.

Using an interface provided by Bacmman, I performed a manual revision and correction of mistakes in the segmentation and tracking of all the processed experiments. Then, it can be extracted the cell size, division time, total fluorescence, etc. for all detected cells over time.

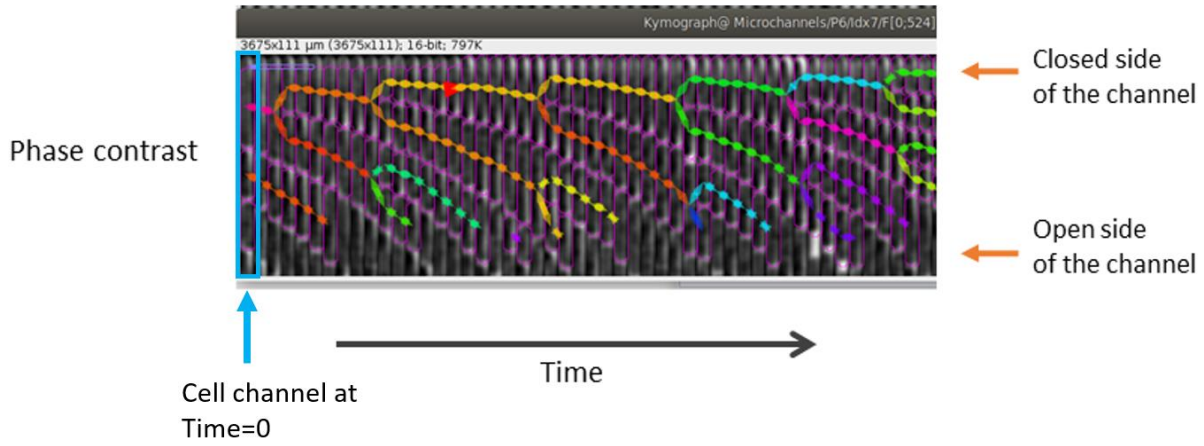

Figure 2.7. Segmentation and tracking results of cells confined on a channel. The image is a screenshot of the Bacmman software interface. It shows a single channel over a 2 hours. The time between two images (the units of the x-axis) is 5 minutes. A typical experiment from this work lasts ~24 hours. The segmented cells are shown with the pink outline. The tracking is represented with the arrows that connect the cells among images from the previous and posterior time points. Each time a division is detected, the color of the joining lines changes.

3. Cost of unnecessary proteins in the growth of *E. coli*

3.1 Background and Introduction

There are different kinds of perturbations that can change bacterial growth. For instance, by modulating the nutrient quality that feeds the cells, their size changes following an exponential dependence on the growth rate, a relation known as the "nutritional growth law" [2, 6]. Also, directly changing the configuration of the proteome by overexpressing unnecessary proteins changes the growth rate: it has been observed that as the unnecessary protein production increases, the growth rate decreases [11]. Lastly, by inducing bacteria with non-lethal doses of the antibiotic chloramphenicol, the translation of proteins is inhibited while decreasing cell growth [2, 16, 17].

In [4], Scott and Gunderson et al. performed a series of population-level experiments in *E. coli*, to characterize the growth rate and protein content of bacteria under the mentioned perturbations.

Based on their results, they presented a phenomenological model that describes and predicts the growth rate λ of a strain in different conditions, with the equation:

$$\lambda = \kappa_t(1 - \Phi)\left(\frac{\kappa_n}{\kappa_n + \kappa_t}\right) \tag{3.1}$$

where the 'nutritional effectiveness' κ_n reflects the nutrient quality of the growth media; κ_t, the 'translational effectiveness' is a parameter that correlates linearly with the speed of translational elongation; Φ is the fraction of proteins in the cells that do not change when there are nutrient variations.

Equation 3.1 is analogous to the equation that describes an electrical current in a circuit with two resistors in series. This resemblance led Scott and Gunderson et al. to make the analogy of the bacterial growth with a simple electric circuit, where λ is the current flowing through the circuit with the resistors in series with conductance κ_n and κ_t, while the total voltage is $1 - \Phi$ (see Fig.3.1).

Having a rich media is analogous to having a high conductance κ_n; inhibiting translation with a dose of chloramphenicol is like decreasing the conductance κ_t; if the cells have an expression of unnecessary proteins, an increase of the fraction of nutrient-independent proteins leads to a decrease in the voltage (1- Φ).

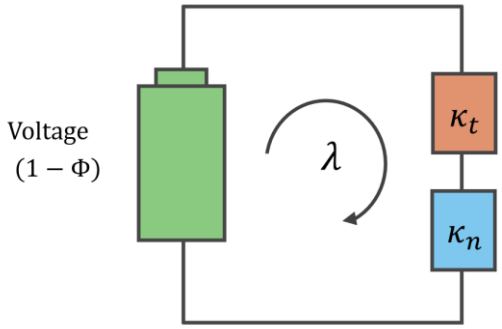

Figure 3.1. The expression of growth rate (Eq. 3.1) is identical to the equation obtained with Ohm's law for a circuit with two resistors connected in series. The voltage is equivalent to 1-Φ, and the growth rate λ to the current that passes through the resistors with conductance κ_t and κ_n. Changing to a richer nutrient is as decreasing the blue resistor with conductance κ_n, for which case the current would increase. Increasing translational inhibition with antibiotics is as increasing the brown resistor with conductance κ_t, then the current would decrease. Expressing unnecessary proteins would be as decreasing the voltage $1 - \Phi$. Then by decreasing the voltage $1 - \Phi$ while the resistances remain constant, the whole current λ decreases. Figure modified from [3].

The main observation that led Scott and Gunderson et al. to Eq.3.1 is that there are different kinds of proteins whose fraction on the proteome follow a different growth rate function. They found that by modulating the nutrient quality to increase the growth rate λ, the fraction ϕ_R of ribosome-related proteins, increases linearly as in Fig.3.2a, with the mathematical expression:

$$\phi_R = \lambda/\kappa_t + \phi_0 \tag{3.2}$$

where ϕ_0, is the vertical intercept of ribosomal proteins and κ_t is the inverse of the slope They also found that when inhibiting translation, ϕ_R follows a linearly inverse function

$$\phi_R = \phi_{max} - \lambda/\kappa_n \tag{3.3}$$

As illustrated in Fig. 3.2 with the dashed lines (each of them corresponding to different growth media). ϕ_{max} is the vertical intercept of the of ribosomal proteins and κ_n the inverse of the slope. In contrast with the ribosomal proteins, as shown in Fig.3.2b, the fraction ϕ_P of "other" constitutive proteins P decreases linearly as the nutrient-dependent growth rate λ increases. Lastly, the fraction ϕ_Q of the housekeeping proteins, Q, remains fixed, independently on the nutrient conditions. Finally, overexpressing an unnecessary protein U takes an imposed faction ϕ_U of the

proteome, therefore it is also independent of the nutrient. Note that equation 3.1 is obtained directly from Eq.3.2 and Eq. 3.3, with $\Phi = \phi_Q + \phi_U = 1 - \phi_{max} + \phi_0$.

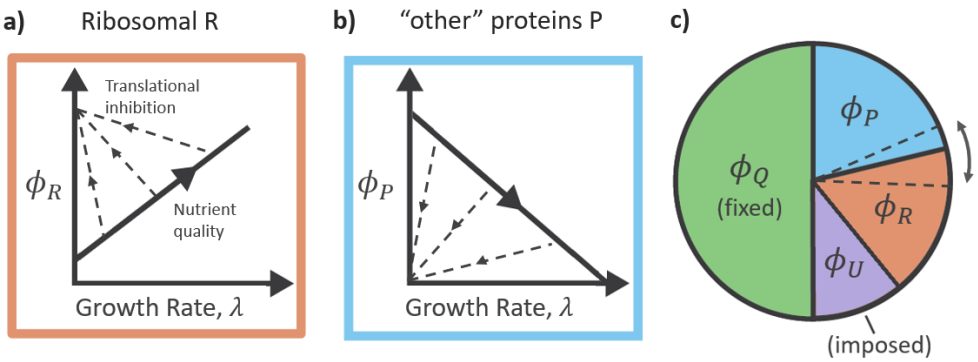

Figure 3.2. Bacterial growth laws. **a)** The fraction of ribosomal proteins ϕ_R, is a linear function of growth rate when the nutrient quality varies (dark line), while when there is translational inhibition (dashed lines), the ribosomal proteins follow a decreasing linear function of the growth rate. **b)** By contrast, the fraction of constitutive proteins ϕ_P decreases as the growth rate increases when nutrient quality becomes poorer, while (dashed lines) the growth rate decreases due to translational inhibition with antibiotics. **c)** The proteome can be divided at least into three sectors: the sector associated with housekeeping proteins Q is fixed whose fraction ϕ_Q of the total proteome, has been experimentally found to be ~0.5 for *E. coli*; the ribosomal related proteins *R* are represented by the fraction ϕ_R, and "other" constitutive proteins P by the fraction ϕ_P. If the cells have artificially imposed expression of unnecessary proteins U, that occupy a fraction ϕ_U, those decrease the size of the sectors P and R. The fraction of the ribosomal and other proteins change depending on the growth conditions, following the growth laws from (a) and (b), and $\phi_R + \phi_P + \phi_Q + \phi_U = 1$. Figure modified from [4].

Considering that the sectors R, P, Q, and U, integrate the total proteome ($\phi_Q + \phi_P + \phi_R + \phi_U = 1$), the linear relations of the proteins described in Fig.3.2 (known as growth laws) can be understood as the cell allocating resources between the protein sectors, differently depending on what is optimal for growth at a given condition.

The growth rate of a population of cells that overexpress unnecessary protein U can be written in terms of the fraction that it takes from the proteome as:

$$\lambda(U) = \lambda(U = 0) \cdot \left(1 - \frac{\phi_U}{(1 - \phi_Q)}\right) \tag{3.4}$$

Since $(1-\phi_Q)$ ~0.5 is fixed, the equation above shows that increasing the fraction of unnecessary proteins can only decrease (linearly) the growth rate.

This framework from Scott et, al., allows us to understand in terms of Ohm's law and predict the growth rate of bacteria without the need to describe their underlying molecular mechanisms.

In a further analysis, Basan et al., [11], also analyzed the cell size under the three mentioned perturbations: nutrient quality variations, translational inhibition, and unnecessary protein production.

Their experiments also were at the population level, as they consisted in obtaining the exponential bacterial growth curve in batch culture, from which subsamples were taken to measure the average cell size. They corroborate the nutritional growth law, namely, that the cell size is an exponential function of the growth rate when nutritional content is varied. Interestingly, they also found that when growing bacteria that produce unnecessary proteins, the growth rate decreases while the cell size increases, which is a different tendency than the one given by the growth law, Fig.3.3. To explain such behavior, they also propose an allocation resource model, in which there is a 'division' kind of protein *X*, for which an individual cell needs to reach a certain value since the cell is born and while it grows, in order for the cell to divide.

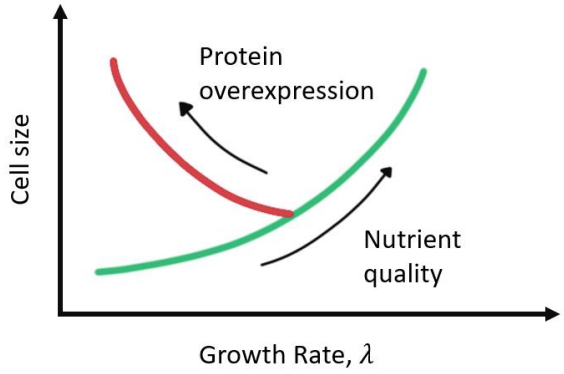

Figure 3.3. Cell size shows a different trend as a function of growth rate when it is modulated by nutrient quality (green) than when the expression of an unnecessary protein is varied (red). When the growth rate is modulated by nutrient quality, cell size follows an exponential function [2, 11] which is known as a "nutritional growth law". The relation when there is unnecessary expression is reported experimentally by Basan et al. in [11]. The image is a representation of the results from [11].

Here I present the results of a series of experiments in *E. coli* strains, which have a different level of the unnecessary fluorescent protein Venus and grown in three different growing media.

Different from what was done by Scott and Gunderson et al. and Basan's experiments, as described in chapter 2, the experiments I performed consisted of monitoring and measuring *single cells* over time, by using a microfluidic device [14]. Therefore, rather than having the populational growth rate (the inverse of the time that it takes for the population's size to double), I analyze the relation of the average of cell size, division time, etc., of individual cells.

Since the unnecessary protein that the strains produce is fluorescent, measuring their fluorescence gives a relative amount of unnecessary production.

In this chapter, first I compare my results with the population-level results from Scott and Gunderson et al. and Basan et al. and analyze if this Venus dataset follows the predictions established by their models.

3.2 Fluorescence distribution of ProVenus series

The ProVenus strains differ among them in the strength of the promoter that controls the expression of the fluorescent protein Venus. As described in chapter 2, the promoters used in such strains (listed from low to high strength) are Pro1, Pro4, Pro5, ProA, ProB, ProC, and ProD [22]. A strain with a weak promoter will produce few fluorescent proteins and therefore its fluorescence will be lower in comparison with a strain that has a stronger promoter.

Fig.3.4a shows the mean fluorescence (total fluorescence/cell size) over time of one mother cell for each strain in the ProVenus set. Those time traces were obtained by growing and monitoring bacteria in a *Mother Machine* device, fed by a constant flux of rich liquid growth medium. In Fig.3.4b is the fluorescence distribution of many cells for each ProVenus set.

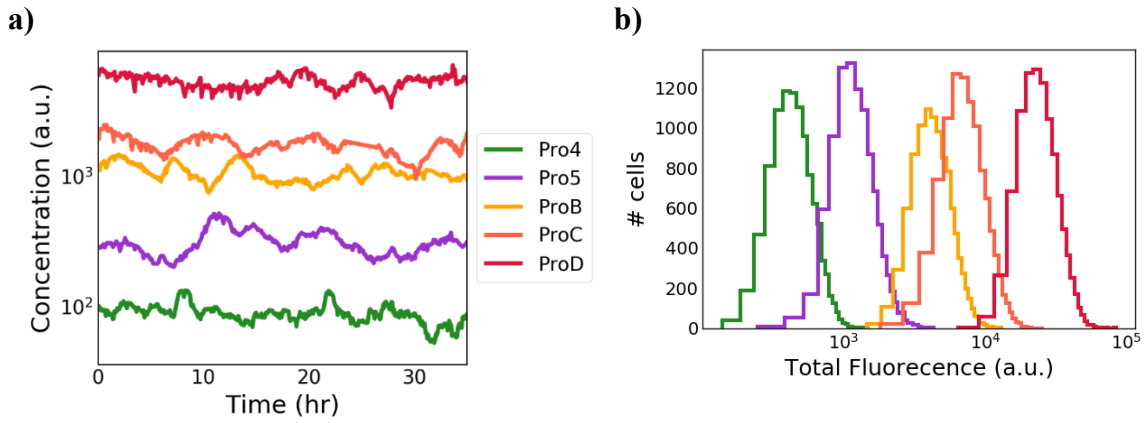

Figure 3.4 ProVenus series's Fluorescence. **a)** Time series of the mean fluorescence (total fluorescence divided by size) of a mother cell from each strain of the pProVenus set. Such strains have promoters with different strengths (Pro4, Pro5, …, ProD, [22]) controlling the expression of the fluorescent protein Venus. **b)** Distributions of fluorescence for a population of each strain. Fluorescent measurements were obtained from microfluidics (mother machine) experiments.

3.3 Effect of Venus production on Size

The size distribution of the wild type strain, when grown in the mother machine, are right-skewed as it is shown in Fig.3.5, which is a characteristic that has been widely reported [92, 9, 6, 14].

The mean size, when grown in poor medium, is 2.4 μm^2 (blue), in the intermediate medium, 2.6 μm^2(orange), and even bigger, in the rich one (red) the mean is 3.10 μm^2. Therefore, using the mean of the distributions as the measurement representative for the population agrees with the second growth law, which says that for many microorganisms, on average, the size increases when increased the nutritional content of the growth media [2].

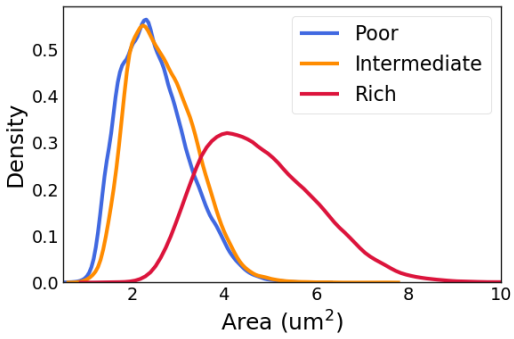

Figure 3.5. Distribution of size of the wild type bacteria (no fluorescent protein production) when grown in different growth media with different nutritional content: poor medium (blue), intermediate (orange), and rich (red). Although there is a big overlap in the distributions, their mean values do show the increment in size, being $\langle S \rangle_{Poor} = 2.4\ um^2$, $\langle S \rangle_{Interm} = 2.6\ um^2$ and $\langle S \rangle_{Rich} = 3.10\ \mu m^2$.

Besides the growth media, the overproduction of a protein also induces a change in the cell size [11]. Accordingly, Fig.3.6 shows the cell size distribution (using kernel density plots) of the ProVenus strains in different media. In the poor and intermediate media, there is a clear shift of the size distribution for the strains that produce more Venus, being the difference between wild type (WT) and the ProD (the strain that produces the most Venus, black line), $\Delta S(D, WT)_{Poor} = 45\%$. For the intermediate, the difference is $\Delta S(D, WT)_{Interm} = 40\%$. In contrast, in the case of cells growing in rich medium, the size of the population is very small among the series, being the biggest difference $\Delta S(D, WT)_{Rich} = 2\%$. The difference in size between wild type and ProD is not conserved between different growth media. On the right side of Fig.3.6 it is shown the mean and variance of the ProVenus strains in the three different media, poor (blue), intermediate (orange), and rich (red).

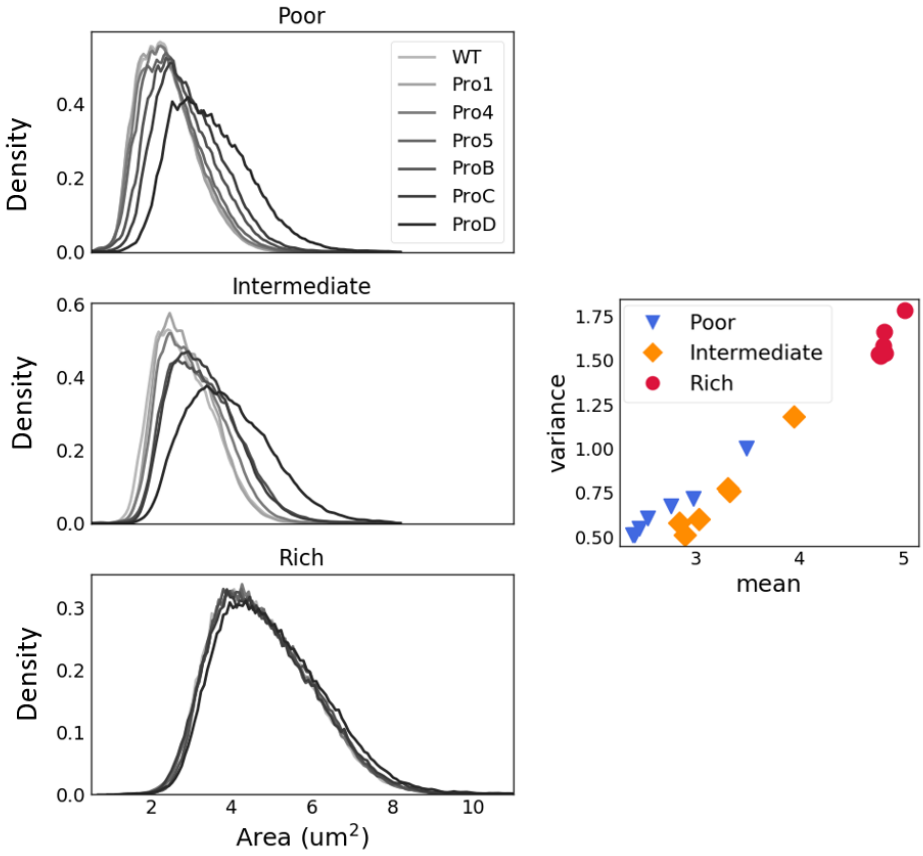

Figure 3.6. Left: Size of ProVenus strains grown in three different media, poor (top), intermediate, (middle), and rich (bottom). The color code corresponds to the amount of the unnecessary protein Venus produced on each stain: light grey corresponds to the wild type strain, that does not produce Venus, and the darkest to the strain that has the strongest promoter for Venus expression, ProD. For the three plots, kernel density plots are shown rather than the histograms of the data, to have a better visualization of the differences among strains. **Right:** Mean and variance of the size distribution of ProVenus strains growing in the three different media, poor (blue triangles): intermediate (orange diamonds), and rich (red circles).

Fig 3.6 and Fig 3.7, show the size distributions of the cells at all time points; these distributions include the measurements in size of the cells regardless of their stage in the division cycle: whether they just divided, about to divide or anytime in between. To verify if this inclusion of all time points could mask a possible difference among the ProVenus strains in the rich media, I calculated the difference of the size at birth S_b, and size just before division S_{div}, between WT and the strain with ProD. These are, respectively: $\Delta S_b(D, WT)_{Rich} = 5.3\%$ and $\Delta S_{div}(D, WT)_{Rich} = 5.4\%$. Although these differences are higher than when taking all the data points (which is 2%), it is fair

to say that the production of the Venus protein does not induce much change in the size of the cells when grown in rich medium.

To characterize the effect in size due to Venus production I will first analyze some quantities related to size. To know what is a relevant measure for the size to reflects changes due to the protein production on a population of bacteria, I analyzed the relationship between cell size, cell size at birth S_b, at division S_{div} and the average size $\bar{S}$ (see diagram in Fig.3.7a), among strains in different media. Fig.3.7b shows the relation between the average cell size when cells are born $\langle S_b \rangle$ and the average when cells are about to divide $\langle S_{div} \rangle$. It can be seen that they follow a linear relationship and not surprisingly, with a slope that is close to 2, confirming that on average cells divide approximately in half.

I also calculate the average size throughout the division time, $\bar{S}$, and then take the average over the population, $\langle \bar{S} \rangle$. For the ProVenus strains in the three different media, the population average of the mean size $\langle \bar{S} \rangle$ is a linear function of the size at birth $\langle S_b \rangle$ with a slope of ~1/ln(2), Fig.3.7c. Considering that the cell size increases exponentially, $S(t) = S_b 2^{\alpha t}$, then the average over the doubling time is:

$$\bar{S} = \frac{1}{T_d}\int_0^{Td} S(t)dt = \frac{S_b}{T_d\, \alpha \ln(2)}[2^{\alpha T_d} - 1]. \qquad (3.5)$$

Then, since the average division time and elongation rate of a population is $\langle \alpha \rangle \sim \langle 1/T_d \rangle$, [6, 23], then it is fulfilled the relation $\langle \bar{S} \rangle = \langle S_b \rangle / \ln 2$ from Fig.3.7c

For a cell on a specific time t, its total fluorescence $F(t)$ is a proxy for the number of Venus proteins at that time. To quantify the fluorescence on a single cell, it could be considered the average over time, since the cell is born until its division. Nonetheless, similar to the size, the average over the population of the average fluorescence over division time is approximately $\langle \bar{F} \rangle = \ln(2) * \langle F_b \rangle$, and the average of fluorescence at birth and division are proportional such that $\langle F_{div} \rangle = 2 * \langle F_b \rangle$.

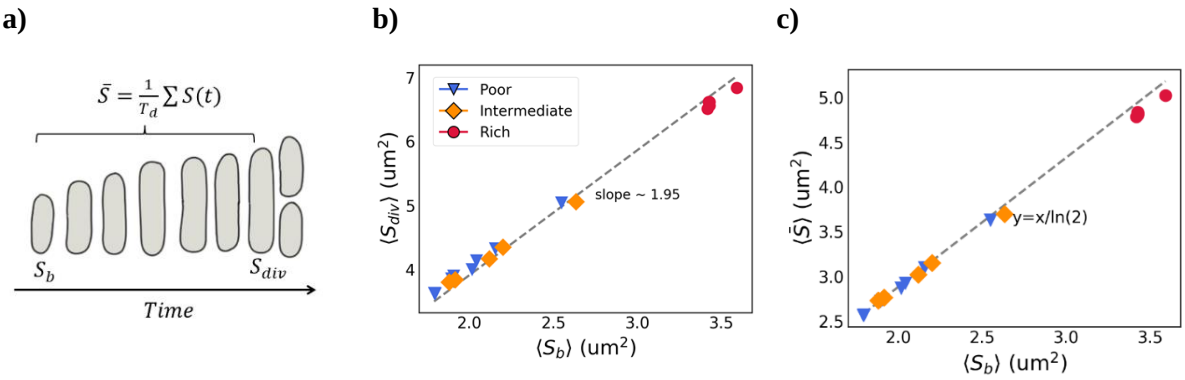

Figure 3.7. Average Size of ProVenus strains. **(a)** Illustration of a growing bacteria with size at birth S_b, and size just before division S_{div}, at time point T_d. $\bar{S}$ is the average size of the cell, from its birth until its division. **(b)** Average size before division $\langle S_{div} \rangle$ as a function of the size at birth $\langle S_b \rangle$, of a population of each ProVenus strain on the three different growth media: poor (blue triangles), intermediate (orange diamonds), and rich (red circles). The dashed line shows the best linear fit to the data, which gives a slope of ~1.95. **(c)** Population average of the mean size of cells $\bar{S}$ (mean size of a cell from birth until division) as a function of the average size at birth $\langle S_b \rangle$. The color code is the same as in **(b)** and the dashed line shows the linear function with slope 1/ln(2).

Fig. 3.8 reports the average size at birth $\langle S_b \rangle$ relative to the size of the strain with no fluorescence. as a function of the fluorescence at birth $\langle F_b \rangle$. The relative difference of the size is computed by using:

$$\text{R.D.}\left(X^i, X^{WT}\right) = \frac{X^i - X^{wt}}{X^{WT}} \tag{3.6}$$

where X^i corresponds to the average of a variable X in a population of strain i (one of the ProVenus strains), and X^{WT} is the average of the same variable for the wild type strain. The size of the cells growing in poor and intermediate media are bigger as the fluorescence gets higher, while in rich media, does not seems to be any appreciable change on size except by the strongest promoter (in red—see the data point at the extreme right of the plot, corresponding to the highest fluorescence).

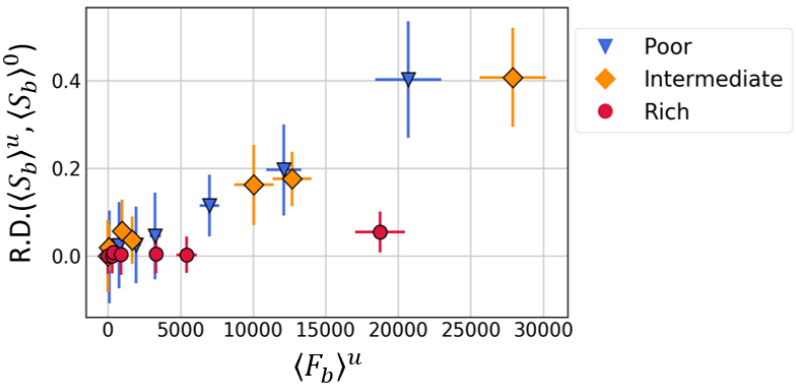

Figure 3.8. Relative difference of the mean size $\langle S_b \rangle^u$ of each ProVenus strain u respect to the mean size at of the strain with no Venus production $\langle S_b \rangle^0$ as a function of the mean fluorescence at birth $\langle F_b \rangle^u$. The different style of markers corresponds to each growth media, blue for poor, orange for intermediate and red for rich media. The relative difference for each strain in a given medium is calculated respective to the wild type strain growth in the same growth medium. The bars show the standard deviation of the mother cells for each strain and growth media condition.

This result qualitatively agrees with what Basan et al. observed in [11]: the average cell size in a population increases when it is forced to overproduce unnecessary protein and the effect on the bacteria at a given load of unnecessary protein is different depending on the growing conditions.

The effect on cell size due to the production of an amount U (or fluorescence F) of Venus proteins, (relative to the case of no Venus production, Eq.3.4), is higher in the poorest media than in the rich one, as seen in Fig.3.8.

This result could be understood by considering that, for an originally small cell with mass m_c (bacteria in poor media), an extra mass, Δm_u added to it (the mass corresponding to unnecessary production), will comprise a higher fraction of the original mass m_c than when the original mass is bigger, (which is the case of cells grown in rich medium). This simplistic view is suggested by considering, as Scott and Gunderson et al. did, that the production of unnecessary protein increases the fixed fraction of proteome, but not the relative fractions of other sectors.

3.4 Effect of Venus production on Division Time

Fig.3.9 shows the distribution of the division time, T_{div}, for the wild type strain, grown in the three different growth media. The mean division time in the rich medium is $\langle T_{div} \rangle_{Rich}$=41min. For the other two media, their mean value, shown in Fig.3.9b, are $\langle T_{div} \rangle_{Interm.}$=85min, and $\langle T_{div} \rangle_{Poor}$=92.5min, which suggest the cells divide faster in the intermediate medium than in the poor one. But, in contrast with the mean, the mode of the distributions in intermediate medium is 75min and 65min for the poor. Since the mean and mode of the size distribution are smaller for the poor medium, followed by the intermediate and then by the rich medium (Fig.3.9), according to the growth law, the same trend should be followed by the average elongation rate (the inverse of the division time). Remember that the growth law states that the cell size is an exponential function of the growth rate when the latter is modulated with the nutritional content [2, 6]. Considering this law, since the mean (not the mode) of division time, is the function that meets the expected relationship with the size for the different growth media, I would keep the mean as the measurement to quantify and describe different variables of the populations.

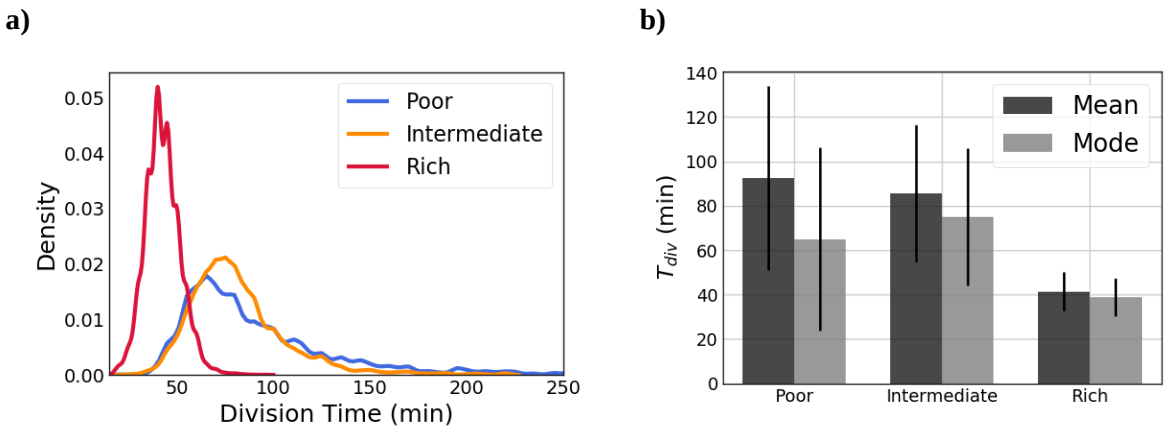

Figure 3.9. Division time, T_{div}, of WT in three different growth media. (a) Division time distributions of the WT strain (strain with no Venus production), grown in various growth media: poor (blue), intermediate (orange), and rich (red). (b) Mean (dark gray), mode (light gray) and standard deviation (error bar), of the T_{div} distributions from (a).

The differences in the distribution of the division time T_{div} among the different ProVenus are not as drastic as in the distributions of size, which can be noted in Fig.3.10. In Fig 3.10 top, it is shown that in intermediate medium the distribution for all ProVenus strains and wild type (where the

lightest gray corresponds to no Venus production and the darkest the maximum production) are similar among them. The top right panel of this figure shows the corresponding mean and standard deviation for each strain, relative to the wild type.

In the rich media, Fig.3.10 bottom, the mean value of the division time distributions increases as the expression of Venus becomes higher. Both the mean and standard deviation are higher for strains with a higher Venus production. This in concordance with Scott and Gunderson et al. observations [12]: bacteria overexpressing unnecessary protein have a lower growth rate than when there is no overexpression.

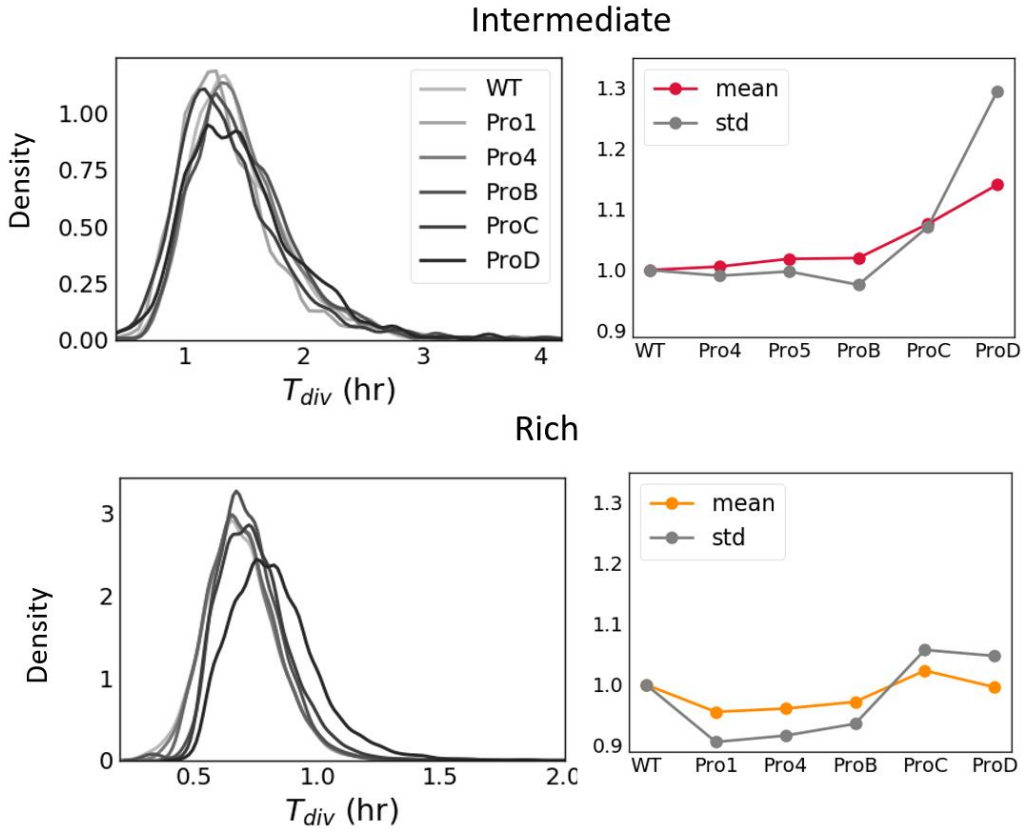

Figure 3.10. Left: Distribution of the division time T_{div} of the ProVenus and WT strains grown in the intermediate and rich media. Right: corresponding mean and standard deviation of the division time distributions for all the strains. Values are divided by the respective mean and standard deviation of the WT strain.

The division time distributions of cells growing in poor medium, Fig. 3.11 show a slight decrease in the mean and standard deviation as the production of Venus becomes higher, but the mode of the distribution is similar among the strains.

The decrease in division time when unnecessary proteins are being produced has not yet reported before, and it goes in contradiction with what is established from some cell size and growth models and reported from experiments [19,12, 21,11, 20]. Although in the following chapters this relationship is be persistent, further analysis and experiments need to be done to demonstrate it true and if so, understand the mechanism behind it.

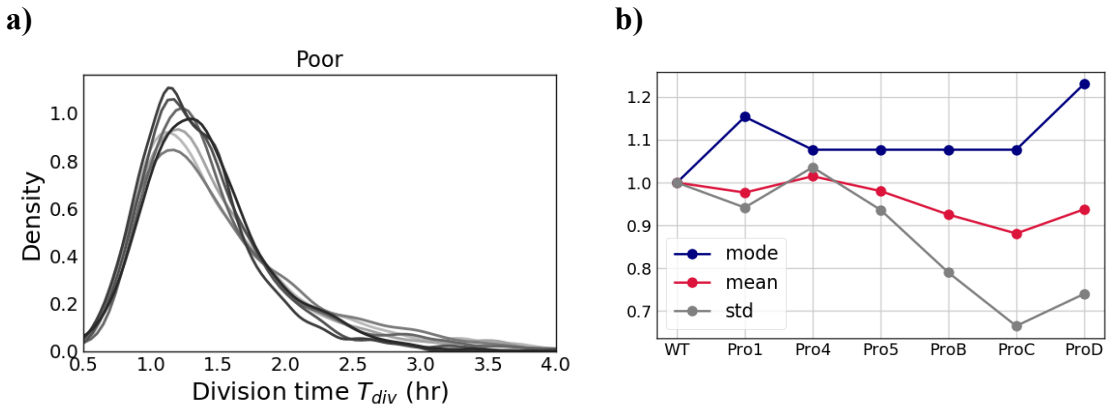

Figure 3.11 Division time of the ProVenus strains when grown in a poor medium. **a)** The shape of the distributions of T_{div} changes for the different strains. As the promoter becomes stronger, the mode of the distributions slightly increases (blue circles, in (b)), while the standard deviation and the mean decrease (red and gray circles); the three measurements are relative to WT's respective values. Missing describing **b).**

On Fig.3.12 it is shown the mean division time of the ProVenus strains as a function of their fluorescence at birth $\langle F_b \rangle$, when grown with the three different growth media. As before, this figure shows the division time relative to the wild type strain (Eq. 3.4), to make it easier to compare the increment among the strains and growth media.

Cells growing in rich media (red circles, Fig.3.12) divide slower as a function of fluorescence; the strain with the highest fluorescence has an average division time approximately 16% larger than wild type. The bars correspond to the standard deviation of T_{div} for different mother cells. For the intermediate medium (orange diamonds) the division time of the ProVenus strains slightly increases compared with the wild type, although the variation among mother cells is bigger as the size of the bars suggests. For the poor media (blue triangles) the mean T_{div} describes a tendency of the population dividing faster as the fluorescence increases. It is worth noticing that there is a higher variation in T_{div} in poor and intermediate media than in the case of the rich media. Given

that the division time distributions have long tails (Fig.3.11), more data might be necessary to accurately calculate the mean values $\langle T_{div} \rangle$. Further analysis needs to be done to give a better measurement of the division time that characterizes a population of individual cells in poor media, maybe by considering more than the first moment of the distribution.

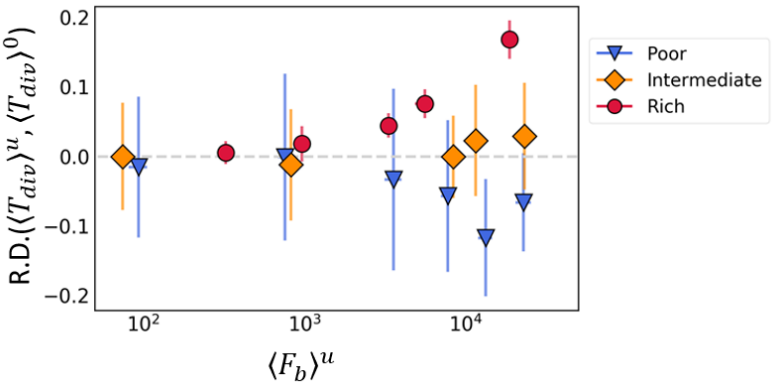

Figure 3.12. Relative difference of the mean division time $\langle T_{div} \rangle^u$ for each ProVenus strain u, relative to the mean division time of the wild-type strain (strain with no fluorescent protein expression) $\langle T_{div} \rangle^0$ (Eq.3.6), as a function of the mean fluorescence at birth $\langle F_b \rangle^u$, when cells are grown in different media. The bars show the standard deviation of the average division time of the mother cells, for each strain and growth media condition.

3.5 Effect of Venus production on Elongation Rate

Another relevant quantity that describes the physiology of the cells is the elongation rate: the rate at which a cell changes its size. If an individual cell i that grows exponentially as $S^i(t) = S_b^i 2^{\alpha^i t}$, then α^i, which is its instantaneous elongation rate, can be calculated from the time traces of the bacteria, taking its derivative:

$$\frac{1}{S^u}\frac{\mathrm{d}S^u}{\mathrm{d}t} = \ln(2) * \alpha_u \tag{3.7}$$

As mentioned before, the inverse of the average elongation rate, $1/\langle \alpha^u \rangle$, of a population should be equal to the average division time of a population $\langle T_{div}^u \rangle$, which is true for the ProVenus strains in the three different media, as seen in Fig.3.13. A linear fit to these averages was applied and the resulting slope is ~1.03.

It is important to note that what I obtain from my experiments is the elongation rate α of *individual cells* (calculated from Eq.3.5), while in the populational experiments the growth rate, λ is the rate at which *the population* doubles its size. In other words, from one populational experiment, it is obtained one measurement of λ and from a single-cell experiment, what is obtained is a distribution of the elongation rate α. Nonetheless, it has been observed that λ and the population average $\langle\alpha\rangle$ obey the relationship [6]:

$$\langle 1/\mathrm{S}\ \mathrm{dS/dt}\rangle = \langle\alpha\rangle * \ln(2) = \langle 1/T_{div}\rangle * \ln(2) = \lambda \qquad (3.8)$$

Then we can investigate the growth rate relations known from previous population-level studies with the average of the elongation rate of a population of single cell, given that $\langle\alpha\rangle = \lambda/\ln(2)$.

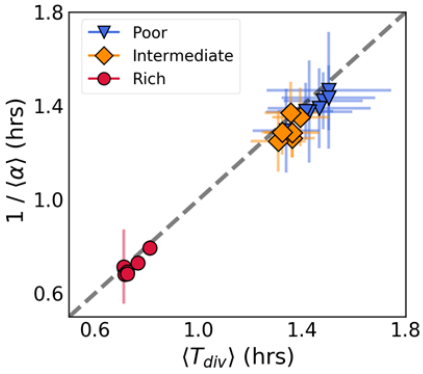

Figure 3.13. Comparison of the mean division time $\langle T_{div}\rangle$ and the inverse of the elongation rate, $1/\langle\alpha\rangle$, for the ProVenus series in poor, intermediate, and rich media. The bars show the standard deviation of average $\langle T_{div}\rangle$ and $1/\langle\alpha\rangle$ of various mother cells, for each strain and growth media. The dashed line represents the identity function. The best fit for these data with a linear function gives a slope of ~1.03.

To compare my result with the theory developed by Scott and Gunderson et al., Eq.3.4, it is important to notice that the fluorescence F that I measured experimentally comes only from the expression of the Venus protein. It is then expected for F to be proportional to the number of unnecessary proteins U (Venus) produced in the cell. By contrast, from Eq. 3.4 what is obtained is the growth rate as a function of the fraction of the unnecessary proteins from the proteome ϕ_U. Considering the cell size to be proportional to the total amount of proteins in the cell (over two-thirds of dry-mass in different conditions [11]), then $\phi_U \sim U/size$, where U is the number of unnecessary proteins, and $\phi_U \sim F/size$. The size here is given in a number of pixels from our

image and has no physical dimension; similarly, the intensity F of the fluorescent signal is presented as a dimensionless quantity.

Then, according to Eq.3.4 and the above considerations, the relative difference of growth rate $\lambda^U = \lambda(U)$ of a strain that produces U unnecessary proteins, relative to the growth rate λ^0 of a strain with no unnecessary production, R.D. (λ^U, λ^0) is:

$$R.D.(\lambda^U, \lambda^0) = \frac{\lambda^U - \lambda^0}{\lambda^0} = -\frac{\phi_U}{1-\phi_Q} \sim -\frac{F}{size} \quad . \tag{3.7}$$

The relation from above holds for the mean elongation rate as well, $R.D.(\langle\alpha\rangle^u, \langle\alpha\rangle^0) = \langle F\rangle^u/\ln(2)$, where u is an index to indicate the different ProVenus strains with different amount of Venus expression, $u = \{Pro1, \ldots, ProD\}$, and $\langle\alpha\rangle^0$ is the average elongation rate for the strain with no Venus production.

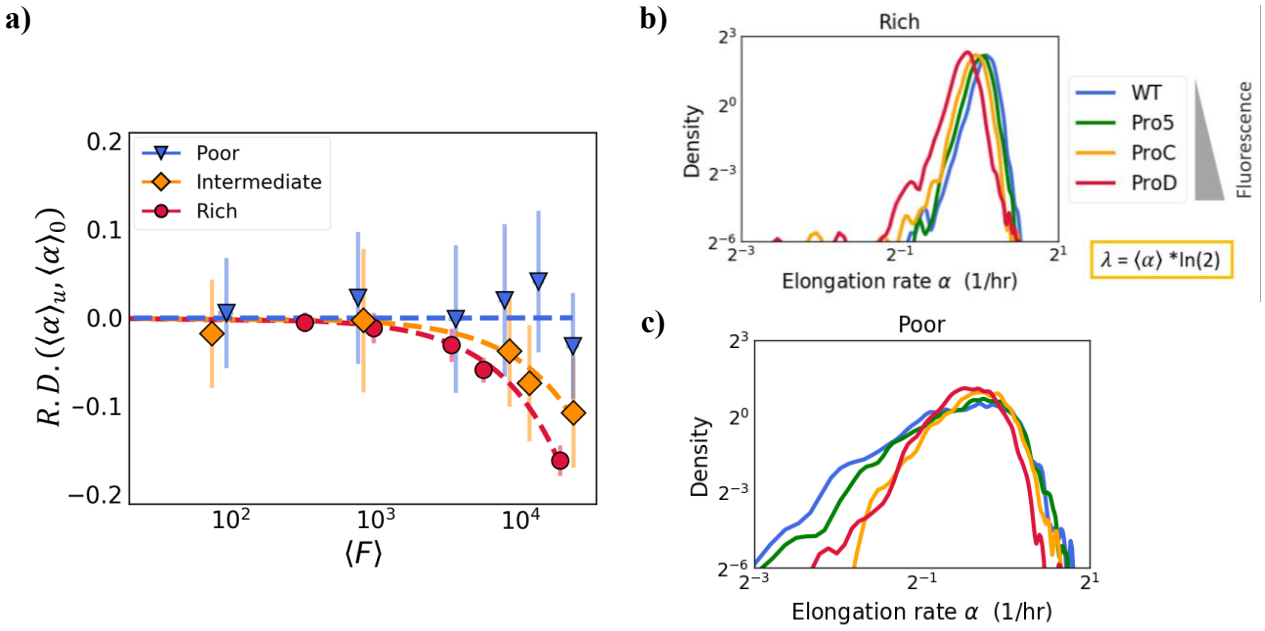

Figure 3.14. a) Relative difference, of the mean elongation rate $\langle\alpha\rangle^u$ of the ProVenus strains u that produce the unnecessary fluorescent protein Venus, with respect to the mean elongation rate $\langle\alpha\rangle^0$ WT strain (without Venus production) as a function of the fluorescence mean $\langle F\rangle^u$. The color code corresponds to different growth media in which the strains were grown. The elongation rate was calculated by taking the mean of the elongation rate α^i, obtained by fitting the size of each individual cell i to $S^i(t)=S^i_{birth}2^{\alpha^i t}$. Then for the population u of cells, $\lambda^u = \ln(2)\,\langle\alpha^i\rangle^u$, the bracket means the population average. The bars show the standard error for each strain and the dotted line is the best linear fit to the data for each growth media. **b)** Kernel density estimation for 4 of the Venus set of strains; in order of fluorescence WT (no fluorescence), Pro5, ProC, and ProD, grown in the rich media. **c)** Density for the same strains as in (b) but grown in poor media. For each

strain, the elongation rate was calculated from 1500 individual cells. For each strain in rich medium, it was analyzed ~3000 individual cells and ~1500 for each strain in intermediate and poor media.

Fig.3.14 shows the difference of the average elongation rate for each Venus strain, relative to the strain with no Venus $R.D.(\langle\alpha\rangle_u, \langle\alpha\rangle_0)$ for the Venus set in three different growth media, Rich, Intermediate and Poor, as a function of the average fluorescence. The markers show the mean values for each strain, the error bars correspond to the standard deviation from single cell measurements, and the dashed lines, the best fit for the data-points of the strains in each media. The rich and intermediate media curves show a decrease of the elongation rate as the fluorescence gets larger, as expected from Eq.3.6. However, in poor media the noise is too large to draw any conclusions. Nonetheless, the mean value of the elongation rate is not enough to understand the noise emerging poor medium case. In Fig.3.14b and c, I show the distribution of elongation rate α for 4 strains, WT, that do not produce any Venus, and Pro5, ProC, ProD, in the Rich and Poor media. In Rich media, as the fluorescence is larger, the elongation rate distributions shift to the left, so the mean of α clearly decreases, relatively to that of WT ($\langle\alpha\rangle_0$).

In Poor medium, the peaks of the distributions are close and have a long-left tail that seems to decrease as the fluorescence increases. Because of this, the calculation of the mean, and therefore the relative difference, has high noise. But considering the shape of the distribution, not only the mean value of the elongation rate might be necessary to understand the noise emerging from the poorest media.

Considering that the nutritional growth law, which establishes that cells are bigger when grown in rich media than in a poor one, $size^{Rich} > size^{Poor}$, then the absolute relative difference of the growth rate (Eq.3.7) should be larger for cells growing in poor than in rich media:

$$\left|\text{R. D.}\left(\lambda^{U}_{Rich}, \lambda^{0}_{Rich}\right)\right| < \left|\text{R. D.}\left(\lambda^{U}_{Poor}, \lambda^{0}_{Poor}\right)\right| \tag{3.9}$$

The same relation should hold in the case of the relative elongation rate. Nevertheless, data from Fig.3.14a suggest it might not be the case since the absolute difference is larger in the rich medium than in the poor one for the higher values or $\langle F \rangle$.

One possible reason for these observed discrepancies between model predictions and the experimental results can be explained as follows:

I assumed the fluorescence to be proportional to the number of proteins U:

$$F = a * U = a * \phi_U * size\,, \tag{3.10}$$

with a being a proportionality factor that relates the number of fluorescent proteins and the fluorescence they produce. If a depends on the quality of the growth media, then the X-axis in Fig.3.14a needs to be adjusted to represent correctly Eq.3.9. To prove or disprove this point, it would be necessary to make calibration experiments of the Fluorescence produced by a number (or fraction) of Venus proteins. However, if a is the same for all media and Fig.3.14 is correct, then the deviation observed in this figure cannot be explained by considering that the unnecessary protein only changes the "fixed" sector of the proteome (the "voltage" in the Ohm's law analogy) but also affects the "capacitance" of the resistors.

3.6 Nutritional growth law and unnecessary expression

As mentioned in this chapter's introduction, the size of bacteria has an exponential dependence on the nutrient-imposed growth rate, a relation known as the 'nutritional growth law'.

In Fig.3.15a, I show with big markers the average size at birth, S_{birth}, as a function of the average elongation rate α, for the WT strain (that does not produce any fluorescent protein) growing in the three different growth media. The small circles are averages of individual lineages, while the dashed line is the best exponential fit for this relation. As already shown by Taheri-Araghi et al. [6], the average size as a function of the average elongation rate, measured for individual cells with Eq.3.7, reproduces the nutrient-imposed curve of size and growth rate.

As the level of unnecessary production increases, the relation between size and growth rate separates from the nutrient-quality curve, as seen in Fig.3.15b, as previously reported by Basan et al. for population-level experiments [11]. While in the three different growth media the cell size increases with Venus production (as indicated by the brown arrow), the elongation rate shows a

tendency to decrease in the rich and intermediate media, while in the poor one it is not conclusive. These observations are the same as in sections 3.6 and 3.5, where the size and the elongation rate were analyzed as functions of the fluorescence.

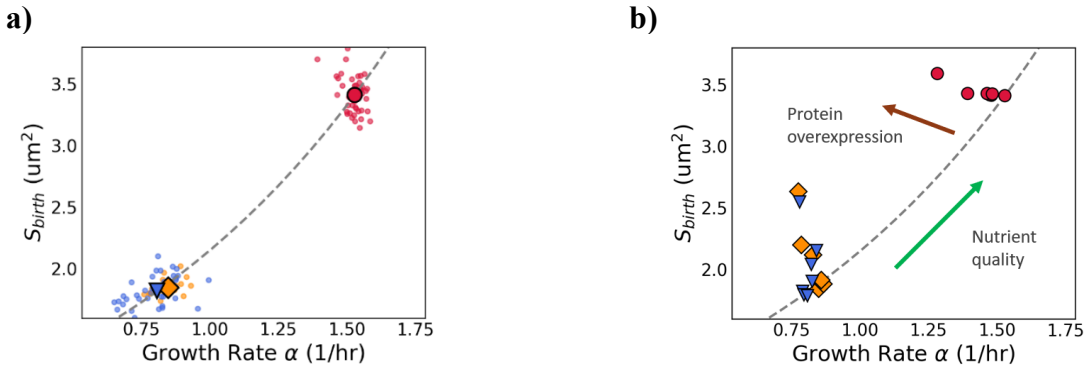

Figure 3.15. Average size at birth, S_{birth}, as a function of the average growth (elongation) rate α. **a)** The big markers correspond to the averages of all single cells of the strain with no Venus, grown in the three different growth media. The smaller circles are averages of different lineages in the population, red for the rich media, orange for the intermediate and blue for the poor. The dashed line is the best exponential fit. **b)** Average size vs average elongation rate for all the ProVenus strains in the three different growth media. As the strains produce more Venus, the averages separate from the dashed line, which is the same as in (a). The green arrow indicates the curve of nutrient modulated growth, and the brown arrow the direction of the curves with a higher level of production (or fluorescence).

3.7 Discussion

The relations among different physiological parameters when considering the averages of the single-cell measurements of the ProVenus strains coincide with most of the relations known from populational/bulk experiments.

The negative correlation between protein overexpression and growth rate follows a linear negative function [4]. From the three different growth media in which the ProVenus series were grown, in two of them (rich and intermediate), such a linear negative relationship was observed. In the other growth medium used (poor), there is a slight positive tendency of increased mean elongation rate for the strains that produce the most unnecessary protein, but because of the high variation in elongation rate in this specific media, there is still further acquisition of data and analysis to be performed before making any conclusion about this contra-intuitive observation. The effect that unnecessary protein production has on the elongation rate, as defined with the relative difference

with no-unnecessary production, is larger for rich media than for other media. This result does not agree with the Scott and Gunderson et al. model. To understand the reason for this discrepancy it would be necessary to make “calibration experiments”, to actually map the fraction of the Venus content in the strains and their fluorescence, on the different growth media. This would help to prove/disprove the theory or identify if there are missing considerations in the treatment of the fluorescent data.

In agreement with Basan et al, the average cell size increases when there is unnecessary overproduction, and since under this same perturbation the elongation rate decreases, the size as a function of elongation rate shows a negative correlation, displaying a different tendency as the one predicted by the nutrient-limiting growth relation (the nutritional growth curve).

In summary, here I presented an analysis for the growth of *E. coli* under various conditions: different growth media and levels of overexpression of unnecessary protein. This analysis mostly consisted of relating the average values of the growth variables, which confirm the results already obtained at the population level and raise new questions for further analysis. Given the experimental setup I used in this dataset, I can also analyze how these variables relate to a single-cell level. Such an analysis is presented in the following chapter.

4. Correlation between cell growth and unnecessary protein synthesis at single-cell level

4.1 Introduction

A population of bacteria has a stable and reproducible average cell size, division time, or proteome content when grown under a steady condition. Some of these physiological parameters can even be predicted using the so-called growth laws, as described in Chapter 3 [2, 4, 8]. However, the mean population behavior of bacteria does not give enough information to understand the process by which individual cells control their growth.

Over the years, different cell size control models have been proposed [8], which are briefly described in Fig.4.1. The 'sizer' model states that cells monitor their size and divide once they reach a target size. The 'timer' model claims that cells divide after a fixed time since birth. Finally, the 'adder' control model states that there is a continuous expansion of length until it has added a fixed length Δ regardless of birth size.

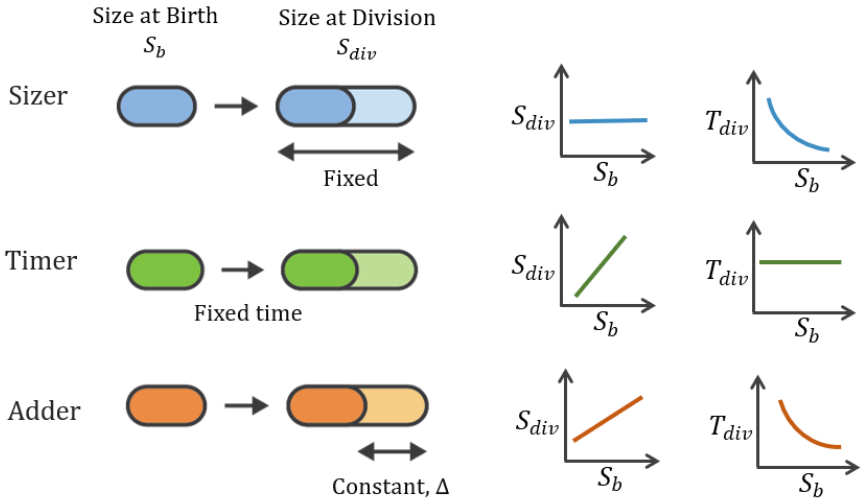

Figure 4.1. Bacterial size control models. In the 'sizer' model (top), cells divide once they reached a fixed size S_{div}, independent of the size at birth S_b. In the 'timer' model (middle), the size depends solely on the age of the cells and divide after a fixed duration since birth, such that the division time T_{div} is constant. In the 'adder' model (bottom), there is a constant mass (or content) Δ that cells need to reach to triggers its division. The relations between the variations in size at division S_{div} and division time T_{div} as functions of variations of size at birth S_b for a population of bacteria that follows each model are shown on the right side. Those relations help determine which model is that a certain bacteria or strain follows. Figure modified from [8].

The specific relationships between size at birth, size at division, and division time are distinct for these different models and can be used to discriminate between the three different hypotheses (see illustration in Fig.4.1). It has been observed that different species of bacteria follow one or a combination of these mechanisms [6, 7, 9, 31-37]; for *E. coli*, it has been reported by several single-cell studies that the model that best describes its growth is the adder model [5, 6, 7, 9, 33].

Specifically, Taheri-Aragui et al., using the mother machine, monitored *E. coli* cells and found that the adder model relations are verified when bacteria grow in media with different nutrient quality. The same study also found deviations in the nutrient growth law at the single-cell level [6, 23].

As shown in Chapter 3, at the population level, overproducing unnecessary proteins changes the rate of growth. Therefore, one could ask: what is the effect on growth at the individual cell level when the cells overproduce unnecessary proteins? Are the relationships described by the Adder model conserved at the individual cell level?

Presumably, the only systematic analysis of the effect on growth when cells produce different levels of unnecessary proteins, including cell size measurements, is the one from Basan et al. [11]. Their main observation (presented in Chapter 3, Fig.3.3) is that when there is an expression of unnecessary proteins, the mean cell size of a population increases while the growth rate decreases. Such relation goes in the 'opposite direction' than the nutrient growth law.

Their experiments consisted of growing bacteria in bulk, where the individual behavior of cells cannot be distinguished from each other. In other words, they did not have access to single-cell parameters, such as the distributions of size at birth and division, elongation rate, and division time of their populations.

Nevertheless, they presented a possible mechanism for individual cells to explain their results.

This hypothesis is that there is a 'division protein' X, which a cell synthesizes and accumulates over its cell cycle, and once it reaches a threshold X_{div} it triggers cell division, as illustrated in Fig.4.2. In their model, as in Scott and Gunderson et al.'s model (Fig.3.2), the cell allocates resources among the different sectors of proteins: housekeeping Q, ribosome-associated R, and 'others' P, including the X sector. The fraction of each sector depends on nutrient quality.

Then, if the cell is forced to overproduce unnecessary proteins U, the resources are split to synthesize such U proteins, which takes away resources otherwise destined to the other sectors. Under this condition, the cell needs a longer time for X to reach the threshold X_{div}, making division time longer than if the cell did not have to produce U.

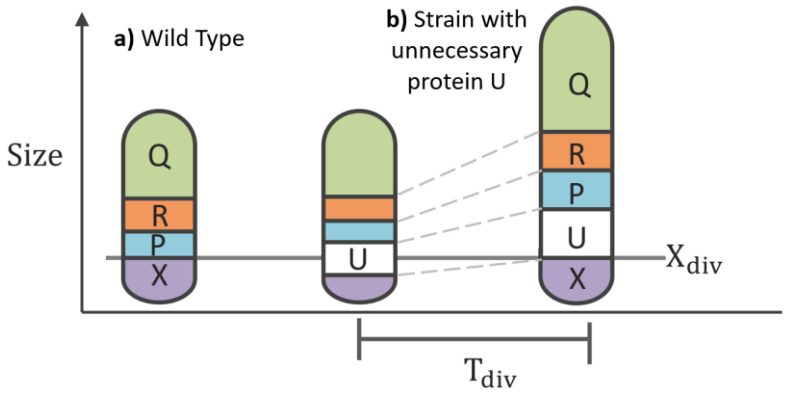

Figure 4.2 Diagram of Basan et al. model [11]. There is a kind of protein X, 'division protein', which the cell needs to accumulate and reach up to a threshold X_{div} to trigger division. In **a)** a wild type strain is represented with its different protein sectors, as in Scott and Gunderson et al. (see chapter 3): housekeeping Q, ribosome-affiliated proteins R, constitutive P, plus the division proteins 'X'. According to experimental results, the fraction of Q proteins is fixed. **b)** If a cell that produces unnecessary protein U is born with the same cell size as (a), the fraction of the protein sectors R, P, and X are compressed, since the fraction of Q is fixed and of U is imposed. Therefore, since the initial amount of X is less, it will take the cell a longer time T_{div} to reach the threshold X_{div} of X than if there was no U protein.

In this section, I present the analysis of a new single-cell dataset for different strains that overproduce the unnecessary protein Venus grown in different growth media. With this dataset, I check the validity of Basan et al.'s hypothesis by relating the size, and fluorescence at birth and division, with the division time. Also, I explore the extension of the adder model for the strains that have different levels of unnecessary proteins.

Overall, I analyze the deviations from the relations at the population level presented in chapter 3 and identify mathematical relations that describe the effect on the protein production on the different growth variables at the single-cell level.

4.2 Control of cell size

As I mentioned above, *E. coli* growth is phenomenology consistent with the adder model [5, 6, 7, 9, 33]. That is, a cell i add a fixed amount Δ of mass at each generation, so that the size at division S_{div}^{i} and the size at birth S_{b}^{i} obey the following relationship:

$$S_{div}^{i} = S_{b}^{i} + \Delta \,. \qquad (4.1)$$

To determine whether or not the overproduction of protein affects this relationship (Fig.4.1), in Fig.4.3 I show the size at division as a function of the size at birth for the Venus strains grown in the intermediate medium. The triangles correspond to the population average for each strain $j = \{\mathrm{WT}, \mathrm{Pro1}, \mathrm{Pro4}, \ldots\}$, which, as shown in chapter 3, follow the function $\langle S_{div}^{i} \rangle^{j} = 2\langle S_{b}^{i} \rangle^{j}$ (the brackets define an ensemble average over the population j of N cells).

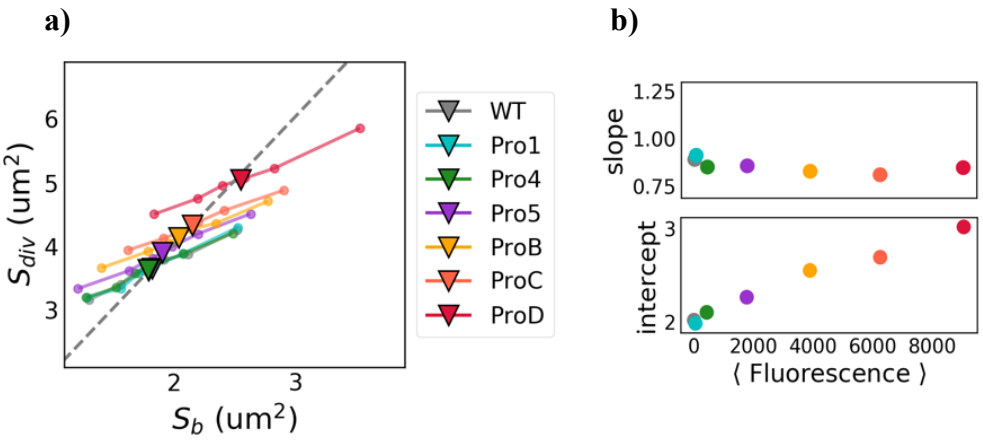

Figure 4.3. **a)** Size at division S_{div} as a function of the size at birth S_b for each ProVenus strain u growing in the "intermediate" medium. The larger markers show the mean over a population of individual cells i, $\langle S_{div}^{i} \rangle^{j}$ vs $\langle S_{b}^{i} \rangle^{j}$, and the dashed line corresponds to the best linear fit, which has a slope 2.01. For each strain, the cells were grouped by their cell size at birth into six intervals. The small markers show the mean of the size at division S_{div}^{j} as a function of the mean size at birth S_{b}^{j} of those six groups per each strain j (connected lines). The rainbow color code represents the level of fluorescence of the strains. **b)** Slope and intercept obtained from the best linear fit for each strain in (a), as a function of the mean fluorescence.

I divided each population j, into six equally sized intervals depending on the value of the size at birth, S_{div}^{j}. The small circles show the mean size at division of the individual cells (indicated with

the i index) corresponding to each interval k, $\bar{S}_{div}^{jk} \coloneqq \langle S_{div}^{i} \rangle^{jk}$, as a function of the mean size at birth for each interval and each strain $\bar{S}_{b}^{jk}$. For simplicity, henceforth I will indicate the mean of a variable X over individual cells i, belonging to a bin k of a population j, such as $\langle X^{i} \rangle^{jk}$, only as $\bar{X}_{b}^{j}$. This representation with the binning of some variables helps to visualize the relationship at the single-cell level, so I refer to it as the 'single-cell trend', a term also used in other work [6, 20].

The single-cell trend for all strains shows deviations from the population trend, which coincides with Eq.4.1 since, as displayed in Fig4.3b, the calculated slope obtained from the best fit of each curve in Fig.4.3a is positive and relatively constant among strains. The intercept for each strain then corresponds approximately to the added size Δ^{j}, which gets larger as the fluorescence (unnecessary production) of the strain u increases, Fig.4.3b.

Similarly, each ProVenus strain grown in the other two growth media have a positive correlation between $\bar{S}_{b}^{j}$ and $\bar{S}_{div}^{j}$, as can be observed in Fig.4.4a, where the mean $\bar{S}_{div}^{j}$ is shown as a function of the binned size at birth $\bar{S}_{b}^{j}$, rescaled by the populational mean $\bar{S}_{b}^{j}/\langle S_{b}^{i} \rangle^{j}$ for each strain j (continuous lines) in the three different media, poor (circles in blue), intermediate (in orange), and rich (in red). The slopes corresponding to each strain's linear fit are in Fig.4.4b, as a function of the mean fluorescence of each strain. The slope has a low correlation with the fluorescence, with a Pearson correlation coefficient of -0.17, showing that there is no clear bias on the size regulation due to the unnecessary protein production.

Given that an individual cell i, (from the population j), grows exponentially with time $S^{ij}(t) = S_{b}^{ij} 2^{\alpha_{ij} t}$, then at the time of division

$$S^{ij}\left(T_{div}^{ij}\right) = S_{div}^{ij} = S_{b}^{ij} 2^{\alpha_{ij} T_{div}^{ij}}, \tag{4.2}$$

therefore, considering Eq.4.1, the division time is:

$$T_{div}^{ij} = \frac{1}{\alpha_{ij}} \log_2 \left(1 + \frac{\Delta^{j}}{S_{b}^{ij}} \right) \tag{4.3}$$

In Fig.4.4c is presented the mean of the division time T_{div}^{j}, as a function of the binned scaled size at birth, $\bar{S}_b^j/\langle S_b^i\rangle^j$, for all ProVenus strains in the three different growth media. All populations show a negative correlation between $1/T_{div}^{ij}$ and S_b^{ij} which is consistent with the functional form of Eq.4.3, if Δ^j=fixed.

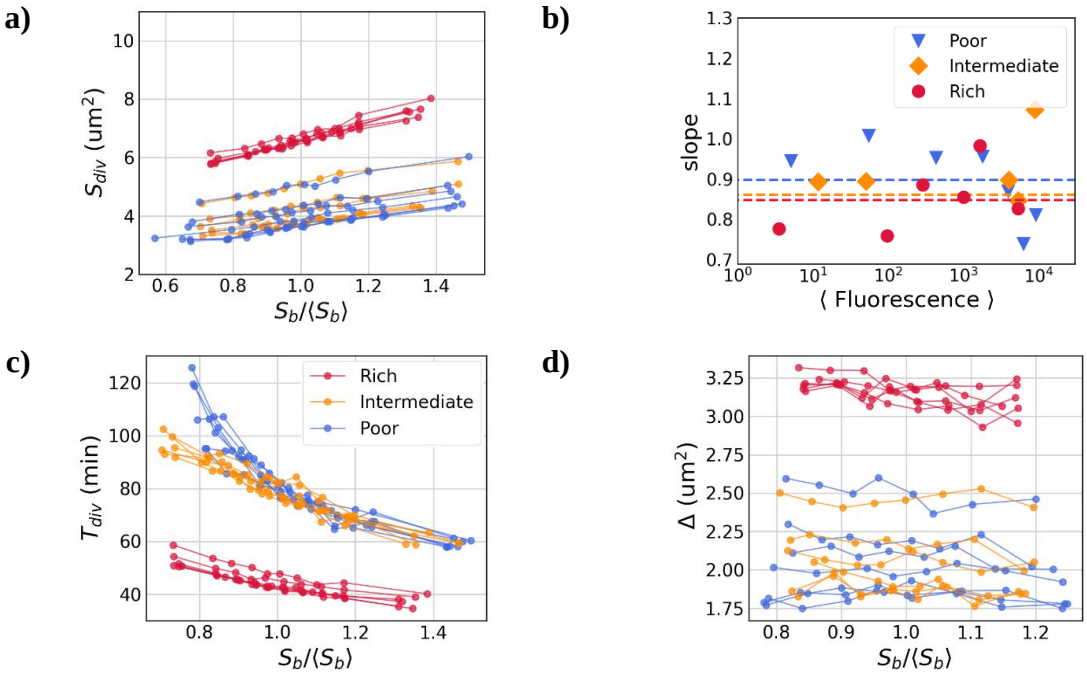

Figure 4.4. a) Mean size at division $\bar{S}_{div}^{j}$ as a function of the binned rescaled size at birth $\bar{S}_b^j/\langle S_b^i\rangle^j$ (rescaled by the average size at birth over all individual cells i), for each ProVenus strain j (connected lines) growing in three different media, rich (red), intermediate (orange), and poor (blue). **b)** Slope obtained from the linear fit to the single-cell (binned) relation $\bar{S}_{div}^{j}$vs $\bar{S}_b^j$ for each strain and condition in (a). The dashed lines correspond to the average of the slopes for each growth media, with the color being the same as the data points. **c)** and **d)** Division time $\bar{T}_{div}^{j}$, and the mean added size $\bar{\Delta}^j$ (defined for a cell i $\Delta^{ij} := S_{div}^{ij} - S_b^{ij}$) , as functions of the binned rescaled size at birth $\bar{S}_b^j/\langle S_b^i\rangle^j$, for each ProVenus strain j grown in three different media. The color code is the same as in (a).

Lastly, similar to Fig.4.4a and b, Fig4.4d shows the mean Δ^j of the added size as a function of $\bar{S}_b^j/\langle S_b^i\rangle^j$ for each strain growing in the different media. It can be appreciated that some of the

curves do not show a completely flat trend, which is consistent with the slope for $\bar{S}_{div}^{j}$ vs $\bar{S}_{b}^{j}$ not being precisely 1. Despite these small deviations, which can be explained by molecular and segmentation noise [38], the relations among the growth variables are more aligned with the adder model, even so, that the name 'near adder' control has been used to describe the size control of *E. coli* [49]. Then, the adder control mechanism still holds during the overproduction of unnecessary proteins.

Although the molecular basis of the adder regulation is unclear, [6,8,9], as mentioned in the introduction, one hypothesis is that there is a specific kind of "division" proteins that are responsible for cells to trigger division [11, 20, 45]. This analysis shows that the added size (or protein) increases as the strains produce more unnecessary proteins. In the following sections, I will further discuss this point.

4.3 Deviations from "population" behavior

When considering a single cell i, the elongation rate α^i (how fast the cell's body grows) obtained by fitting the temporal evolution of its size by the function $S^i(t) = S_b^i 2^{\alpha t}$, and the frequency of division $1/T_{div}^i$ (how fast they divide), are different variables. Such distinction is not possible to do at a population level, where, as seen in Chapter 3, the averages over a population result to be the same $\langle 1/T_{div}^i \rangle = \langle \alpha^i \rangle$.

To analyze this distinction, in Fig.4.5a I show the mean size at birth $\bar{S}_b^j$ as a function of the binned inverse of the division time $1/\bar{T}_{div}^j$ for the ProVenus distributions for each growth media j. First, there is a noticeable difference between media: In poor (blue) and intermediate (orange) media, for the slowest dividing bacteria the relation is closely similar to the one obtained at the population level (circles). However, when division is faster, the correlation between division time and elongation rate decreases. In rich media (red), this correlation is lost, as indicated by the zero slope for all the strains observed in the bottom plot of Fig.4.5a. The X-axis indicates the mean fluorescence of each strain to relate Pearson's correlations with the amount of protein they produce on average: In the poor and intermediate media, as the population has higher fluorescence, the correlation $R(\alpha, 1/T_{div})$ decreases, while in the rich media, all the strains show close to zero correlation, independent of Venus's amount.

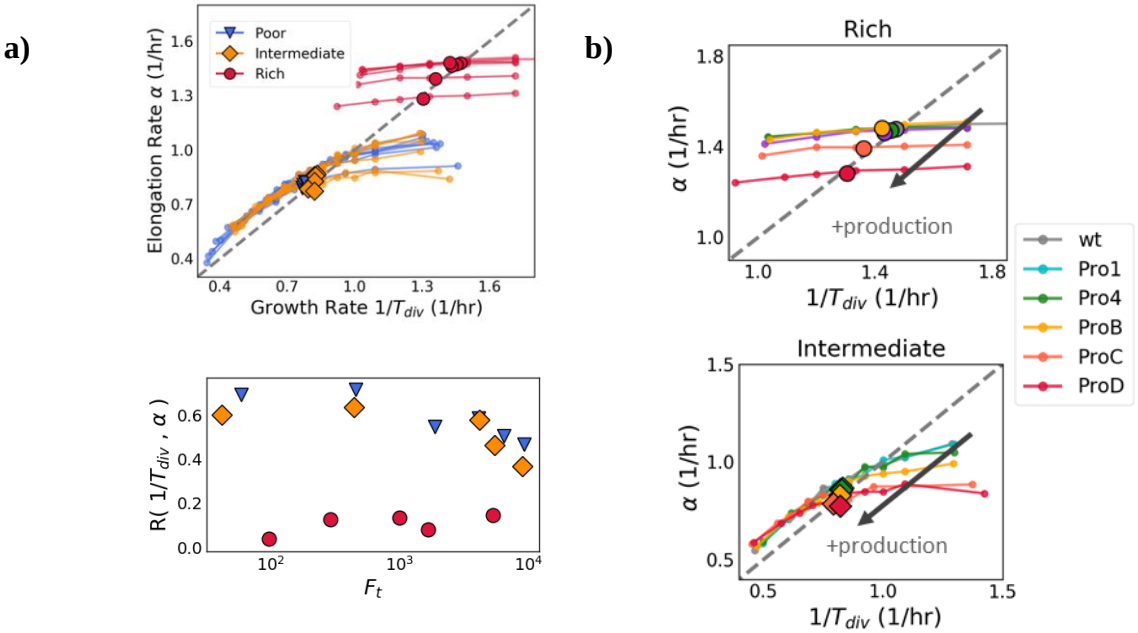

Figure 4.5. Elongation rate α versus the inverse division time $1/T_{div}$. **a)** The larger markers correspond to the population averages for each ProVenus series in poor (blue), intermediate (orange), and rich (red). The smaller markers correspond to the mean value of the data binned $1/\bar{T}_{div}$. The bottom plot shows the average of the Pearson's correlation coefficient between α and $1/T_{div}$, $R(\alpha, 1/T_{div})$ calculated for many mother cells. **b)** Enlarged elongation rate versus division time plots, for the strains grown in rich (top) and intermediate (bottom) media. The rainbow color code corresponds to different fluorescence levels, from gray, which corresponds to the WT strain with no unnecessary production, to the strain with the highest production, ProD (red). The arrows indicate the direction of increasing protein production.

This observation was made by Kennard et al. [23] for strains grown in different growth media, but they did not explore the effect on growth due to unnecessary protein production.

In Fig.4.5b, I show the close-up of the ProVenus strains in the rich and intermediate media. The rainbow code color represents the fluorescence level, from wild-type in gray (no fluorescence) until ProD strain in red, which is the strain with highest Venus production (higher fluorescence). The arrows also indicate the direction of increasing fluorescence. In rich media, the slope across strains seems to be the same and is almost horizontal, which means that α does not depend on the levels of unnecessary protein produced within each strain. In the intermediate media, cells with long division times have the same relationship with α across strains, and they are close to the $y = x$ function. For shorter division times, cells deviate from the identity, and they deviate more as they produce more unnecessary protein.

From Eq.4.3, the case of $1/T_{div} \sim \alpha$ is obtained when the size at birth is close to the added size, $\Delta \sim S_b$.

With this, it can be interpreted from Fig.4.5b that for the WT strain there is a majority of cells for which $\Delta \sim S_b$. But then, since producing more Venus increases the size (mass) of the cells, for the strains with higher production, the relation deviates more from the identity/population curve.

The phenomenological interpretation from Kennard et. al, which is based on considering these deviations due only to the growth media, is that when bacteria are divide slowly, they have enough time to respond to transient environmental fluctuations and equally coordinate the elongation rate and division frequency. Whereas in rich media, individual cells do not have enough time to react and adapt their divisions. This hypothesis could be extended to include deviations due to the overproduction of proteins, considering that it may also introduce fluctuations in the allocation of resources and the number of proteins.

4.4 Effect on division time of overexpression of the fluorescent protein Venus

To study the effects on division time of overexpression of the fluorescent protein Venus, I analyzed the relationship between division time T_{div} for various fluorescence levels in single cells. More specifically, I measured the fluorescence at birth F_{birth}, just before division F_{div}, and the difference $\Delta F = F_{div} - F_{birth}$.

First, in Fig.4.6a, I show the relationship between T_{div} and F_{birth}. As discussed in Chapter 3, I take the mean of division time $\langle T_{div} \rangle^j$, and fluorescence $\langle F_{birth} \rangle^j$ over the population j of individual cells for each ProVenus strain, and plot $\langle T_{div} \rangle^j$ versus $\langle F_{birth} \rangle^j$. The relationship shows a positive slope in rich and intermediate medium (large red circles and orange diamonds). For poor medium $\langle T_{div} \rangle^j$ decreases with $\langle F_{birth} \rangle^j$, but as mentioned before, a larger data set is needed to support this claim.

Contrary to the observed behavior at the population level, the relation at the single-cell level of division time and fluorescence at birth, $\bar{T}^j_{div}$ versus $\bar{F}^j_{birth}$, shows a negative slope. In Fig.4.6a, this effect is shown with the small markers and joined by continuous lines corresponding to each strain j. I quantified this negative correlation between T^j_{div} and F^j_{birth} using Pearson's correlation

coefficient as shown in Fig.4.6a, right panel. This result demonstrates that cells that are born with fewer fluorescent proteins take longer to divide than those born with more fluorescent proteins.

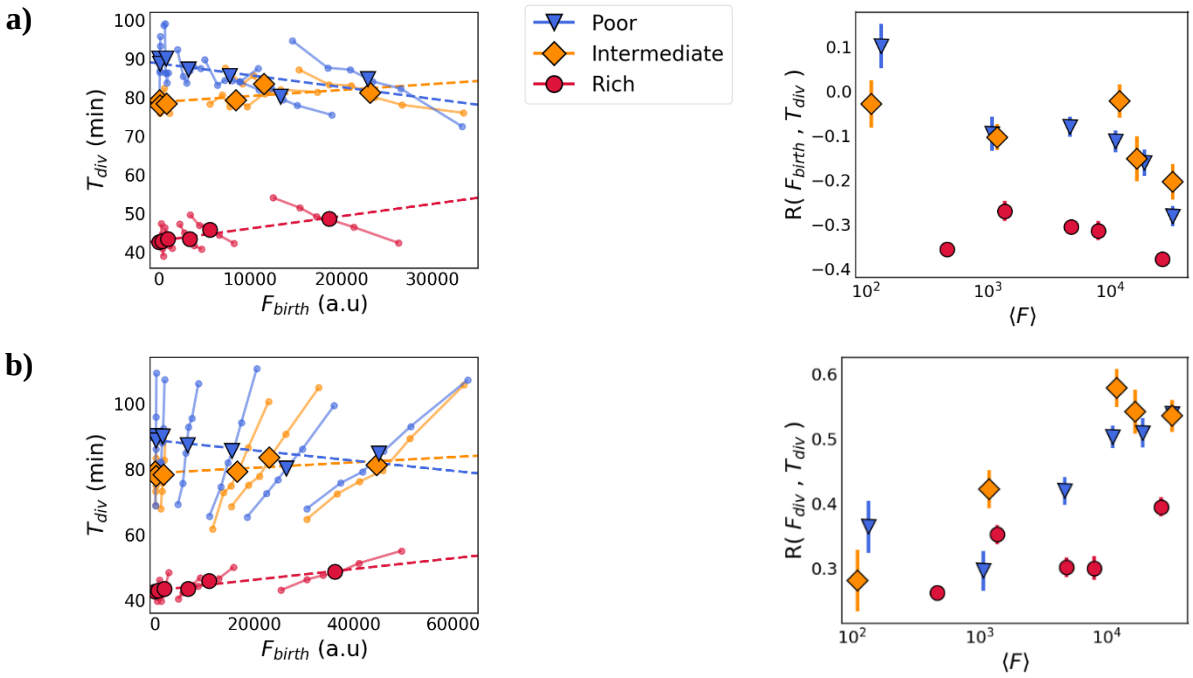

Figure 4.6. **a)** Relation between the division time, T_{div}, and the fluorescence at birth, F_{birth}. On the left, the large markers (triangles, diamonds, and circles) indicate the average for the ProVenus strain in the three different media (poor, intermediate, and rich, respectively). The smaller circles joined by lines correspond to the binned $\bar{F}_{div}$ versus $\bar{F}_{birth}$ for each strain at different media. The right pane shows the average Pearson's correlation $R(F_{birth}, T_{div})$ over all mother cells for each ProVenus strain on each growth media. Similarly, in **(b)** is shown T_{div} as a function of the fluorescence at the division time, F_{div}.

In Fig.4.6b, I show the relation between T_{div} and the fluorescence just before dividing, F_{div}. Each strain j also has a positive correlation between T_{div}^{j} and F_{div}^{j}. In other words, the cells with higher fluorescence at the time of division grew for a longer time before division. The right panel contains the mean Pearson's coefficient $R(F_{div}, T_{div})$ calculated for each lineage as a function of each strain's mean fluorescence, which corroborates the positive correlation.

These two relationships showing opposite slopes between F^j_{birth} and T^j_{div} and between F^j_{div} and T_{div} suggest that what correlates with the division time is the accumulation of unnecessary protein during the cell cycle. Indeed, in Fig.4.7a, I show T_{div} as a function of the fluorescence accumulated during the cell cycle $\Delta F = F_{div} - F_{birth}$, which shows a positive correlation for all strains in different media. The Pearson's correlation $R(\Delta F, T_{div})$ in Fig.4.7a increases as the strains produce more Venus and is larger than the one obtained in Fig.4.6b

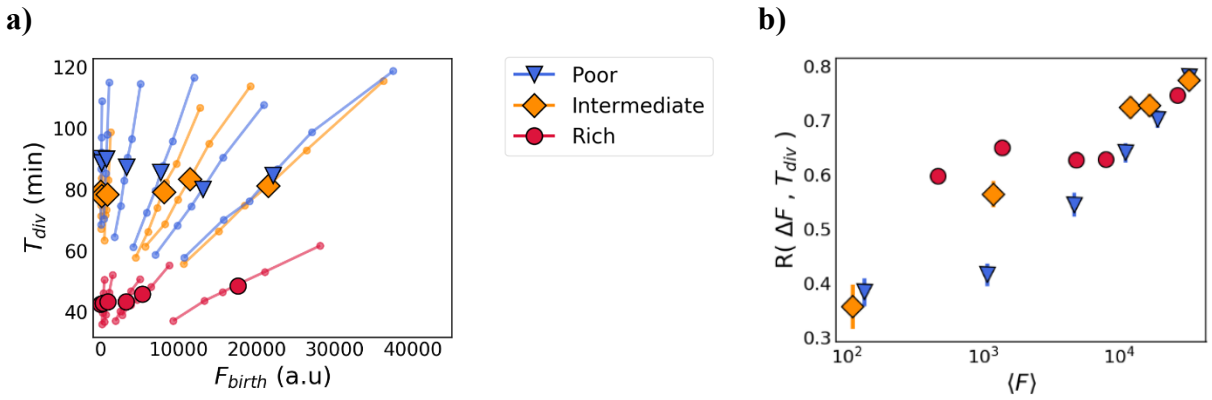

Figure 4.7. **a)** Relation between the division time, T_{div}, and the accumulated fluorescence $\Delta F = F_{div} - F_{birth}$. On the left, the large markers (triangles, diamonds, and circles) indicate the average for the ProVenus strain in the three different media (poor, intermediate, and rich, respectively). The circles correspond to the mean $\overline{T}_{div}$ as a function of the binned mean $\overline{F}_{birth}$ for each strain at different media. **b)** Average Pearson's correlation $R(\Delta F, T_{div})$ over all the mother cells for each ProVenus strain on each growth media.

Variation in fluorescence in a population of cells is due to the difference in the number of fluorescent proteins it contains. Since cells also vary in size, one can imagine the case in which there are variations in the number of fluorescent proteins while the concentration (its fraction in the proteome) remains invariant, or the case in which this fraction also changes.

According to Scott and Gunderson et al., a population of bacteria growing under a steady condition l (l index indicates both the strain with constitutive production and growth condition) would have a stable fraction of unnecessary protein U, ϕ^l_U, and also a stable fraction of division protein X, ϕ^l_X. By contrast, changing the growth condition would change the protein sectors' fraction and affect

the mean elongation rate, division time, and cell size. This point, discussed in Chapter 3, explains why the mean division time $\langle T_{div} \rangle$ over a population of cells is longer as it has a larger mean fluorescence (either $\langle F_{birth} \rangle$ or $\langle F_{div} \rangle$): each strain has a different mean fraction of unnecessary production ϕ_U^l that 'takes away' resources from other sectors, including from X. Therefore, as ϕ_U^l gets larger, ϕ_X^l lowers making the mean division time of the population to increase.

By definition, the number of division protein X and unnecessary proteins U in a cell i are:

$$X^{li}(t) = M^{li}(t) * \phi_X^l(t), \tag{4.4}$$

$$U^{li}(t) = M^{li}(t) * \phi_U^l(t) \tag{4.5}$$

where M^{li} is the total amount of protein in the cell i.

If ϕ_U^l and ϕ_x^l are approximately constant, the fluorescence F^{li} of a cell will be positive proportional to the amount of both proteins U^{li} and X^{li}.

$$F^{li}(t) \propto U^{li}(t) = \frac{\phi_U^l}{\phi_X^l} * X^{li}(t) \tag{4.6}$$

According to Basan's model, the number of division proteins X^{li} needs to cross the threshold X_{div} (which is assumed the same for all conditions) to trigger division.

Therefore, considering this model and Eq.4.5, cells with a low level of fluorescence F^{li} at the beginning of a cell cycle would also have few X^{li} proteins and would take longer to reach X_{div} and divide (after a time T_{div}^{li}) than a cell born with a lower fluorescence. This negative correlation between F_{birth}^l and T_{div}^l for a strain j is observed in Fig.4.6a for almost all ProVenus strains.

We assume that the unnecessary proteins are produced at a constant rate since the promoters are constitutive and cells are growing at a steady rate. Consequently, the longer a cell takes to divide, the more Venus proteins accumulate from birth to division. Therefore in individual cells, the accumulated fluorescence should be positively correlated with division time, which is the result observed in Fig.4.7.

We hypothesize that, at least for the cells in rich media, the fraction of protein sectors is approximately constant among individual cells under stable conditions and that the number of unnecessary proteins U and division proteins X are positively correlated.

Under this hypothesis, the ribosomal related proteins R can synthesize simultaneously the proteins of both sectors, X and U. In this way, the variations in the abundance of ribosomes drive variations in proteins X and U.

That a population of cells has their fractions of proteins constant is a strong assumption. These sectors most probably have variations among individual cells, which would add noise to the division time of a population. Those variations might even depend on the growth media. I discuss this point in the following section.

4.5 Correlation between Cell Size and Expression Levels of Fluorescent Proteins

To visualize the relationship of cell size and unnecessary proteins in individual cells, I show in Fig.4.8 the mean size at birth S_b^l, as a function of the binned fluorescence at birth, F_{birth}^l, for each ProVenus stain l in three different growth media (small circles joined by straight lines).

The single-cell relations for each strain do not fall onto the mean population behavior curve (large markers) of each corresponding growth media. Nonetheless, there is a positive correlation between S_b^l, and F_{birth}^l for each strain in the three different growth media: the cells that have more Venus protein are also larger.

All the ProVenus strains have a positive Pearson's correlation $R(F_{birth}, S_b)$, which becomes larger as the strains produce more fluorescent proteins, indicated in Fig.4.8b. In the case of the rich media, all the strains have a correlation $R(F_{birth}, S_b)$ higher than in the other media (>0.5 for all strains). For poor medium it is noticeable that the correlation depends on the production of Venus of each population being low for small production (0.15 for the strain that produces the lower fluorescence, Pro1) and higher for high amounts of production (0.75 for the strain that synthesizes the higher fluorescence, ProD).

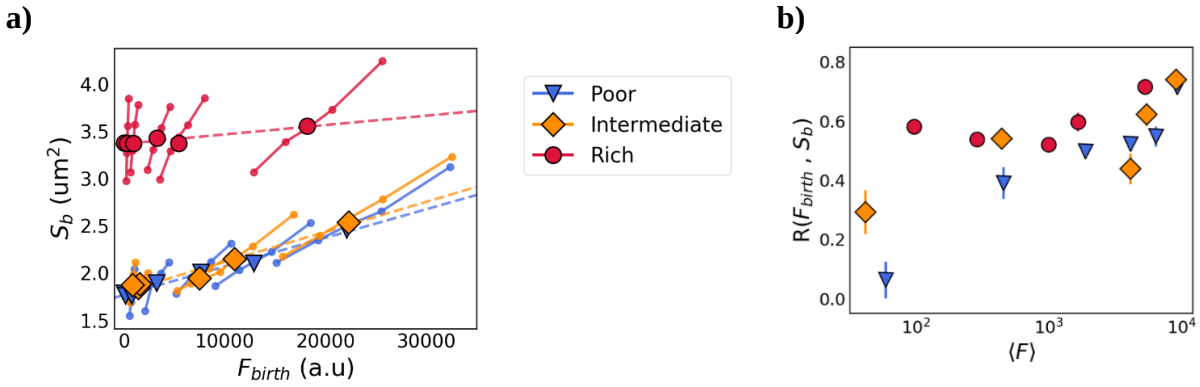

Figure 4.8. a) For each ProVenus strain grown in a specific media, the cells were grouped by level of fluorescence at birth F_{birth} in five intervals. The small dots joined with continuous lines show the mean of the cell size at birth $\bar{S}_b$ and fluorescence $\bar{F}_{birth}$ of those groups for each strain in different media. The blue triangles, orange diamonds, and red circles show the population averages for the strains grown in the three media, poor, intermediate, and rich, respectively. The dashed lines indicate the trend of the population averages of the ProVenus on each media. **b)** Average Pearson's coefficient of size and fluorescence calculated for each mother cell from the ProVenus strains in poor, intermediate, and rich media. The color code is the same as the average values in (a).

As already mentioned, the proteome can be divided into different types of proteins (or sectors). If cells express unnecessary proteins, these proteins make up a sector U and add extra mass to the cell's total mass (and volume) [12,11,39,40]. Also, cells increase the number of endogenous proteins when there is unnecessary protein production [11, 41]. Therefore, the extra cellular mass when there is overexpression is a combination of the unnecessary proteins and proteins from other sectors.

Since the mass M^{li} of a cell i is proportional to its size S^{li} [11], and the fluorescence level F^{li} is a proxy of the number of U^{li}, equation Eq.4.5 leads to

$$F^{li}(t) \propto S^{li}(t) * \phi_U^l(t). \tag{4.7}$$

If the fraction of unnecessary protein ϕ_U^l is the same over time and independent of the mass and size of the cell i, the fluorescence level would be approximately proportional to the size, $F^{il} \propto S^{il}$. Rescaling by the respective mean value of each population of strains l, these quantities would be approximatively $\bar{F}^{il}/\langle F^i \rangle^l = \bar{S}^{il}/\langle S^i \rangle^l$.

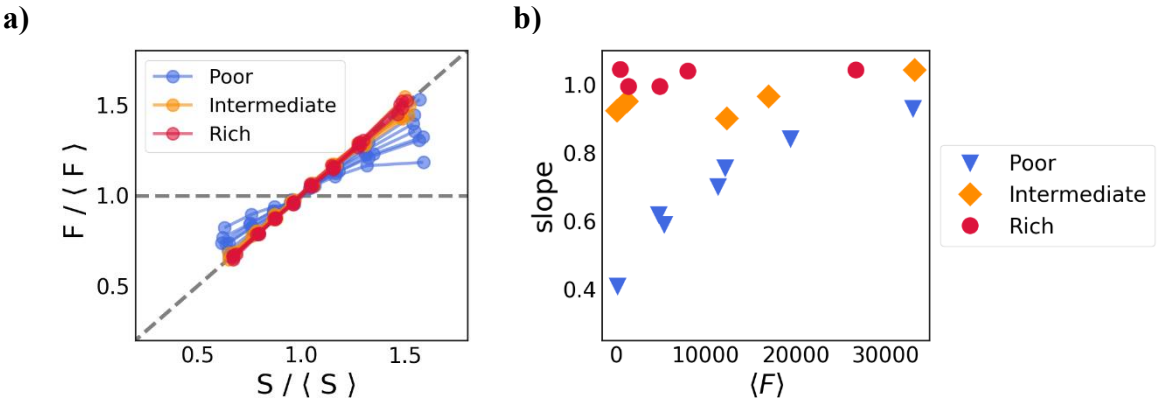

Figure 4.9. On the left is the fluorescence $\bar{F}$ as a function of the binned cell size $\bar{S}$ of the ProVenus strains at birth (a) and at division (b), all variables scaled by the mean value of the population. The color corresponds to the growth media in which the cells were grown, poor in blue, intermediate medium in orange and rich medium in red. On the right is the slope of the best linear fit of each of the curves, as a function of the average fluorescence of each strain in different growth media, the color code corresponds as well to the growth media.

I tested this relation for the ProVenus strains. In Fig.4.9a, I show the rescaled fluorescence as a function of the binned rescaled size for each ProVenus strain in the three different growth media. Fig.4.9b shows the slopes of the curves from Fig.4.9a and how they depend on the average fluorescence per population. In the rich and intermediate media, the proportionality constant is closer to one and similar for all the strains (Fig.4.9b). It can be concluded that, in such media, the fraction of the unnecessary fluorescent proteins ϕ_U^l is well conserved among cells of each ProVenus strain. In poor media, the curves corresponding to strains with low Venus fall outside the identity curve more than in the other two media (blue curves in Fig.4.9a), meaning that they have a significant cell-to-cell variation in the fraction to Venus ϕ_U^l. The slope for the strains with low Venus production is close to zero, but it increases as the strain's fluorescence $\langle F^i \rangle^l$. Therefore, the strains with a higher level of unnecessary production have a more conserved fraction of proteins ϕ_U^l.

We do not have a model to simulate cell growth under different protein production and growth conditions that accounts for the noise in the size of the protein sectors. Nevertheless, I present below a hypothesis about why the fraction of unnecessary protein is stable in rich media but not in the poor.

In rich media, the resources are in excess and always available to robustly allocate them among the different protein sectors. By contrast, since the nutrients are more limited in poor media, cells need to make a trade-off among the different sectors to distribute the resources, then the noise in allocation among sectors is bigger.

For cells that produce a low level of unnecessary protein U, other sectors of proteins constitute a larger percentage of the total proteome; therefore, the cells' size is mainly subject to variations of other sectors other than ϕ_U^l . When cells are forced to synthesize Venus in greater quantities, Venus has a greater fraction of the proteome, thus has a higher effect on the cell size. Therefore, the high unnecessary protein concentration exceeds the intrinsic noise in allocation due to the low resources.

4.6 Correlation between elongation rate and Expression Levels of Fluorescent Proteins

Data in Figure 4.10a show the elongation rate α^l as a function of the binned fluorescence F_{birth}^l for each ProVenus strain l in different growth media (small circles joined by straight lines), and the mean for each population, $\langle\alpha\rangle^l$ versus $\langle F_{birth}\rangle^l$ (large markers).

For rich media, while the mean elongation rate of a population decreases as the strain has a higher fluorescence, at the single-cell level, the correlation between α^l and F_{birth}^l is close to zero for all strains (Fig.4.10b). There is a smaller change between the mean of populations of different strains in the other two media. Nevertheless, at the single-cell level, there is a weak negative correlation between α and F_{birth} (Fig.4.10b).

Previous work that analyzed single-cell measurements from *E. coli* found that the elongation rate has a weak correlation with other cell parameters, such as cell size and division time [53]. They assume that the cell must control α independent of other parameters. Such result coincides with the case of cells growing in rich media in this work.

Why is there a negative correlation at the single-cell level at poor media while there is no correlation in rich media? The answer could be related to the hypothesis proposed in the previous section: there are bigger variations on the fraction of different protein sectors among individual cells of a population when the resources are scarce.

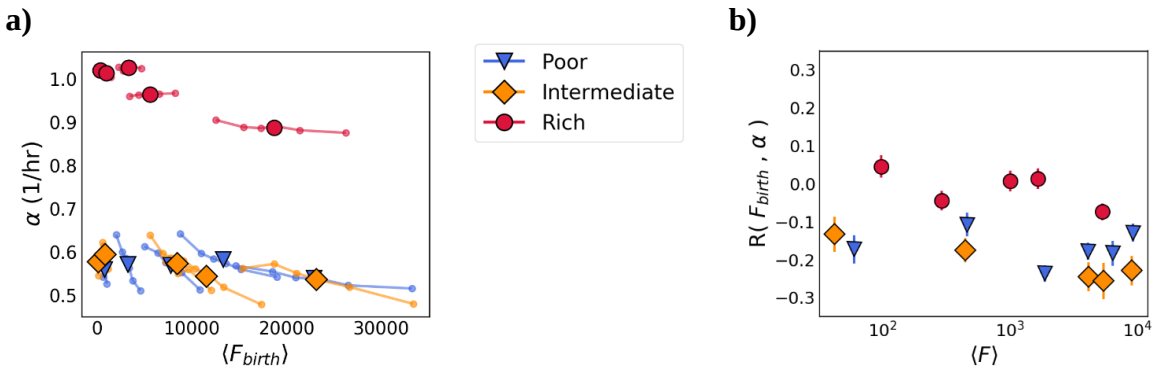

Figure 4.10. a) For each ProVenus strain grown in a specific media, the cells were grouped by level of fluorescence at birth F_{birth} in five intervals. The small dots joined with continuous lines show the mean of the elongation rate $\bar{\alpha}^j$ and fluorescence $\bar{F}^j_{birth}$ of those groups for each strain j in different media. The blue triangles, orange diamonds, and red circles show the cells' mean values per strain grown in the three media, poor, intermediate, and rich, respectively. **b)** Average of the Pearson's coefficient between α and F_{birth} of each mother cell from the ProVenus strains in poor, intermediate, and rich media. The color code is the same as the average values in (a).

4.7 Single-cell deviations from the growth law

As mentioned before, for many microorganisms, the average size of a population across different growth media (diverse nutrient quality) follows an exponential function of its growth. In recent years by using microscopy and microfluidic techniques, Taheri-Araghi et al. [6] revealed that the trend of the relationship 'size versus division frequency' within a population of individual cells deviates from the nutrient growth law. In Fig.4.11a, I show the same result for the wild-type strain in three growth media. The larger markers indicate the mean size as a function of the frequency of division time in each media. As seen in Eq.3.8 and Fig.3.16, the same relation of the population averages follows in the 'mean size versus mean elongation rate' and would be similar as well with the growth rate ($\langle\alpha\rangle * \ln(2) = \langle 1/T_{div}\rangle * \ln(2) = \lambda$). The small circles show the mean size $\bar{S}^l_b$ versus the mean frequency of division $1/\bar{T}^l_{div}$ for each population l binned by the frequency of division. The dashed curve corresponds to exponential best fit to the averages of the populations.

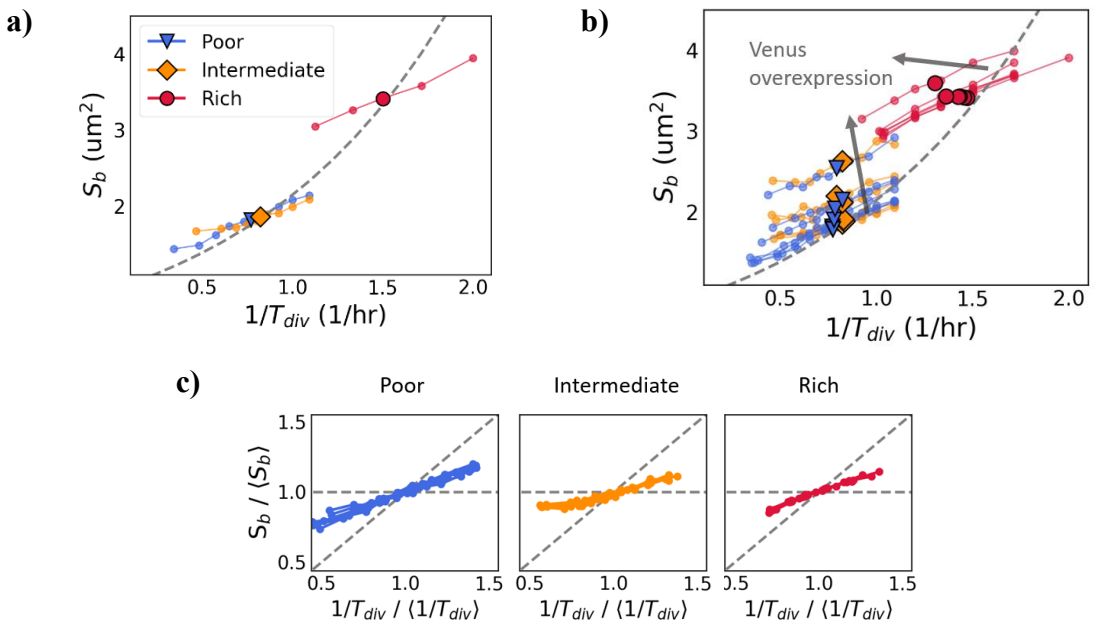

Figure 4.11 a): Size at birth S_b versus division frequency $1/T_{div}$ for the wild-type strain grown in three different media. In red, the large marker corresponds to the mean values of the cells growing in the rich medium, while the small markers show the single-cell relationship (mean values of the data binned by $1/T_{div}$) division frequency in equal size bins. Similarly, the markers in orange and blue correspond to cells growing in the intermediate and poor media. The dashed line is the best fit of an exponential function to the data, only to illustrate the known relation of the nutrient growth law [6]. **b)** S_b versus $1/T_{div}$ for the different ProVenus strains growing in different media. As in (a), the large markers show each population's respective mean and the small markers the relation for the data binned by division frequency values. The arrows indicate the order of increasing protein production, from lower to higher. **c)** Rescaled version of the single-cell relations in (b), $\bar{S}_b/\langle S_b \rangle$ versus $1/\bar{T}_{div}/\langle 1/T_{div} \rangle$ for the ProVenus strains in poor (right), intermediate (middle), and rich (right) media.

These single-cell level deviations have been observed when the growth rate (division frequency) was controlled by changing the media's nutrient content [6, 23]. In this work I extend the analysis for growth changes due to the overexpression of the unnecessary protein, for the ProVenus series. The results are reports in Fig.4.11b. As the strains produce more Venus, the mean deviates from the 'nutritional growth law' as indicated by the arrows. The single-cell relations for the strains with different production (small circles) exhibit a similar relationship across various media.

As presented in Fig.4.11c, for each growth media, the size at birth rescaled by its mean $\bar{T}_b/\langle S_b \rangle$ versus the rescaled division frequency $1/\bar{T}_{div}/\langle 1/T_{div} \rangle$ for each ProVenus strain and media fall into the same curve.

The deviations from the population trend when there is overexpression of unnecessary proteins and the rescaling with the mean expression of unnecessary proteins is a novel result; however, they were predicted by a model for bacterial growth, which I discuss in the section that follows.

4.8 Using Bertaux' allocation model to interpret single-cell data

In a recently published work, Bertaux et al. [11] present a cell physiology model that considers the allocation and dynamics of different kinds of proteins and their effect on single-cell growth. This model is more detailed than Scott and Gunderson et al.'s model described in chapter 3, which only considers changes of the protein composition at the population level but not variations in individual cells. As illustrated in Fig.4.12, there are different kinds of proteins that have different functions.

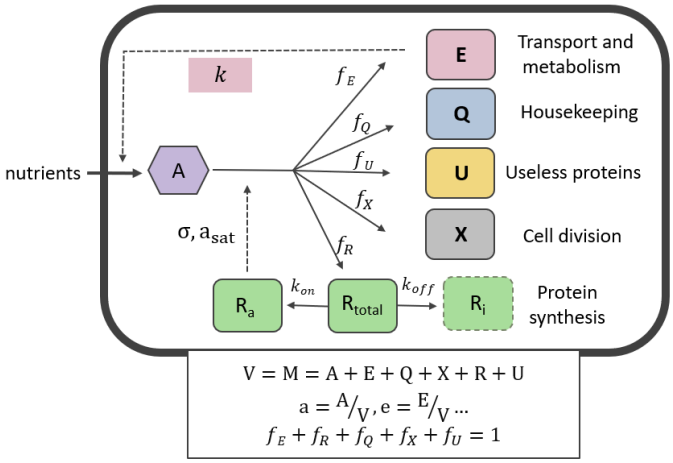

$$\frac{dZ}{dt} = f_Z \sigma R_a \frac{a}{a + a_{sat}}, \qquad Z = \{E, Q, X, U\}$$

$$\frac{dA}{dt} = kE - \sigma R_a \frac{a}{a + a_{sat}},$$

$$\frac{dR_a}{dt} = f_{R_a} \sigma R_a \frac{a}{a + a_{sat}} - k_{on} R_a + k_{off} R_i$$

$$\frac{dR_i}{dt} = k_{on} R_a - k_{off} R_i$$

Figure 4.12. Diagram showing the structure of Bertaux model. The model consists of two kinds of cell components: precursors and proteins. The proteome is divided into different protein sectors: transport E, housekeeping Q, useless proteins U, division X, ribosomal R (active R_a or inactive R_i). The precursors are assigned to a sector i by an allocation fraction f_i. E proteins transform the nutrients, which have a k nutrient quality, into precursors. R proteins synthesize the proteins from precursors at a rate σ, and has a saturation constant a_{sat}. The sum of the proteins and precursors equals the total mass (volume) of a cell. Nutritional limitations are modeled with the parameter k, expression of the unnecessary protein by the fraction f_U and translational inactivation by changing the rate of R_i. Figure modified from [20]. The dynamics of the absolute amounts of coarse-grained cell components are described by the set of differential equations on the left.

The metabolic and transport proteins E transform the nutrients, which have a k nutrient quality, into precursors A, and the ribosomal proteins R synthesize the proteins out the precursors. As proposed by Basan et al.'s (see Fig.4.2), in Bertaux's model, a cell divides when it accumulates X proteins up to a fixed threshold X_{div}. The housekeeping proteins are involved in the basic functioning of a cell and compose a fixed fraction of its proteome, regardless of the growth conditions [24, 12]. Finally, the unnecessary proteins do not have any function in a cell.

The number of precursors assigned to each protein sector Z, ($Z = \{E, R, X, R, U\}$) depends on the allocation fraction f_Z. The fraction of the unnecessary proteins f_U is fixed and imposed in a simulation, and the fraction for the housekeeping f_Q is fixed (~0.5).

Few parameter values were obtained by fitting experimental results previously reported from ribosomal abundance under growth limitations.

This model implements stochasticity using Gillespie's algorithm for a single cell. When cell division occurs, the model keeps tracking the mother's growth. When X reaches the division threshold X_{div}, each molecule (protein and precursor) is kept in the mother cell, with probability ½.

The model reproduces the growth law and Basan's population results, as shown below. The model also displays the 'near-adder' relations as in Fig.4.4.

Using this model, I simulated my experimental conditions: time-lapses of individual cells with different levels of unnecessary protein growing in various growth media. The strains with varying levels of unnecessary protein are simulated by changing the fraction f_u of unnecessary proteins U, $f_u = \{0.2, 0.4, 0.8, 0.1, 0.12\}$, and the diverse growth media with changes in the k parameter, $k = \{1, 4, 8\}$.

Fig.4.13 shows some results of these simulations: the relations of cell size at birth S_b, division time T_{div} and elongation rate α, with the number of unnecessary proteins at birth U_{birth}.

The results are qualitatively similar to the experimental results, both at the population level (the mean over the cells of each simulation, large markers on the right panels of 4.12a, b, and c) and for individual cells (averaging over the binned data, smaller markers joined by a straight line).

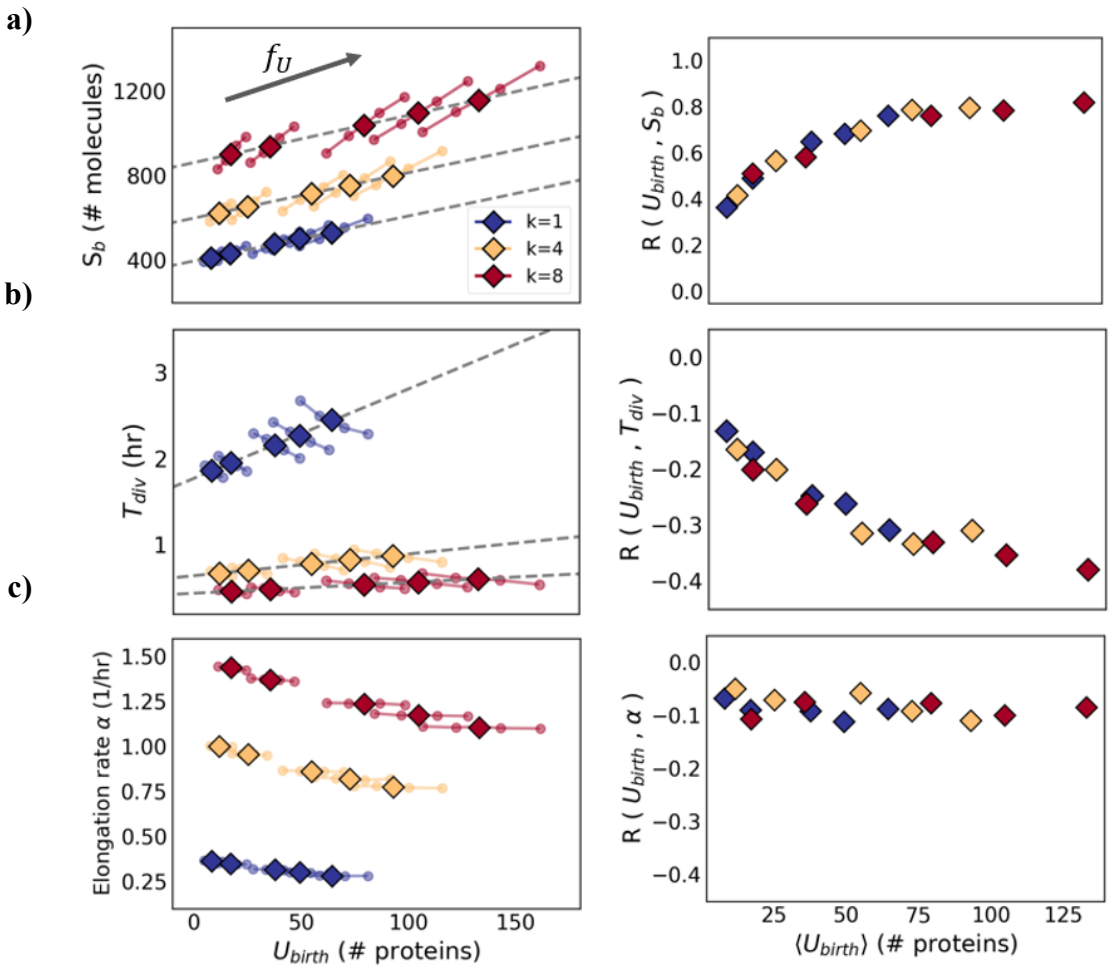

Figure 4.13. Results of several simulations of the growth of cell lineages using Bertaux stochastic model for bacterial growth. The simulations vary in two parameters: the parameter k, representing the nutrient quality of the growth media, $k = \{1, 4, 8\}$ (indicated by different colors), and the fraction of unnecessary proteins f_U=$\{0.2, 0.4, 0.8, 0.1, 0.12\}$ (order in the direction indicated by the arrow). **a)** Left: Size at birth S_b (measured by its total number of proteins plus precursors), as a function of the number of unnecessary proteins at birth U_{birth}. The diamond markers show the mean $\langle S_b \rangle$ versus $\langle U_{birth} \rangle$ over individual cells for different populations. The colors indicate the nutrient quality k and the arrows the order of the populations with low to higher f_U. The circles connected with lines correspond to the cell size over intervals of the data of each population binned by U_{birth}. The gray dashed lines are the best linear fit to the mean values $\langle S_b \rangle$ versus $\langle U_{birth} \rangle$ for each value of the nutrient quality k. Right: Pearson correlation coefficient between the fluorescence and size at birth $R(F_{birth}, S_b)$ for each population as a function of its mean fluorescence at birth. The color markers correspond to the nutrient quality k as in the left plot. **b)** and **c)** Similar plots as in (a), but for the relation of division time T_{div} and elongation rate α with the fluorescence at birth U_{birth} respectively

The mean cell size of a population with a given nutrient quality k increases with the number of U_{birth}. Also, the variations of individual cells increase, although the trend does not fall into the population trend of each k. The correlation between S and U also increases as the strains produce more unnecessary protein, noted in the Pearson's correlation coefficient $R(U_{birth}, S_b)$ in Fig.4.13a, right panel.

By contrast, the relation between the mean division time $\langle T_{div} \rangle$ and the amount of unnecessary protein $\langle U_{birth} \rangle$ for individual cells is the opposite; individual cells that have few proteins at birth U_{birth}, have a longer division time. This negative correlation is observed both in the trend of the binned data and the correlation coefficient in $R(U_{birth}, T_{div})$ on Fig.4.12b. This result is analogous to the one shown in Fig.4.6a.

The coincidence between the experimental and simulation results about the relationship between division time and unnecessary expression supports the scenario discussed in chapter 4.4. This scenario consists of two parts. On the one hand, to divide, cells need to accumulate a quantity of a protein X up to a fixed threshold independent of any growth condition.

On the other hand, the variations in fluorescence in the population of a single strain under stable conditions are mainly due to the variation in the number of fluorescent proteins, while the fraction of these proteins (and the fraction of other proteins) in the cells exhibits small variations.

Then, the fluctuations in the number of unnecessary proteins U are a response to changes in the number of ribosomal proteins R. More ribosomal proteins mean more synthesis of any type of proteins; therefore, the X proteins respond in the same way to R (see equations in Fig.4.12). When there is an increase in U proteins, there is also an increase in X, proteins which make the cells reach the threshold X_{div} and divide faster. Thus U_{birth} (and the fluorescence F_{birth}) and T_{div} are negatively correlated.

Finally, the elongation rate as a function of the unnecessary protein has a weak negative correlation with the number of unnecessary proteins. The correlation is independent of the nutrient parameter k and the fraction f_U, as in the experimental results from Fig.4.10.

The model also reproduces the nutrient growth law. The mean size $\langle S_b \rangle^k$ is an exponential function of the division frequency $\langle 1/T_{div} \rangle^k$, when $f_U = 0$ (large markers that fall on the dashed

exponential curve in Fig.4.14a). The mean values when f_U is higher have a different trend (indicated by the gray arrow), similar to the results in Fig.4.11b and [11].

The single-cell data (smaller markers joined by a line for each population) show that there is a systematic deviation from the population average for all conditions. These deviations are qualitatively similar to the ones of the ProVenus strains in Fig.4.11b. They also collapse onto the same curve when both parameters are rescaled by their population mean, as indicated in Fig.4.14b.

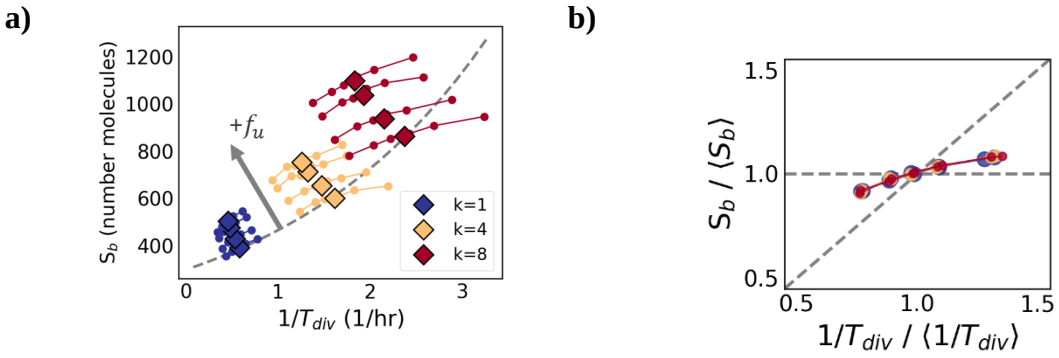

Figure 4.14. Results from Bertaux et. al model. a) Average number of molecules (proteins plus precursors) in the cells at birth S_b vs frequency of division $1/T_{div}$, for various combinations of parameters. The colors show the simulations with the same parameter for nutrient quality k={1, 4, 8}. The fraction of unnecessary protein used are f_U={0, 0.02, 0.04, 0.08, 0.1}, and are displayed in increasing order as indicated by the arrow. The big diamond markers correspond to the average over all the cells for a given condition, whereas the small circles correspond to the mean values for the data being equally binned by $1/T_{div}$. **b)** For all the conditions in (a) (all combinations in the values of k and f_U), the mean of the rescaled size at birth as a function of the binned rescaled elongation rate, overlap in the same curve.

4.9 Discussion

Here I presented an analysis of the correlation between different cell parameters that characterize the production of unnecessary proteins (cell size, division time, and elongation rate) and the fluorescence of individual cells from the ProVenus strains in different growth media.

I showed that the adder size control is robustly conserved for the ProVenus cells growing in the three different growth media. No matter how much "stressed" the cells are due to the overexpression of unnecessary proteins, the cell size and division time obey the adder relations.

Although the adder relations have been widely observed for many conditions and microorganisms in a steady-state, their underlying biophysical and molecular mechanisms are still unknown [45].

A possible dynamical mechanism proposes a division protein, X, which a cell accumulates during growth, and once reached a fixed threshold, the cell divides [11].

Like the other types of protein (ribosomal, housekeeping, etc.), this X protein composes a sector on the cells' proteome, which changes depending on the nutrient (described by Scott and Gunderson [12], see chapter 3.1). This model of the accumulation threshold explains why the mean cell size of a population increases while the elongation rate decreases when the cells overexpress unnecessary proteins [11].

Recent work by Panlilo et al. showed experimentally that single cells change their size, elongation rate, and division time when they switch on nutrients [45]. They found that these changes can be explained with the accumulation/threshold hypothesis better than with other division mechanisms [46].

The results presented in this chapter, particularly the correlation between size, division time, and fluorescence at birth, can be as well understood under the accumulation/threshold model and some considerations described below.

I found that individual cells' fluorescence is proportional to their size in rich media, which implies that the unnecessary (fluorescent) U protein fraction is well conserved in a population.

Since any type of protein needs ribosome-related proteins R to be synthesized, if the protein fractions are fixed, the accumulation of unnecessary and division proteins will be positively correlated (both subject to the variations on R proteins). Hence a positive correlation between fluorescence level and size at birth and a negative correlation between fluorescence at birth and division time. In other words, a small cell has also a small number of unnecessary proteins (making the fluorescence low) and a low number of X proteins, causing the cell to take a longer time to accumulate division proteins until the threshold is reached and the cell divides. On the contrary, bigger cells have more proteins, therefore higher fluorescence, and consequently reach faster the division threshold (Fig.4.15)

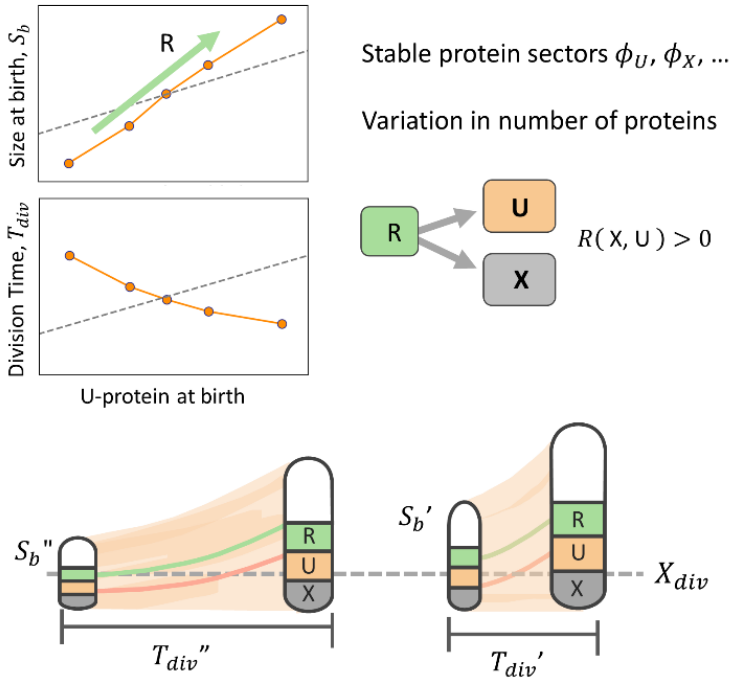

Figure 4.15. The correlations at the single-cell level between the size at birth S_b and division time T_{div} with the number of unnecessary U proteins at birth can be explained by the simultaneous synthesis of U proteins and division proteins X by the ribosomal proteins R. At a steady-state, this simultaneous synthesis implies stable protein sectors, ϕ_U, ϕ_X, …, which do not compete for the R proteins. Since the ribosomes drive changes both in U and X proteins, there is a correlation between them. Below is a representation of two cells with a low (left) and high (right) level of R proteins at birth. An increased number of R proteins in a cell yields a higher protein synthesis, thus a large cell mass and size. Hight load of R also implies more X protein synthesis, hence a shorter time for the cell to reach the threshold X_{div} and divide.

In poor media, the correlation between division time and fluorescence at birth is close to zero for strains with low mean Venus synthesis. Such correlation decreases and is negative as the average Venus synthesis of the population is greater. Besides, Venus proteins concentration is poorly conserved among cells from the strains with low fluorescence levels. We hypothesize that in poor media, the proteome sectors have a big cell-to-cell variability since there is competition between different proteins because of the low resources available.

Bertaux's model, which I discussed above, is of particular interest because it is based on the proteome allocation theory and because it modeled cell division with the accumulation of a

division protein [45]. This model can reproduce qualitatively well single-cell relations between the growth parameters: The relations proper of the adder mechanism and the deviations on the nutrient growth law. With the model, I simulated my experimental conditions: populations with different levels of unnecessary protein growing in various nutrient conditions.

The correlation between unnecessary proteins and division time from the model agrees better with the results obtained in the rich media experiments. Nonetheless, it does not reproduce all the behavior in poor conditions, a case for which we hypothesize there is significant noise in the protein concentrations.

Overall, the analysis of the experimental data shown in this chapter reproduces different results of the effect of unnecessary proteins from single and population levels and encompasses various cell growth models such as the adder model, size growth laws, and the threshold initiator model.

5. Growth dependance on protein synthesis with pulse dynamics

5.1 Introduction

Classically, the study on how microorganisms control cell size and division has been addressed by measuring physiological parameters as the cell size and doubling time, under balanced growth. This is achieved by growing bacteria while maintaining the same growth conditions, such as keeping a constant flux of growth media, constant temperature, and, as I presented in Chapters 2 and 3, maintaining a steady production of unnecessary protein. Independent experiments under different conditions contributed to identifying the growth laws and the adder mechanism as the underlying principles that govern cell growth [2, 3, 4, 6, 11].

However, this empirical description is a mean-field theory of cellular growth that predicts neither the time dependence of the growth parameters (cell size, division time, elongation rate) nor the causal relationships between them [45]. With this in mind, I decided to analyze the dynamics of individual cells when subject to big temporal fluctuations in the production of proteins and the associated effect on the growth. To do this, I chose to study the dynamics of the synthesis of flagellar proteins in *E. coli*, which, as I demonstrated with others in Kim et al. [48], exhibit large pulses during the flagellum synthesis. For this reason, the flagellar system is a good system to characterize the effect that large pulses on protein synthesis have on cellular growth.

As briefly described in Chapter 1, the promoters that control flagellar genes show sharp bursts of activity followed by long periods with no activity that can extend across several cell divisions. The flagellar system consists of three classes of promoters that activate and control flagellar proteins' production in an organized way to coordinate the synthesis of the flagella [52], as illustrated in Fig.5.1. The class-1 promoter *flhDp* regulates the expression of the proteins FlhD and FlhC, which together form a macromolecular complex $FlhD_4C_2$, also called the master regulator of the system. $FlhD_4C_2$ governs the activation of the class-2 promoters that control the expression of the genes for the flagellar hook and basal body. One of the class-2 promoters controls the production of the protein FliA that mediates the expression of the class-3 genes for the filament synthesis and motor elements that power the flagellum rotation.

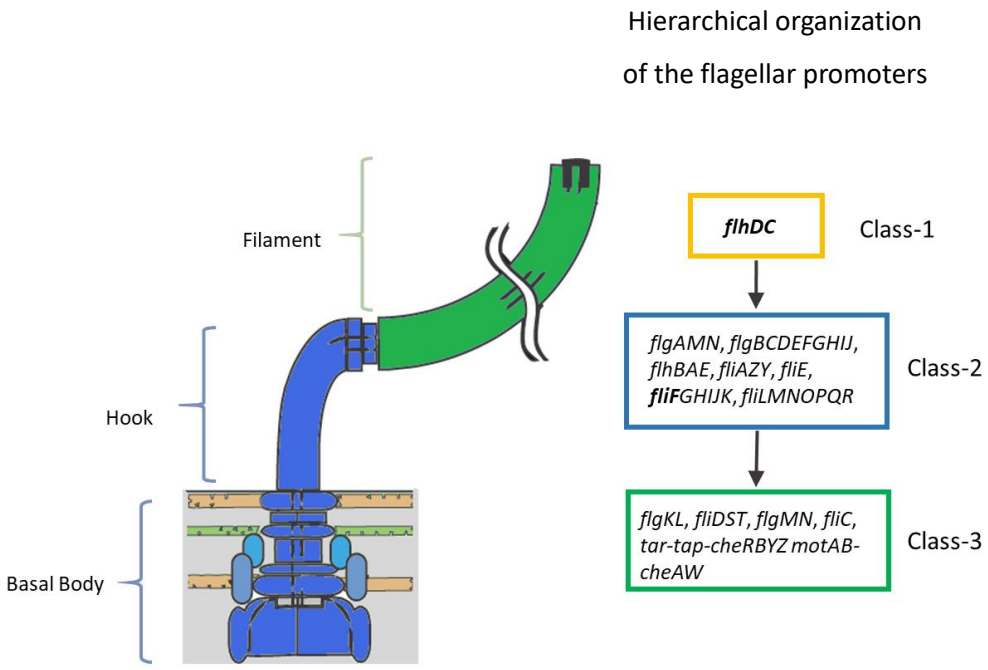

Figure 5.1 The diagram indicates the main components of the flagellum of *E. coli*. The organized activation of flagellar promoters coordinates the assembly of the different elements. There is a class-1 promoter, *flhDp*, the master regulator of the system and regulates the class-2 promoters, which controls the genes that encode the basal body and hook's molecular elements. *fliA*, a class-2 gene, encodes the sigma factor FliA, which drives the transcription of the class-3 operons. The class-3 operons encode products needed in the late flagellar assembly, such as the proteins that integrate the filament and the motor's components.

Although the master regulator $FlhD_4C_2$ governs the class-2 promoters' expression, the observed pulses of the class-2 are not deterministically determined by temporal variations of the class-1 promoter activity. We proposed in [56] a model in which another non-flagellar protein, YdiV, sequesters the master regulator $FlhD_4C_2$. YdiV serves as a filter that eliminates small-amplitude $FlhD_4C_2$ fluctuations and integrates over time fast fluctuations, creating intermittency in the class-2 expression. For this reason, the activity in class-2 presents pulses even when the class-1 promoter exhibits steady dynamics similar to that of a constitutive (i.e., unregulated) promoter.

Particularly, the synthesis of flagella represents a high energetic cost for the bacterium as refs. [54, 55] established at a population level. For instance, using competition experiments, it has been demonstrated that a population of cells that do not produce flagella (strain with the master regulator

genes deleted, ΔflhDC) grows faster than a population that synthesizes flagella [55]. Besides, flagella are composed of dozens of proteins whose assembly requires the expression of more than 50 different genes that manage the logistics of component production [51, 52, 53].

Because of the high burden that flagellar protein synthesis represents on populations of cells, we can expect it to affect the bacteria's cell growth. However, since its synthesis has pulse-like dynamics, it is unclear how it will be affected over time: how do size, elongation rate, and division time change and respond to pulses of the flagellar promoter activity?

To investigate this question I monitored single cells of the strain DCF (the description of the strain construction is in Chapter 2.2) growing under stable conditions in the mother machine. The DCF strain reports the activity of the class-1 promoter *flhDp* with the yellow fluorescent protein.

In previous chapters, I analyzed the growth of strains with different levels of steady synthesis of unnecessary proteins. In contrast, here, I explore the effect on the growth of temporal fluctuations of protein synthesis within the same strain.

I found some noticeable changes in the cell's physiology associated with the flagellar expression. The cell size and elongation rate increase with the (flagellar) protein expression while division time decreases.

Interestingly, the relation between protein expression and elongation rate and the division time is contrary to the relation of the mean values across strains. As seen in past chapters, a population of a strain with high protein production has, on average, a slower growth (and longer division time) than another population with a lower protein expression. As I will show in this chapter, for individual cells, when there is a higher expression of unnecessary protein, the cells grow more and faster.

Studying the time series of individual cells also revealed a shift in elongation rate respect to the promoter activity: the elongation rate increase precedes the expression pulses. This observation then challenges the notion of the growth rate changing as a direct consequence of the protein production pulses.

5.2 Pulsating behavior in the synthesis of flagellar proteins

As mentioned above, under certain conditions, *E. coli* synthesizes flagellar proteins with pulse-like dynamics. I constructed the DCF strain to monitor such activity, which expresses two fluorescent proteins, Venus and CFP, controlled by the class-1(*flhDp*) and class-2 (*fliFp*) flagellar promoters, respectively. Contrary to the ProVenus strains, which I analyzed in previous chapters, in DCF we are interested in the correlation between the production of flagellar proteins and growth, while the fluorescent proteins serve to report the activity of the flagellar promoters.

While the CFP total fluorescence does not represent the amount of all class-2 flagellar proteins, the derivative of the fluorescence does measure the promoter activity of the class-2 promoter *fliFp*. Besides, since all class-2 promoters have synchronous activity, we consider the calculated promoter activity for *fliFp*, a robust proxy for the activity of all class-2 promoters.

Fig.5.2a shows an example of various time traces of the DCF strain. At the top is the total fluorescence controlled by the class-1 (yellow) and class-2 (blue) promoters, and in the middle the promoter activity for both classes, $PA_{class-1}$ and $PA_{class-2}$, is shown. These plots show that the class-1 promoter activity does not vary much over time compared to the variation of class-2 activity, which shows the pulse-like behavior we reported in [48] — periods of high activity followed by periods of no activity.

In Fig.5.2a bottom, I plotted the area of a cell lineage (the track of a mother cell over time). The green points correspond to the measured area of the cells. The gray curves show the best exponential fit to the area of each cell (we used the function $S(t) = S_b 2^{\alpha t}$). Each discontinuity corresponds to an event of cell division, indicated by the vertical lines in the three panels of Fig.5.2a. It can be observed that the pulses can last longer than one cell generation.

a)

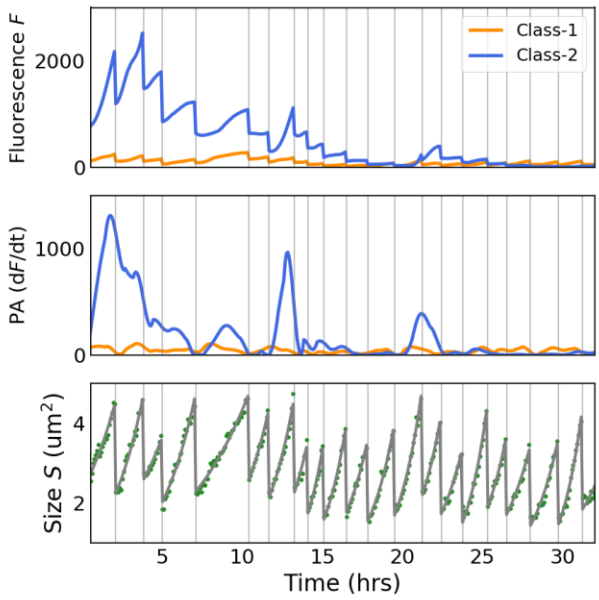

b)

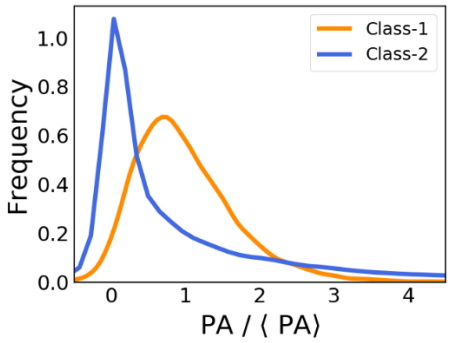

Figure 5.2. a) Time series corresponding to a cell lineage from the strain DCF, which has fluorescent markers for the class-1 (yellow) and class-2 (blue) flagellar promoters. The top panel shows the measured fluorescence as a function of time. The middle pannel shows the calculated Promoter Activity, PA, smoothed using the Savitzky–Golay filter. The bottom pannel displays the measured size (surface area, green dots) and the best exponential fit to the points for each cell (gray curves). b) Distribution of class-1 and class-2 Promoter Activities for cells of the DCF strain. Both distributions are rescaled by the respective mean of the population. They correspond to the measurements of 50 lineages, tracked by ~47 hours.

There are noticeable differences in the class-1 and class-2 promoter activity distributions for many mother cells, as can be seen in Fig.5.2b which shows the promoter activity normalized by its mean to facilitate the comparison between the class-1 and class-2 distributions. $PA_{class-2}$ has a long tail on the right, corresponding to the pulses, with a mean $\mu_2 = 197.35$, coefficient of variation CV_2=1.50 and skewness $\tilde{\mu}_{3_2}$=2.44. On the other hand, class-1 shows a distribution with mean $\mu_1 = 46.87$, coefficient of variation CV_1=0.682 and skewness $\tilde{\mu}_{3_1}$=0.95.

Class-1 and class-2 promoter activities are dynamically different: the autocorrelation function for class-1 activity decays sharply, while class-2 decays slowly, showing longer correlation times, as shown in Fig.5.3a. In other words, the class-1 signal loses the memory from its past states faster than that of class-2. This difference in the dynamics of the two classes indicates that the class-2

pulses are not a direct consequence of the transcription or translational regulation of *flhDC,* the class-1 regulator.

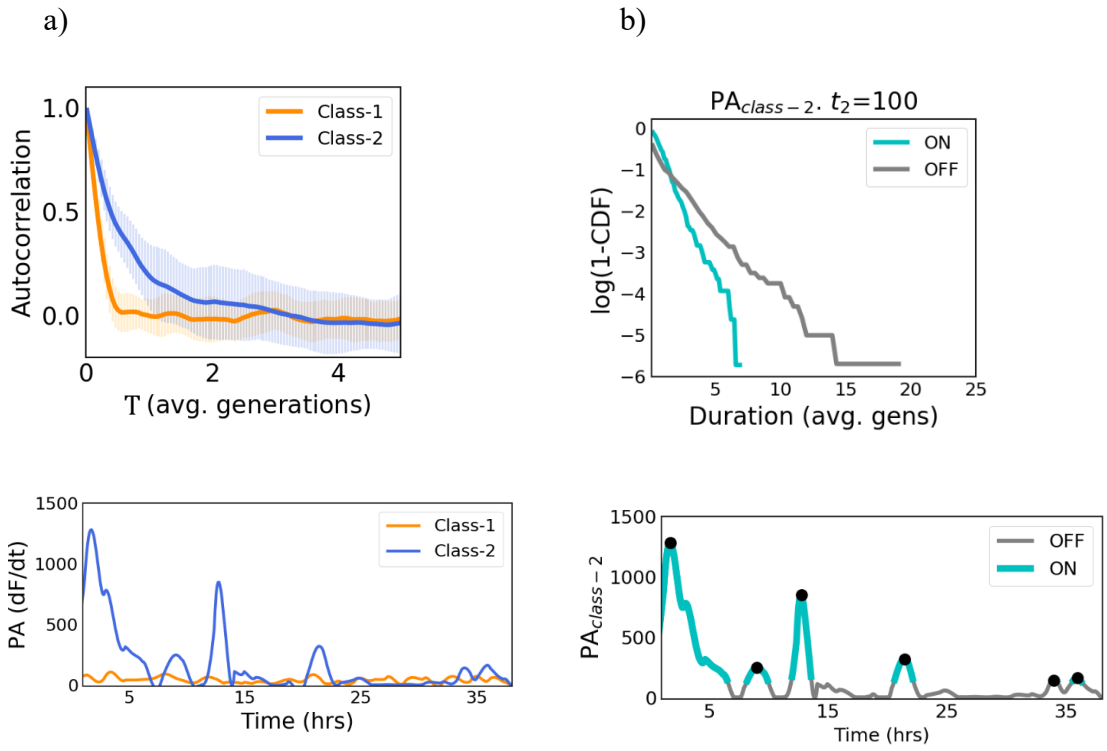

Figure 5.3. a) Normalized autocorrelation function of the flagellar promoter activity of class-1 (yellow) and class-2 (blue) time series. At the bottom, an example of a lineage time series with the same color cod is shown. For each promoter, I estimated the autocorrelation from 50 lineages, each at least 30 generations long. b) Cumulative distribution of the ON (cyan) and OFF (gray) durations of the class-2 promoter activity $PA_{class-2}$ plotted as log(1 − CDF). Below is the $PA_{class-2}$ series of a lineage with the same color code, for the ON and OFF states, defined by the threshold $t_2 = 100$.

I defined a pulse by considering a fixed threshold t_2 such that when $PA_{class-2}$ is above it, the system is 'ON' and below it, the system is 'OFF'. We set the threshold by taking the mean of the derivative of the autofluorescence (the natural emission of the cells, which is not controlled by any promoter) plus two standard deviations. Any signal below the threshold corresponds to zero promoter activity of the cells. The duration of the class-2 ON and OFF state are approximated by exponential distributions, with mean values $\mu_{ON} = 1.4$ and $\mu_{OFF} = 2.1$, respectively. The cumulative distribution of the ON and OFF state duration is represented in Fig.5.3b as the

logarithm of 1-CDF (Cumulative Distribution Function), showing longer periods of inactivity than the pulses' duration.

Class-2 promoters display activity in pulses with different amplitudes and different periods, and the periods of no activity have on average a longer duration than the ON states. Thus, this experimental system is well suited to study the effects of temporal fluctuations of protein synthesis on the cell growth parameters, such as cell size, elongation rate, etc., as I will present in the following sections.

5.3 Correlation between class-2 flagellar protein production and cell size

To characterize the relationship between the synthesis of flagellar proteins and cell size, I sorted all the cells of the CDF strain by their size at birth S_b in equally spaced bins. Then, I calculated the mean promoter activity of the class-1 and class-2 promoters within each bin. Fig.5.4a indicates the mean promoter activity rescaled by its mean as a function of the mean rescaled cell size S_b.

This plot allows us to see that cells with different sizes have a similar class-1 promoter activity (orange circles) as can be seen from the close to the zero-slope of the orange line. There is a noticeable difference in the class-2 promoter (blue circles). The relationship between size and promoter activity has a greater slope than for class-1; cells that are smaller at birth also have low promoter activity than larger cells at birth.

As a reference, I plotted in Fig.5.4a the relationship between size and the activity of the constitutive promoter Pro4, which controls the steady expression of the fluorescent protein Venus (from the strain Pro4Venus analyzed in previous chapters). This Pro4 strain does not pulse, and the slope of the size versus promoter activity nears zero.

Variations in the class-2 protein synthesis have a stronger correlation with the cell size than for the class-1 proteins. While the class-1 promoter involves the synthesis of only two different class-1 proteins, several class-2 promoters synchronously control the expression of many more proteins, therefore more mass is associated with increments in the class-2 activity.

As we can see in Fig.5.4b, for low values of the class-2 promoter activity, (lower than $PA_{class-2} = 100$), S_{birth} does maintain similar values. However, as $PA_{class-2}$ increases, (which corresponds to the cells during pulses), the cell size also increases.

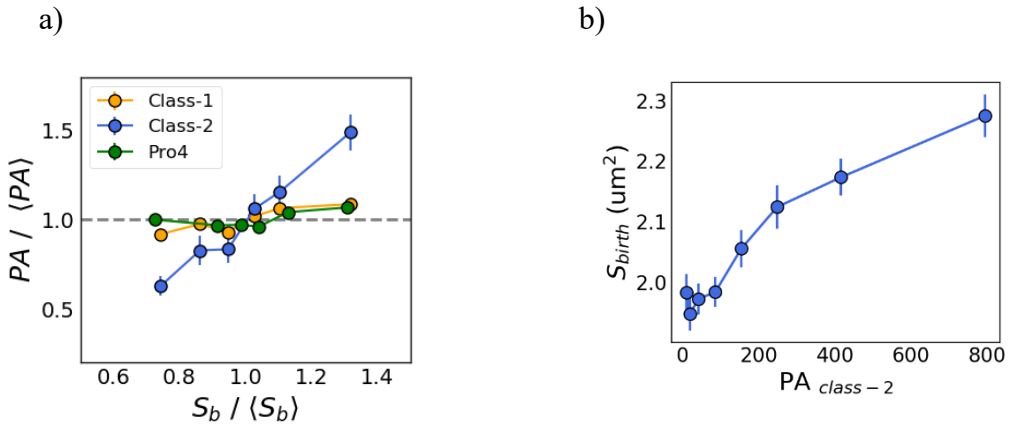

Figure 5.4. a) Mean of the normalized flagellar class-1 (orange) and class-2 (blue) promoter activity, PA, as functions of the binned cell size at birth, S_{birth}, rescaled by their mean. The green data points correspond to the Pro4Venus strain, which has a constitutive promoter Pro4 that controls the expression of Venus (see chapter 4). b) Mean size at birth for equally spaced bins of the class-2 promoter activity, $PA_{class-2}$.

To visualize the variations in cell size during the pulses, I divided the time traces into peak-to-peak intervals that include a peak of a pulse, the following OFF state, and the next pulse, as exemplified in Fig.5.5a. Then, I organized the intervals into two distinct families whose durations are either within 3-5hours or 5-8hours. Finally, I rescaled each interval's duration so that they all start at 0 and end at 1.

I show the average of the peak-to-peak intervals for the $PA_{class-2}$ that originally has a duration between 3-5 hours (blue) and 5-8 hours (gray) in the top panel of Fig.5.5b, and below it, the cell size $S(t)$ for the same intervals.

The average size displays some fluctuations, which are similar for the two sets of intervals. There are peaks at the beginning and end of the curves that coincide with the peaks of the $PA_{class-2}$, indicating their positive correlation on time. Nevertheless, there are two other peaks during the OFF state for which we do not have a biological explanation. However, we speculate it might be

related to the activation of the class-3 genes. Further analysis and experiments are needed to understand this.

To better understand the relation between cell size and class-2 activity, I calculated the cross-correlation between the size S(t) and the $PA_{class-2}(t)$. In Fig.5.3, in gray is the cross-correlation between the time series $S^i(t+\tau)$ and $PA^i{}_{class-2}(t)$, for different time lags τ, for each cell lineage i. The lag τ refers to how far the series are offset, and its sign determines which series is shifted. Then, the correlations in Fig.5.3 shows the similarity of the time series in different times. In blue is the average correlation over the cells, which has a maximum value at lag zero.

From the cross-correlation of each mother I obtained the lag that corresponds to the higher correlation, the lag at which there is a higher similitude between S(t) and $PA_{class-2}(t)$. The histogram of the lags is in Fig.5.5b, and shows that there is a higher statistical correlation between $PA_{class-2}$(t) and S(t) when the latter has a zero and positive delay smaller than 25 minutes, relative to $PA_{class-2}(t)$.

We conclude that the changes in size occur in a time immediately after the pulses. When a single cell has a class-2 pulse, it triggers the production of flagella proteins resulting in an immediate increase in cell mass simply because of the addition of new proteins, the flagellar proteins.

Once the production is decreased or stopped, the cell starts reducing its size as the flagellar proteins get diluted after cell division, exported out of the cell, or degraded.

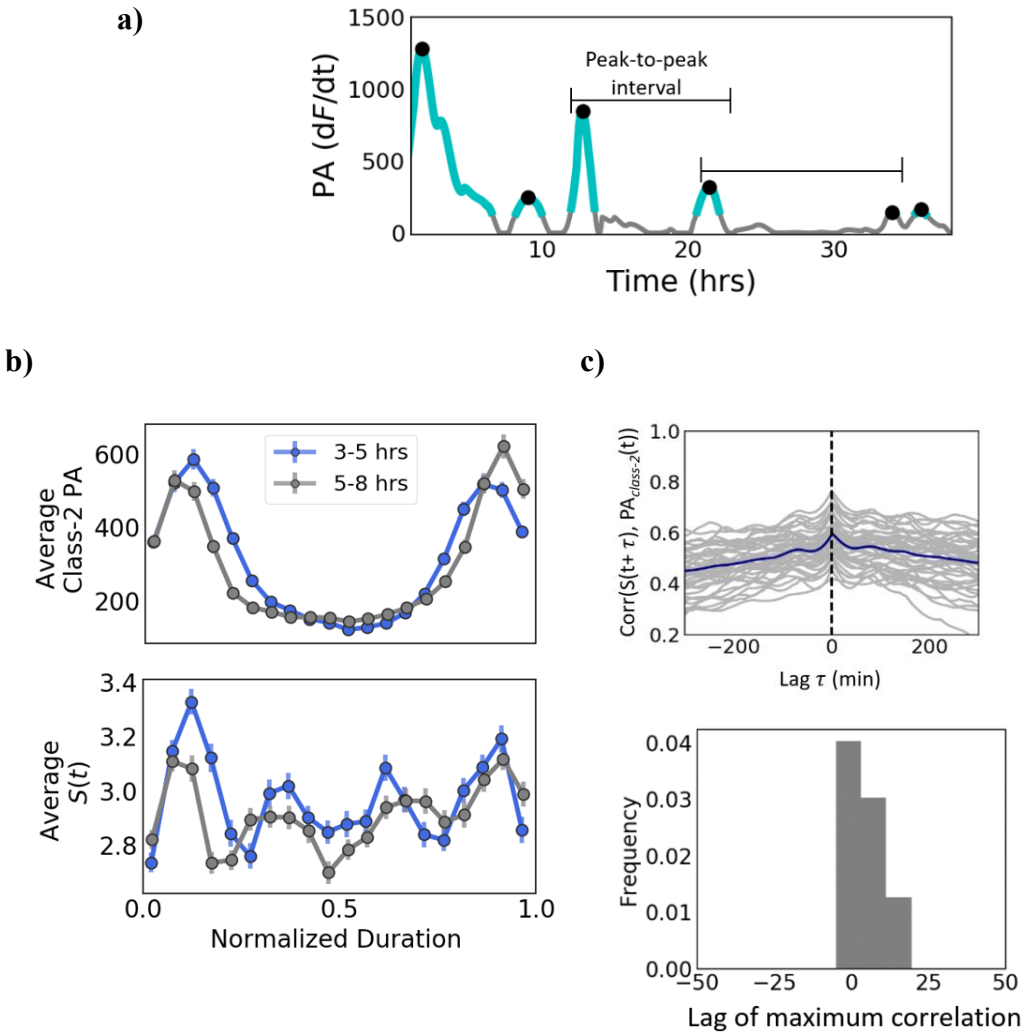

Figure 5.5. a) Each peak-to-peak interval was rescaled to have a duration from 0 to 1. The top panel shows the average of $PA_{class-2}$ of such intervals that originally had a duration between 3-5 hours (blue) and 5-8 hours (gray). At the bottom is the average of the area at birth S_{birth} corresponding to the same peak-to-peak intervals. I computed the averages by dividing the normalized time into evenly spaced intervals. c) top: In gray is the cross-correlation between $PA_{class-2}(t)$ and size $S(t+\tau)$ for many cell lineages, and in blue is the average for each lag τ. Bottom: histogram of the lags corresponding to the maximum correlation per each lineage from the top panel.

5.4 Correlation between class-2 flagellar protein production and elongation rate

The average elongation rate of a population decreases when forced to increase the number of unnecessary synthetized proteins [11, 13]. As discussed in Chapter 3, when the fraction of

unnecessary proteins increases, the resources invested in its synthesis are "taken away" from being used on other proteins needed for cell growth (principally ribosomal proteins).

However, as I showed in Chapter 4, single-cells of a population have a weak correlation between elongation rate and the number of unnecessary proteins, when its expression is constitutive.

Here I analyze elongation rate as a function of class-2 promoter activity in individual cells of the DCF strain. In Fig.5.6, I show the mean elongation rate α over cells of different equal-sized groups of the population selected by their value of class-2 promoter activity. The plot shows that the elongation rate and the promoter activity are positively correlated. Also, the Pearson's correlation coefficient between them is $R(\alpha, PA_{class-2}) = 0.287$. By contrast, the class-1 activity showed a weak correlation, $R(\alpha, PA_{class-1}) = 0.081$.

To compare with the behavior of cells that have a constitutive expression, in Fig.5.6 (in brown) is displayed the elongation rate as a function of the binned activity corresponding to the Pro4Venus strain. Similar to the flagellar promoter, the constitutive expression of the unnecessary protein Venus has a positive correlation with α.

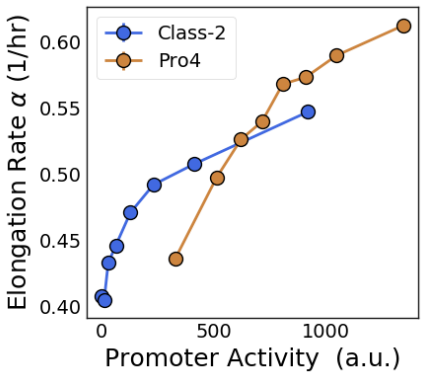

Figure 5.6. Individual cells of the DCF strain were grouped as depending on their class-2 promoter activity in 7 equally sized groups. In blue is the mean elongation rate of each bin as a function of the mean promoter activity. Similarly, the brown markers correspond to the mean elongation rate as a function of the mean activity of the constitutive promoter Pro4 in the Pro4Venus strain.

An interesting observation is that while the mean growth rate of a population of cells is negatively correlated with the mean value of the unnecessary protein expression across strains, at the single

cell level (Fig.3.14), for one strain the correlation among such variables is positive (as demonstrated in Fig.5.6).

Generally, the activity of a promoter describes the rate of synthesis of the protein it controls, while the elongation rate α measures the rate at which a cell grows or acquires its mass. Since the cell's mass is composed ~95% of proteins (which includes the flagellar proteins) [11], α is affected by the synthesis rate of its different proteins. Therefore, both α and promoter activity (constitutive or flagellar promoter) depends positively on the synthesis capacity of the cell, which in turn depends on the ribosomal protein R. I interpret the relations in Fig.5.6 as reflecting the elongation rate and promoter activity dependence on the ribosomal content.

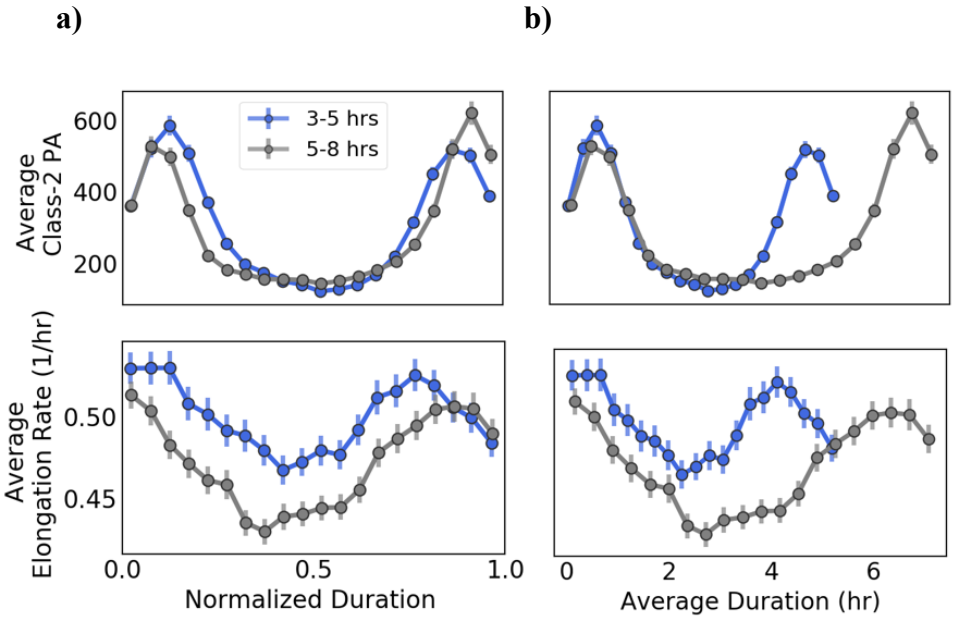

Figure 5.7. a) Average Promoter Activity of many peak-to-peak intervals that were rescaled to have a duration from 0 to 1. The averages include intervals that originally lasted between 3 and 5 hours (blue curves) and 5 to 8 hours (in gray). At the bottom is the average of the elongation rate for the same rescaled intervals. b) Same averages as in a) but with the x-axis multiplied by the intervals' average duration. I computed all averages by dividing the normalized time into evenly spaced intervals. The number of peak-to-peak intervals on each group is 84 and 72 for 3-5 hrs and 5-8 hrs, respectively.

To relate α with the actual pulses of $PA_{class-2}$ I present in Fig.5.7a the average $PA_{class-2}$ (at the top) and the average α (at the bottom) over the binned peak-to-peak intervals (same interval groups

as in Fig.5.5b). The mean α over time presents a similar shape than $PA_{class-2}$: α is high during the average of the is first peaks, it decreases when the $PA_{class-2}$ is OFF, and then increases again around the same time as the average of the second peak. As can be seen in Figure 5.5, the α time-series is shifted to the left when compared to that of $PA_{class-2}$, and contains broader 'peaks'.

In Fig.5.7b, I show the same intervals as in the left, but with the normalized duration multiplied by the mean of the original duration of each group's intervals. With such transformation, it is easier to observe that there is more decrease in the elongation rate in the curve corresponding to 5-8 hours. A possible interpretation is that as more time passes after a pulse, the cell has more time to "relax" and reach a steady elongation rate before it increases again.

From Fig.5.7 it can be observed that the first maximum of the elongation rate precedes the promoter activity's first peak. To verify this, in Fig.5.8a in gray, I show the cross-correlation between the $PA_{class-2}$ and α, Corr$(\alpha(t+\tau), PA_{class-2})$, as a function of the time lag τ for various time series, each corresponding to a cell lineage. In blue is the average of the correlation for each lag. The maximum of the average correlation is at a lag time of -20 minutes. In Fig.5.8b is the histogram of the lags with maximum correlation for all the lineages, which shows that the lag with higher frequency is 25±5 minutes. In other words, there is a greater similarity of $PA_{class-2}$ time-series with the elongation rate shifted ~20 minutes negatively. On average, the cells' elongation rate changes before the synthesis of class-2 proteins.

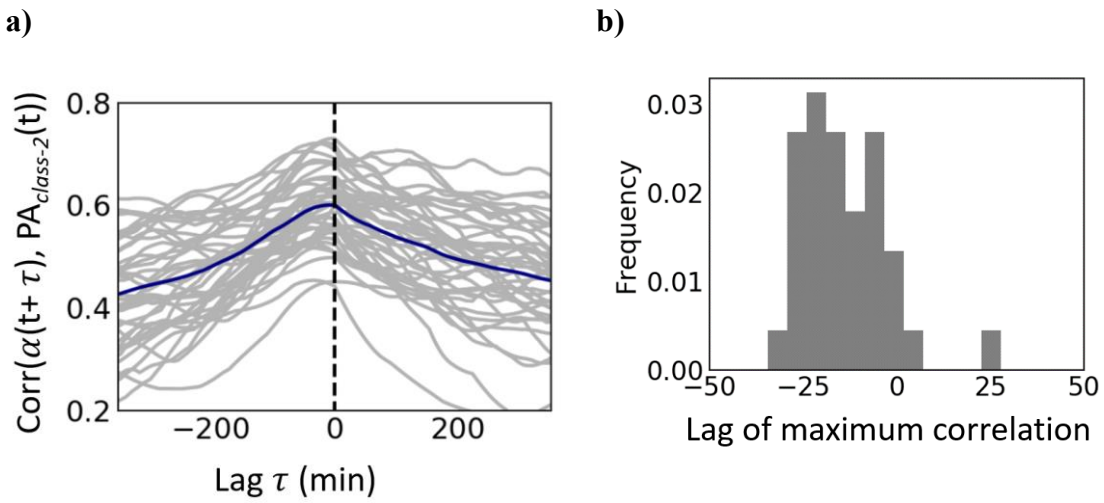

Figure 5.8. a) Cross-correlation between the class-2 prompter activity $PA_{class-2}$ and the elongation rate α, $\mathrm{Corr}(\alpha(t+\tau), PA_{class-2}(t))$ as a function of the time lag τ, for many lineages (gray) and the average per lag (blue). The dashed vertical line is placed at lag $\tau = 0$. The maximum value of the average correlation corresponds to lag $\tau = 20$min. **b)** Histogram of the lags that correspond to the maximum value of each cell lineage's correlation in a). The lag with a higher frequency is -25 minutes.

This result is unexpected for us since it goes against the scenario in which the sudden increase in class-2 protein synthesis is the cause of the change in the elongation rate.

More experiments are necessary to elucidate if the mechanism by which cells modify the elongation rate previous to a pulse of protein production is inherent to the flagellar system or if, in general, cells "prepare" for a sudden perturbation on the proteome.

To consider the effect of the amplitude of the class-2 pulses, I sorted all the intervals of the promoter activity series that presented a pulse into three equally sized groups by amplitude. Each interval starts at the begging of a pulse and lasts all the subsequent OFF state before a second pulse appears. I aligned the series of each group so that the maximum pulses match into the same timepoint and then calculated the average of the promoter activity at each time (see Fig.5, left). For those same groups, I calculated the mean of the elongation rate, shown in the right panel, where the blue vertical line indicates the time point that corresponds to the maximum value of the promoter activity. By comparing these two plots, it is noticeable that the elongation rate is higher for the pulses with bigger amplitude. After that, for the three groups, there is a decrease in the elongation rate. Therefore, the elongation rate during the $PA_{class-2}$ also depends on its amplitude.

This result, reported in Fig.5.9, also shows that the elongation rate has memory since its value after a pulse will depend as well on the amplitude of the previous pulses.

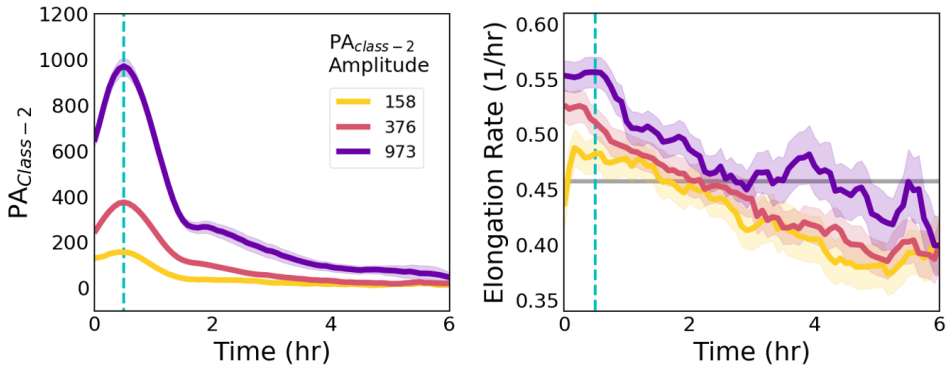

Figure. 5.9. Intervals containing a $PA_{class-2}$ pulse and the following OFF state are divided into three equally sized groups depending on the pulses' amplitude. On the left it is shown the average $PA_{class-2}$ for each group. The average elongation rate for the same four groups is plotted at the right, while the gray horizontal line marks the population's mean elongation rate. The color code corresponds to each group's level of promoter activity, and the label is the mean amplitude of the pulses. The shaded regions in each curve show the respective standard deviation at each time point for each group. The vertical dashed line corresponds to the time of the maximum value of the promoter activity, to which all peaks were aligned.

5.5 Correlation between class-2 flagellar protein production and division time

There are also changes in division time related to the production of flagellar proteins. In Fig.5.10 in blue is the mean division time T_{div} as a function of the binned class-2 promoter activity, calculated from the DCF strain. They have a negative correlation, with a Pearson's coefficient of $R(T_{div}, PA_{class-2}) = -0.228$. Class-1 activity had a very weak correlation with T_{div} with a coefficient $R(T_{div}, PA_{class-1}) = -0.061$ (not include it in the plot). Similarly, in brown is the mean T_{div} as a function of the binned activity of the constitutive promoter Pro4, from the Pro4Venus strain. T_{div} also has a negative correlation with the constitutive promoter activity, with a Person's coefficient $R(PA_{Pro4}, T_{div}) = -0.351$.

Fig.5.11a shows the average class-2 promoter activity (top panel) and the average division time (bottom panel) of the peak-to-peak intervals as a function of the normalized duration. Same interval groups as in Fig.5.7, one with a duration of 3-5 hours and the other of 5-8 hours. The figure

shows a negative correlation between the division time T_{div} and the promoter activity $PA_{class-2}$ during the pulses and the OFF state.

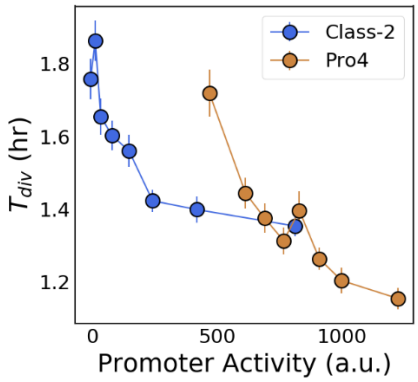

Figure 5.10. Division Time T_{div} as a function of the binned promoter activity of the class-2 promoter measured from DCF strain (blue markers), and constitutive promoter Pro4 from Pro4Venus strain (brown markers). The number of DCF cells is 1388, and 937 of the Pro4Venus. The bins are equally sized, and the error bars show the standard error for each bin.

In Fig.5.11b, the same averages as in (a) are plotted, but the normalized duration is multiplied by the mean duration of each group's interval in order to illustrate the difference in the average of the intervals depending on the duration between peaks. It is noticeable that the average division time is longer when there is a longer duration between peaks (for the intervals from 5-8 hours), as if due to the fact that there is a longer OFF duration after a peak, the cells keep adjusting the T_{div} to be longer.

In Chapter 4, I showed a negative correlation between the division time and the number of unnecessary proteins of cells at birth grow (Fig.3.). We proposed a positive correlation between the synthesis of unnecessary proteins U and division proteins X, assuming cells divide after accumulating X until a fixed threshold is reached. In this way, when there is a high production of U proteins, there is an increased synthesis of X proteins, and cells divide faster than when there is a lower synthesis of proteins.

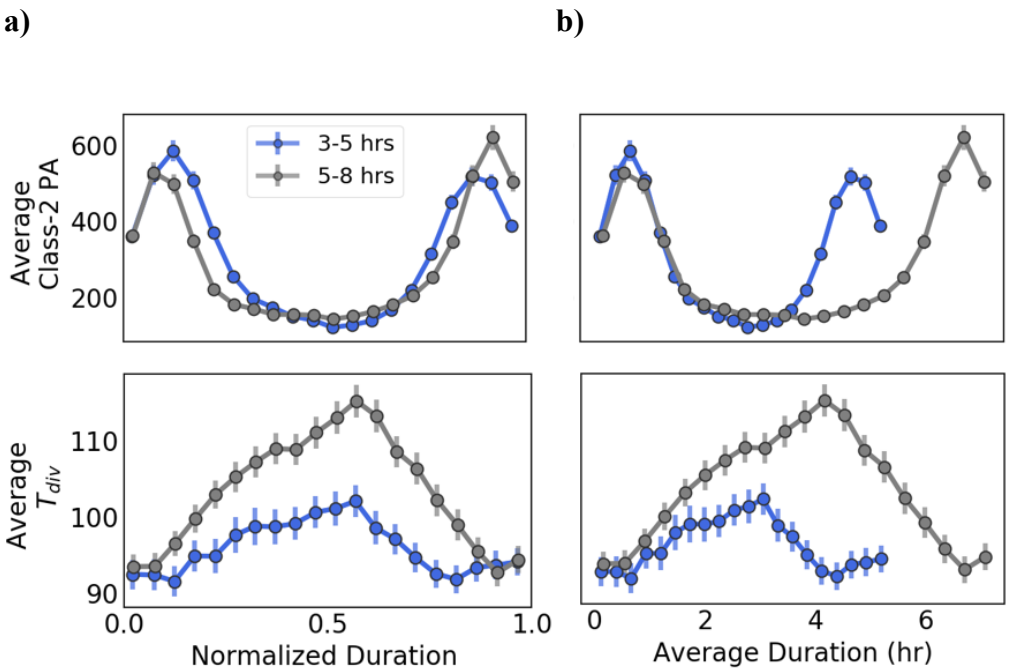

Figure 5.11. a) Peak-to-peak intervals of $PA_{class-2}$ (Fig.5.6a) were rescaled to have a maximum duration of one and averaged over small-time windows. This was done for two groups of intervals, lasting between 3 and 5 hours (blue), and t 5 to 8 hours (gray). The bottom panel shows the average of the division time T_{div} corresponding to the same intervals. b) Same averages as in (a), but the x-axis is multiplied by the mean duration of each group's intervals. The number of peak-to-peak intervals on each group is 84 and 72 for 3-5 hrs and 5-8 hrs, respectively.

Here, in Fig.5.11 and 5.12, I show a negative correlation between $PA_{class-2}$ and T_{div}, also implying a positive relationship between the rate of synthesis of class-2 proteins and X protein synthesis.

It is important to mention that the X and class-2 protein synthesis have different dynamics. The flagellar protein synthesis is coordinated by a complex molecular mechanism involving other flagellar proteins. In contrast, the X proteins might be constitutively expressed [11, 45].

Nonetheless, this analysis demonstrates that both proteins respond to a similar process, probably at the transcriptional or translational level, involving the number of available ribosomal proteins in a cell over time.

5.6 Discussion

In this chapter I presented an analysis of the variation in the parameters that characterize single cell growth (size, elongation rate, and division time) while they produce flagellar proteins with pulse-like dynamics. I performed a single-cell experiment in which I monitored the growth parameters and the activity of the flagellar class-1 and class-2 promoters of *E. coli* over many lineages. As reported in [48], we found that, while the activity of the class-1 flagellar promoter presents a steady expression over time, the class-2 promoters have pulse-like dynamics.

The analysis described in this chapter indicates that the cells exhibit variations in the cell parameters that correlate with the flagellar promoters' activity, particularly with class-2. The correlations between the flagellar promoters' activity and growth parameters (cell size, division time, and elongation rate) are similar as in the case when cells overexpress the unnecessary proteins Venus with the promoter Pro4. While Pro4 is a constitutive promoter, the flagella promoters are involved in a complex system that coordinates the flagella's assembly and functioning. Nevertheless, in both cases, cells are bigger when they synthesize more proteins; the synthesis rate is positively correlated with the elongation rate and negatively correlated with the division time.

The similarity in the correlations between the promoter activity and cell parameters suggests an upstream mechanism that both Venus and class-2 proteins are subjected to, probably in the transcription and translation processes. For instance, the elongation rate and the promoter activity will respond to fluctuations in the number of ribosomes since both directly involve protein synthesis. In the same context, the relation between promoter activity and division time makes sense when assuming that cells divide when they accumulate a division protein up to a fixed threshold (chapter 4, Fig.4.1). The division proteins and class-2 protein synthesis should be positively correlated due to their dependence on ribosomal proteins, thus leading to the negative correlation between the division time and the class-2 promoter activity.

At first sight, these results challenge the scenario that, if cells produce unnecessary proteins, there will be a cost on growth (a slower elongation rate), which is what happens at a population level. Here, we observe the opposite at the single-cell level: when the unnecessary protein synthesis increases, the elongation rate and division frequency increase as well.

However, this discrepancy can be reconciled with previous observations by considering that regardless of the level of unnecessary protein production of a certain strain, the ribosome content

of individual cells positively correlates with elongation rate and protein synthesis. When comparing strains, the average ribosome concentration in cells is lower for the population that produces the more unnecessary protein, so the average elongation rate and synthesis capacity decreases (as discussed in chapter 3). It is important to mention that I am considering populations of bacteria that have already reached a steady-state, namely, populations that have adapted to an optimal proteome configuration.

By studying the pulses in individual cells, I analyzed the cell growth response over time. We found that there are big variations in elongation rate, similar to the class-2 promoter activity pulses, but preceding the latter. This result is surprising since it goes against our notion that the elongation rate changes due to the sudden class-2 expression.

Nevertheless, the increase in elongation rate preceding the class-2 promoter activity pulses may reflect the synthesis of other proteins involved in the flagellar system prior to class-2 expression—for example, the synthesis of the protein YdiV, which sequesters the class-1 complex $FlhD_4C_2$ and prevents the activation of class 2 promoters [47, 53, 54, 55]. These results also demonstrate the dependence of flagella production on the cell's intrinsic processes since the correlation between the flagellar pulses and cell parameters can be described with the interactions between flagellar, ribosomal, and division proteins.

In the future, I would like to discriminate if the change in elongation rate before the production of proteins is a specific phenomenon to the flagellar system or if it is related to a general process in the production of any protein. I could address this question by performing experiments to monitor individual cells while artificially inducing the synthesis of an unnecessary protein, such as Venus. This would have a directed protein production, unlike the flagellar proteins, which are part of a complex system that involves several different flagellar proteins. Besides, this suggested experiment would allow us to control the fraction of unnecessary proteins that cells accumulate before they reach steady-state, allowing me to study the transition between the single-cell and population trends.

Although there are still many questions left unanswered, the results presented here describe, for the first time, the growth of single-cells over time when they are subject to sudden protein production. This is an important first step to understand the mechanism of allocation of resources among different protein sectors.

Appendix 1. Microfluidic master fabrication

New designs for the microfluidic device were created in AutoCAD; generally, it consists of two layers, one for the cell channels and a second one for the feeding channels. The cell channels were 1.1μm wide and 25μm long. The edges of the channels were smoothed out to reduce the halo that appears during phase-contrast imaging. We also added a trough at the boundary where the cell channels meet the feeding channel so that the phase contrast halo from the feeding channel does not affect the imaging of the cells inside the channel (Fig.2.6). The feeding channels were 8.1mm long and 100μm wide.

Fabrication of the master mold was carried out using standard UV photolithography in a clean room environment at the Center for Nanoscale Systems at Harvard University. We modified the fabrication procedure from the method described in [24] by exposing the SU-8 using a Heidelberg MLA150 Maskless Aligner (Heidelberg Instruments). The MLA150 enabled us to directly "print" our AutoCAD designs without a mask and often resulted in more accurate printing of smaller features.

To print the microfluidic device master, we used the following protocol. The spin coating parameters shown below are written using the abbreviation: speed (rpm)/acceleration (rpm/sec)/time (sec):

1) First layer: cell channels.

a. Place a 3″ wafer at a spinner and rinse it by adding acetone and isopropyl alcohol (IPA) while it is spinning.
b. Let the wafer dry for 15 minutes on a hotplate at 200°C.
c. Let the wafer cool down for a few minutes and place it on a spin chuck.
d. Slowly pour SU-8 2002 until it covers ~2/3 of the wafer. Here, avoid any bubbles in the resist since even small bubbles can distort the cell channel.
e. Spin the wafer using the program: Step 1: 500/100/10, Step 2: 3500/300/60.
f. Bake the wafer for 1 min at 65°C, 1 min at 95°C, 1 min at 65°C.

g. Expose the wafer with the cell channel design using the MLA150 with a dosage of 2500 mJ/cm2. In our cell channel design, we also include cross-shaped marks which will serve as alignment marks during the exposure of the feeding channel layer.
h. After exposure in the MLA, bake the wafer for 1 min at 65°C, 1 min 95°C and 30 seconds at 65°C.
i. Gently immerse the wafer in a SU-8 developer.
j. Bake the wafer for 15 minutes on a hot plate at 150°C ("hard bake" step).
k. Measure the channel height using a profilometer. The expected high is ~1.2µm.

2) Second layer: feeding channels.

a. Place the wafer with the cell channels on a spin chuck.
b. Slowly pour SU-8 2010 photoresist on the wafer covering ~2/3 of its area.
c. Spin the wafer using the program: Step 1: 500/100/10. Step 2: 3000/300/60.
d. Bake it using hot plates for 1 min at 65°C, 2 min 95°C and 1 min at 65°C.
e. Use cotton swabs soaked with propylene-glycol-methyl-ether-acetate (PGMA) to wipe SU-8 off from the region of the wafer where the alignment crosses are printed.
f. Bake the wafer at 65°C for 1 minute.
g. Load the feeding channel design into the MLA. Place the wafer in the MLA and align the wafer by identifying the crosses using the cameras of the MLA. Once alignment is complete, expose with a dosage of 4500 mJ/cm2 and focus offset ("defoc") -2.
h. Once the design is exposed, bake the wafer at 65°C for 1 min, 95°C for 4 min and 65°C for 1 min.
i. Immerse the wafer in a container with PGMA and shake it very slowly for 1 min. j. Rinse the wafer with IPA to remove the remaining SU-8. k. Let the wafer hard bake at 150ºC for 15 minutes. l. Measure the feeding channel height using the profilometer. The expected height is ~11µm.

References

1. Donachie, W. D. (1968). Relationship between cell size and time of initiation of DNA replication. Nature 219, 1077–1079

2. Schaechter M., Maaloe O., Kjeldgaard N. (1958). Dependency on medium and temperature of cell size and chemical composition during balanced grown of Salmonella typhimurium. J Gen Microbiol, 19:592-606.

3. Helmstetter CE (1968) DNA synthesis during the division cycle of rapidly growing Escherichia coli B/r. J Mol Bio, 31:507-518.

4. Scott, M., & Hwa, T. (2011). Bacterial growth laws and their applications. Current Opinion in Biotechnology, 22(4), 559–565.

5. Koppes, L. J. H., Meyer, M., Oonk, H. B., Jong, M. A. D. E., & Nanninga, N. (1980). Correlation Between Size and Age at Different Events in the Cell Division Cycle of Escherichia coli, 143(3), 1241–1252.

6. Taheri-Araghi, S., Bradde, S., Sauls, J. T., Hill, N. S., Levin, P. A., Paulsson, J., … Jun, S. (2015). Cell-size control and homeostasis in bacteria. Current Biology, 25(3), 385–391.

7. Amir, A. (2014). Cell size regulation in bacteria. Physical Review Letters, 112(20), 1–5.

8. Willis, L., & Huang, K. C. (2017). Sizing up the bacterial cell cycle. Nature Reviews Microbiology, 15(10), 606–620.

9. Campos, M., Surovtsev, I. V., Kato, S., Paintdakhi, A., Beltran, B., Ebmeier, S. E., & Jacobs-Wagner, C. (2014). A constant size extension drives bacterial cell size homeostasis. Cell, 159(6), 1433–1446.

10. Soifer, I., Robert, L., Amir, A., Soifer, I., Robert, L., & Amir, A. (2016). Single-Cell Analysis of Growth in Budding Yeast and Bacteria Reveals a Common Size Regulation Strategy. Current Biology, 26(3),

11. Basan, M., Zhu, M., Dai, X., Warren, M., Sevin, D., Wang, Y.-P., & Hwa, T. (2015). Inflating bacterial cells by increased protein synthesis. Molecular Systems Biology, 11(10), 836–836.

12. Scott, M., Gunderson, C. W., Mateescu, E. M., Zhang, Z., & Hwa, T. (2010). Interdependence of cell growth and gene expression: Origins and consequences. Science, 330(6007), 1099–1102.

13. Chevance, F. F., & Hughes, K. T. (2008). Coordinating assembly of a bacterial macromolecular machine. Nat Rev Microbiol, 6(6), 455–465.

14. Wang, P., Robert, L., Pelletier, J., Dang, W. L., Taddei, F., Wright, A., & Jun, S. (2010). Robust growth of escherichia coli. Current Biology, 20(12), 1099–1103.

15. Basan, M. (2018). Resource allocation and metabolism: the search for governing principles. Current Opinion in Microbiology, 45, 77–83. https://doi.org/10.1016/j.mib.2018.02.008

16. Volkmer B, Heinemann M (2011) Condition-Dependent Cell Volume and Concentration of Escherichia coli to Facilitate Data Conversion for Systems Biology Modeling. PLOS ONE 6(7): e23126.

17. Hill NS, Kadoya R, Chattoraj DK, Levin PA (2012) Cell size and the initiation of DNA replication in bacteria. PLoS Genet 8:e1002549

18. Marshall, W.F., Young, K.D., Swaffer, M., Wood, E., Nurse, P., Kimura, A., Frankel, J., Wallingford, J., Walbot, V., Qu, X., and Roeder, A.H.K. (2012). What determines cell size? BMC Biol. 10, 101.

19. Klumpp, S., & Hwa, T. (2014). Bacterial growth: Global effects on gene expression, growth feedback and proteome partition. Current Opinion in Biotechnology, 28, 96–102.

20. Bertaux, F., Kügelgen, J. Von, & Marguerat, S. (2016). A bacterial size law revealed by a coarse-grained model of cell physiology. 1–21.

21. Scott, M., Klumpp, S., Mateescu, E. M., & Hwa, T. (2014). Emergence of robust growth laws from optimal regulation of ribosome synthesis. Molecular Systems Biology, 10(8), 747.

22. Davis, J. H., Rubin, A. J., & Sauer, R. T. (2011). Design, construction and characterization of a set of insulated bacterial promoters. Nucleic Acids Research, 39(3), 1131–1141. https://doi.org/10.1093/nar/gkq810

23. Kennard, A. S., Osella, M., Javer, A., Grilli, J., Nghe, P., Tans, S. J., Cicuta, P., & Cosentino Lagomarsino, M. (2016). Individuality and universality in the growth-division laws of single E. Coli cells. Physical Review E, 93(1)

24. Kim, J., Darlington, A., Salvador, M., Utrilla, J., & Jiménez, J. I. (2020). Trade-offs between gene expression, growth and phenotypic diversity in microbial populations. Current Opinion in Biotechnology, 62, 29–37. https://doi.org/10.1016/j.copbio.2019.08.004

25. Peebo, K., Valgepea, K., Maser, A., Nahku, R., Adamberg, K., & Vilu, R. (2015). Proteome reallocation in Escherichia coli with increasing specific growth rate. Molecular BioSystems, 11(4), 1184–1193. https://doi.org/10.1039/c4mb00721b

26. Towbin, B. D., Korem, Y., Bren, A., Doron, S., Sorek, R., & Alon, U. (2017). Optimality and sub-optimality in a bacterial growth law. Nature Communications, 8, 1–8. https://doi.org/10.1038/ncomms14123

27. Yuichi Wakamoto, Jeremy Ramsden, and Kenji Yasuda, Single- cell growth and division dynamics showing epigenetic correla- tions, Analyst 130, 311 (2005)

28. Trueba, F. J., Neijssel, O. M., & Woldringh, C. L. (1982). Generality of the growth kinetics of the average individual cell in different bacterial populations. Journal of Bacteriology, 150(3), 1048–1055. https://doi.org/10.1128/jb.150.3.1348-1055.1982

29. Schaechter, M., Williamson, J. P., Hood, J. R., & Kochal. (1962). Growth, cell and nuclear divisions in some bacteria. Journal of General Microbiology, 29, 421–434. https://doi.org/10.1099/00221287-29-3-421

30. Wakamoto, Y., Ramsden, J., & Yasuda, K. (2005). Single-cell growth and division dynamics showing epigenetic correlations. Analyst, 130(3), 311–317. https://doi.org/10.1039/b409860a (adder)

31. Facchetti, G., Chang, F., & Howard, M. (2017). Controlling cell size through sizer mechanisms. Current Opinion in Systems Biology, 5, 86–92. https://doi.org/10.1016/j.coisb.2017.08.010 (slow growth adder deviation)

32. Iyer-Biswas, S., Wright, C. S., Henry, J. T., Lo, K., Burov, S., Lin, Y., Crooks, G. E., Crosson, S., Dinner, A. R., & Scherer, N. F. (2014). Scaling laws governing stochastic growth and division of single bacterial cells. Proceedings of the National Academy of Sciences, 111(45), 15912–15917. https://doi.org/10.1073/pnas.1403232111

33. Tanouchi, Y., Pai, A., Park, H., Huang, S., Stamatov, R., Buchler, N. E., & You, L. (2015). A noisy linear map underlies oscillations in cell size and gene expression in bacteria. Nature, 523(7560), 357–359. https://doi.org/10.1038/nature14562

34. Logsdon, M. M., Ho, P. Y., Papavinasasundaram, K., Richardson, K., Cokol, M., Sassetti, C. M., Amir, A., & Aldridge, B. B. (2017). A Parallel Adder Coordinates Mycobacterial Cell-Cycle Progression and Cell-Size Homeostasis in the Context of Asymmetric Growth and Organization. Current Biology, 27(21), 3367-3374.e7. https://doi.org/10.1016/j.cub.2017.09.046

35. Cadart, C., Monnier, S., Grilli, J., Sáez, P. J., Srivastava, N., Attia, R., Terriac, E., Baum, B., Cosentino-Lagomarsino, M., & Piel, M. (2018). Size control in mammalian cells involves modulation of both growth rate and cell cycle duration. Nature Communications, 9(1). https://doi.org/10.1038/s41467-018-05393-0

36. Priestman, M., Thomas, P., Robertson, B. D., & Shahrezaei, V. (2017). Mycobacteria modify their cell size control under sub-optimal carbon sources. Frontiers in Cell and Developmental Biology, 5(JUL). https://doi.org/10.3389/fcell.2017.00064

37. Chandler-Brown, D., Schmoller, K. M., Winetraub, Y., & Skotheim, J. M. (2017). The Adder Phenomenon Emerges from Independent Control of Pre- and Post-Start Phases of the Budding Yeast Cell Cycle. Current Biology, 27(18), 2774-2783.e3. https://doi.org/10.1016/j.cub.2017.08.015

38. Wallden, M., Fange, D., Lundius, E. G., Baltekin, Ö., & Elf, J. (2016). The Synchronization of Replication and Division Cycles in Individual E. coli Cells. Cell, 166(3), 729–739. https://doi.org/10.1016/j.cell.2016.06.052

39. Erickson, D. W., Schink, S. J., Patsalo, V., Williamson, J. R., Gerland, U., & Hwa, T. (2017). A global resource allocation strategy governs growth transition kinetics of Escherichia coli. Nature, 551(7678), 119–123. https://doi.org/10.1038/nature24299

40. Hui, S., Silverman, J. M., Chen, S. S., Erickson, D. W., Basan, M., Wang, J., Hwa, T., & Williamson, J. R. (2015). Quantitative proteomic analysis reveals a simple strategy of global resource allocation in bacteria. Molecular Systems Biology, 11(2), e784–e784. https://doi.org/10.15252/msb.20145697

41. Kafri, M., Metzl-Raz, E., Jona, G., & Barkai, N. (2016). The Cost of Protein Production. Cell Reports, 14(1), 22–31. https://doi.org/10.1016/j.celrep.2015.12.015

42. Mori, M., Schink, S., Erickson, D. W., Gerland, U., & Hwa, T. (2017). Quantifying the benefit of a proteome reserve in fluctuating environments. Nature Communications, 8(1), 1–8. https://doi.org/10.1038/s41467-017-01242-8

43. Dai, X., Zhu, M., Warren, M., Balakrishnan, R., Patsalo, V., Okano, H., Williamson, J. R., Fredrick, K., Wang, Y. P., & Hwa, T. (2016). Reduction of translating ribosomes enables Escherichia coli to maintain elongation rates during slow growth. Nature Microbiology, 2 https://doi.org/10.1038/nmicrobiol.2016.231

44. Dai, X., & Zhu, M. (2020). Coupling of Ribosome Synthesis and Translational Capacity with Cell Growth. Trends in Biochemical Sciences, 45(8), 681–692. https://doi.org/10.1016/j.tibs.2020.04.010

45. Panlilio, M., Grilli, J., Tallarico, G., Sclavi, B., Cicuta, P., & Lagomarsino, M. C. (2020). Threshold accumulation of a constitutive protein explains E. coli cell division behavior in nutrient upshifts. BioRxiv, 2020.08.03.233908. https://doi.org/10.1101/2020.08.03.233908

46. Si, F., Li, D., Cox, S. E., Sauls, J. T., Azizi, O., Sou, C., Schwartz, A. B., Erickstad, M. J., Jun, Y., Li, X., & Jun, S. (2017). Invariance of Initiation Mass and Predictability of Cell Size in Escherichia coli. Current Biology, 27(9), 1278–1287. https://doi.org/10.1016/j.cub.2017.03.022

47. Mark Kim, J., Garcia-Alcala, M., Balleza, E., & Cluzel, P. (2020). Stochastic transcriptional pulses orchestrate flagellar biosynthesis in Escherichia coli. Science Advances, 6(6). https://doi.org/10.1126/sciadv.aax0947

48. Apel, D., & Surette, M. G. (2008). Bringing order to a complex molecular machine: The assembly of the bacterial flagella. Biochimica et Biophysica Acta - Biomembranes, 1778(9), 1851–1858. https://doi.org/10.1016/j.bbamem.2007.07.005

49. Chilcott, G. S., & Hughes, K. T. (2000). Coupling of Flagellar Gene Expression to Flagellar Assembly in Salmonella enterica Serovar Typhimurium and Escherichia coli. Microbiology and Molecular Biology Reviews, 64(4), 694–708. https://doi.org/10.1128/mmbr.64.4.694-708.2000

50. Chevance, F. F., & Hughes, K. T. (2008). Coordinating assembly of a bacterial macromolecular machine. Nat Rev Microbiol, 6(6), 455–465. https://doi.org/nrmicro1887

51. Fitzgerald, D. M., Bonocora, R. P., & Wade, J. T. (2014). Comprehensive Mapping of the Escherichia coli Flagellar Regulatory Network. PLoS Genetics, 10(10). https://doi.org/10.1371/journal.pgen.1004649

52. Jun, S., Si, F., Pugatch, R., & Scott, M. (2018). Fundamental principles in bacterial physiology-history, recent progress, and the future with focus on cell size control: A review. Reports on Progress in Physics, 81(5). https://doi.org/10.1088/1361-6633/aaa628

53. Sassi, A. S., Garcia-Alcala, M., Kim, M. J., Cluzel, P., & Tu, Y. (2020). Filtering input fluctuations in intensity and in time underlies stochastic transcriptional pulses without feedback. Proceedings of the National Academy of Sciences of the United States of America, 117(43), 26608–26615. https://doi.org/10.1073/pnas.2010849117

54. Wada, T., Hatamoto, Y., & Kutsukake, K. (2012). Functional and expressional analyses of the anti-FlhD4C2 factor gene ydiV in Escherichia coli. Microbiology (United Kingdom), 158(6), 1533–1542. https://doi.org/10.1099/mic.0.056036-0

55. Takaya, A., Erhardt, M., Karata, K., Winterberg, K., Yamamoto, T., & Hughes, K. T. (2012). YdiV: A dual function protein that targets FlhDC for ClpXP-dependent degradation by promoting release of DNA-bound FlhDC complex. Molecular Microbiology, 83(6), 1268–1284. https://doi.org/10.1111/j.1365-2958.2012.08007.x

56. Hui, S., Silverman, J. M., Chen, S. S., Erickson, D. W., Basan, M., Wang, J., Hwa, T., & Williamson, J. R. (2015). Quantitative proteomic analysis reveals a simple strategy of global resource allocation in bacteria. Molecular Systems Biology, 11(2), e784–e784. https://doi.org/10.15252/msb.20145697

57. Leslie M. (2011). Mysteries of the cell. How does a cell know its size? Science. Nov 25;334(6059):1047-8. https://doi.org/10.1126/science.334.6059.1047

58. Ollion, J., Elez, M. & Robert, L. (2019). High-throughput detection and tracking of cells and intracellular spots in mother machine experiments. Nat Protoc 14, 3144–3161. https://doi.org/10.1038/s41596-019-0216-9

59. Friend, J., & Yeo, L. (2010). Fabrication of microfluidic devices using polydimethylsiloxane. Biomicrofluidics, 4(2), 1–5. https://doi.org/10.1063/1.3259624

60. Improved Adhesion/Bonding due to Plasma Treatment of PDMS https://www.azom.com/article.aspx?ArticleID=14346

61. Attwood, TK., & Cammack, R. (2005). Oxford Dictionary of Biochemistry and Molecular Biology. Oxford University Press.